

# Active assistance to the driver for reinforcing the safety on uncertain road surfaces

Nikhil B. Mhaske

A Thesis Submitted to

Indian Institute of Technology Hyderabad

In Partial Fulfillment of the Requirements for

The Degree of Master of Technology



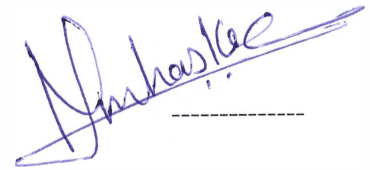
भारतीय प्रौद्योगिकी संस्थान हैदराबाद  
Indian Institute of Technology Hyderabad

Department Of Mechanical and Aerospace Engineering

June 2016

## Declaration

I declare that this written submission represents my ideas in my own words, and where ideas and words of others have been included, I have adequately cited and referenced the original sources. I also declare that I have adhered to all principles of academic honesty and integrity and have not misinterpreted or fabricated or falsified any idea/data/fact/source in my submission. I understand that any violation of the above will be a cause for disciplinary action by the Institute and can also evoke penal action from the sources that have thus not been properly cited, or from whom proper permission has not been taken when needed.



-----  
(Signature)

Nikhil B. Mhaske  
-----


(Student Name)


me14mtech11030  
-----


(Roll No.)

## Approval Sheet

This thesis entitled " Active assistance to the driver for reinforcing the safety on the uncertain road surfaces " by Nikhil Bharat Mhaske is approved for the degree of Master of Technology from IIT Hyderabad.

  
Dr. S Sivesh, Associate professor  
(—————) Examiner  
Dept. of Civil Engineering  
IITH

  
Dr. R Prasanth Kumar, Associate professor  
(—————) Adviser  
Dept. of Mechanical and Aerospace Engineering  
IITH

  
Dr. Venkatesham B, Associate professor  
(—————) Internal examiner  
Dept. of Mechanical and Aerospace Engineering  
IITH

## Acknowledgements

I would like to thank my adviser Dr. R Prasanth Kumar for his continuous support, motivation and valuable guidance. This work could not have been achieved if it was not for his encouragement and solutions to many problems that I faced. Also the help and support provided by my classmates and friends at IIT Hyderabad was exceptional. I specially thank to Mr. Girish Agawane (Former student of IIT Hyderabad), Mr. Bhatia Niket and Mr. Marwadi Sagar for their support and co-operation.

*To my family ...*

# Abstract

This study focuses on the stability and safety of vehicle during constant velocity cornering, when the adhesion coefficient of the road suddenly drops. A vehicle model of 14 **D**egrees **O**f **F**reedom (DOF) is used to implement the controllers which precisely control the yaw moment and side slip angle. The effectiveness of combine implementation of **D**irect **Y**aw moment **C**ontrol (DYC) and **A**ctive **F**ront wheel **S**teering (AFS) is realized using obtained results. The corrective steering angle and yaw moment for above controllers are obtained by non-linear **S**liding **M**ode **C**ontroller (SMC).

The results of non linear dynamic equations of 14 DOF model are verified using ADAMS/Car before implementing controls to it. The position/orientation of roll axis of model is assumed constant, which actually is function of suspension geometry and other parameters. The Magic formula tire model and Tire-Brush model are used to calculate the tire forces generated at tire ground interface. The main function of DYC is to appropriately distribute longitudinal tire forces with the help of differential braking system like **A**ntilock **B**raking **S**ystem (ABS). The controller used in stabilizing the vehicle model, controls yaw moment as well as side slip angle. As to maintain the yaw rate close to the desired one, we may need to turn down the angular velocities of wheels using ABS or speed-up, hence the control system discussed in this research is best suited for electric cars.

# Contents

<b>Declaration</b>	<b>i</b>
<b>Approval Sheet</b>	<b>ii</b>
<b>Acknowledgements</b>	<b>iii</b>
<b>Abstract</b>	<b>v</b>
<b>List of Figures</b>	<b>viii</b>
<b>List of Tables</b>	<b>ix</b>
<b>Nomenclature</b>	<b>xi</b>
<b>1 Introduction</b>	<b>1</b>
1.1 Background . . . . .	1
1.1.1 Controls . . . . .	2
1.1.2 Vehicle Model . . . . .	6
1.1.3 Tire modeling . . . . .	7
1.2 Literature Review . . . . .	8
1.3 Motivation, scope and objectives . . . . .	11
1.4 Thesis layout . . . . .	12
<b>2 14 DOF Vehicle Model</b>	<b>13</b>
2.1 Equivalent Vehicle Model . . . . .	13
2.2 Vehicle Equations Of Motion . . . . .	15
2.3 Tire Model . . . . .	26
2.3.1 Magic Formula . . . . .	26

---

2.3.2	Tire Brush Model . . . . .	28
2.4	Validation of 14 DOF Vehicle Model Using ADAMS/View and ADAMS/Car . . . . .	33
2.4.1	Initial Condition Calculation for MATLAB Model Using Static ADAMS Model . . . . .	33
2.4.2	Validation Using ADAMS/Car . . . . .	34
2.5	Summary . . . . .	38
<b>3</b>	<b>Control of Yaw Rate and Side-Slip by SMC Based DYC and AFS</b>	<b>39</b>
3.1	Introduction . . . . .	39
3.2	Necessity to Control Yaw Rate and Side slip Angle . . . . .	40
3.3	Control law for DYC . . . . .	41
3.4	Control Law for AFS . . . . .	45
3.5	Yaw Stability Controller Structure . . . . .	46
3.6	Summary . . . . .	46
<b>4</b>	<b>Effectiveness of Controllers</b>	<b>48</b>
4.1	Introduction . . . . .	48
4.2	Performance on the Dry Road . . . . .	48
4.2.1	Comparison by Parameters . . . . .	49
4.3	Performance on Slippery Road . . . . .	50
4.4	Performance on Sudden Loss of Adhesion Coefficient of Road . . . . .	53
4.4.1	Introduction of the Case . . . . .	53
4.4.2	Parameters Comparison . . . . .	55
4.5	Summary . . . . .	59
<b>5</b>	<b>Conclusion and Recommendations</b>	<b>60</b>
5.1	Conclusion . . . . .	60
5.2	Recommendations . . . . .	61
<b>A</b>	<b>Support .m file for MATLAB/Simulink Model</b>	<b>62</b>
A.1	.txt File of Initial Conditions for .m File . . . . .	66
A.2	MATLAB Script File and Simulink Model . . . . .	67
	<b>References</b>	<b>82</b>



# List of Figures

1.1	Schematic for application of active systems . . . . .	3
1.2	Schematic for VSC[1] . . . . .	3
1.3	Schematic for AFS[2] . . . . .	5
1.4	Schematic of rigid and suspended vehicle[3] . . . . .	6
1.5	Schematic for direction of tire forces . . . . .	7
1.6	Tire forces . . . . .	8
1.7	Integrated yaw rate controller and rollover avoidance controller[4] . . . . .	11
2.1	Equivalent vehicle model and co-ordinate systems[3] . . . . .	14
2.2	Various force and velocity components at right-front ( <i>rf</i> ) corner of suspension system[3] . . . . .	15
2.3	Schematic of wheel . . . . .	19
2.4	Plan of steered wheel . . . . .	20
2.5	Schematic showing various velocities and forces at right-front corner . . . . .	21
2.6	Longitudinal motion . . . . .	22
2.7	Front view of vehicle model . . . . .	23
2.8	Coordinate axes system on rotating by Cardan angles . . . . .	24
2.9	Sequence of rotation of inertial frame . . . . .	24
2.10	Plan view of tire during combine slip condition [5] . . . . .	28
2.11	Brush model with constant slip angle [6] . . . . .	28
2.12	Braked Tire Brush model without sliding [6] . . . . .	30
2.13	Plan view of contact patch when the tire has constant slip angle and is braked. [6] . . . . .	32
2.14	Static vehicle model in ADAMS/View . . . . .	33
2.15	Compression of various springs in ADAMS for initial conditions . . . . .	34
2.16	Validation of MATLAB model with ADAMS/Car Model . . . . .	35
2.17	Steering angle given to vehicle model in ADAMS/Car . . . . .	35

2.19	Inclination of wheel . . . . .	37
2.20	Reaction time for ADAMS/Car model to the steering input . . . . .	38
3.1	Bicycle model . . . . .	40
3.2	Controller structure . . . . .	46
4.1	Driver input condition during maneuverability . . . . .	49
4.2	Trajectories and yaw rate comparison . . . . .	49
4.3	Heading angle comparison and correction angle by AFS . . . . .	50
4.4	Trajectories and orientation comparison on dry and slippery road . . . . .	51
4.5	Enlarged view of trajectories traced on slippery surface . . . . .	52
4.6	Tracking performance of DYC for sinusoidal steering input on slippery road . . . . .	52
4.7	Side-slip angle on slippery road with sinusoidal steering input . . . . .	53
4.8	Topography of road and vector diagram of yaw orientation at the end of simulation . . . . .	55
4.9	Friction coefficients for different tires and yaw angle comparison . . . . .	56
4.10	Path traced by vehicle over the sudden ice patch and dry road . . . . .	57
4.11	Parameters of vehicle which passed over a sudden ice patch of friction coefficient 0.25 . . . . .	58
A.6	Wheel dynamics in Simulink . . . . .	79
A.7	Dynamics for right-front corner . . . . .	79
A.8	Details of subsystem 'Assembly' . . . . .	80
A.9	Details of subsystem 'Vehicle dynamics' . . . . .	81

# List of Tables

2.1	Magic Formula constants [5]	27
2.2	Various constants in Magic Formula, $F_z$ in $kN$ [5]	27
4.1	Adhesion Coefficient for different road surfaces [7]	54

# Nomenclature

Symbol	Units	Description
$m$	kg	Sprung mass
$J_x, J_y, J_z$	$kg\ m^2$	Moment of inertial about $x, y$ and $z$ axis
$a, b$	$m$	Distance of CG from front and rear axles respectively.
$c$	$m$	Width of the vehicle.
$h$	$m$	Height of the CG from the ground.
$h_{rcf}, h_{rcb}$	$m$	Roll center distance from CG for front and rear suspension resp.
$u, v, w$	$m/s$	Longitudinal, lateral and vertical velocities.
$\omega_x, \omega_y, \omega_z$	$rad/s$	Roll, pitch and yaw velocity.
$\phi, \theta, \psi$	$rad$	Roll, pitch and yaw angle.
$m_u$	kg	Wheel mass
$J_w$	$kg\ m^2$	Wheel inertia
$R_0$	$m$	Free rolling radius
$C_f, C_b$	$N/rad$	Cornering stiffness for front and rear axle.

# Chapter 1

## Introduction

### 1.1 Background

Rigorous research in the field of embedded electronics to shape the intricate circuits has allowed automotive industry to step into era of smart cars. High frequency processing terminals of real time parameter has encouraged the car manufacturers to invest hefty to implement on-board technologies which enhances safety, handling, stability and performance of automobile. More than 30,000 humans lose their lives per year in accidents, and most of them are accounted for driver errors alone [8].

Active stabilization systems installed on-board, helps the driver as a safety assisting functions to avoid roll over during high speed cornering, avoid skidding on low adhesion coefficient roads, maintaining side slip angle in order to have better control over maneuverability etc. Active systems have proven to have superior control on vehicle than passive ones in severe driving conditions, but the complete dependency on these assisting system may not be useful always. For example, while cornering at high speed, with continuous side slip angle correction for vehicle, angular velocities of tires may alter continuously, hence decreasing overall speed and the economy of the vehicle. On account of problem like this, there needs a necessity to find tread-off for usage of these technologies. A smart control system detects the prevailing conditions and stability margin and helps driver to bring the control parameter back to stable region in phase plane.

Roll over being one of the most hazardous events, has been studied throughly by researchers over the years[9, 10]. Even though this study focuses on regaining the stability of vehicle on sudden ice or oil patch during the cornering, the 14 DOF vehicle model explained here can still be used to implement the roll-over avoidance algorithm. The active roll control system includes the systems like,

- Active suspension[11]
- Active Roll bars

- Active steering[12]
- Differential braking[9]

### 1.1.1 Controls

Out of the above four systems, the first two are responsible for directly reducing roll angle of vehicle where as the later two avoid impending roll over by maintaining the yaw rate. Similar to roll prevention phenomenon, the active steering system and differential braking system can also be used to stabilize the swaying side-slip angle and yaw moment. In a driving instance of lane change at low speed on dry asphalt road, the controllability of vehicle is independent of driver's expertise as being non challenging scenario. However, in severe driving condition like sudden lane change on the road covered with ice, driver is forced to take action in the fraction of a second. During situation like this, despite of the level of expertise, many drivers lose the control over vehicle.

To reduce the fatality, automobile manufacturers used passive safety equipments such as air bags. For last three decades, passive safety was preferred over active due to the cost and installation difficulties, but even after implementing all passive majors, the main contributor of such fatal incidences, driver errors, remained untreated. 75% of car accidents are accounted for driver errors[4], which can not be minimized by passive safety equipments.

In view of active safety measures, two systems are identified as very effective. Differential braking control being one of them, mainly works to maintain the yaw moment by generating differential longitudinal forces on left and right tires. Hence by maintaining yaw moment, it improves the yaw angle characteristic and thereby influencing the lateral motion of vehicle which can cause skidding on the slippery road. Active steering control being the other, primarily works as driver assist function. Active steering system can mitigate the difference between actual and desired yaw rate by providing small angle correction to the steering angle given by driver. AFS technology can be implemented via steer-by-wire system in which all the mechanical components of conventional steering mechanisms are replaced by controllers and actuators.

With the help of results obtained which are discussed in chapter 4, it can be inferred that the combine effect of differential braking and active steering forms efficient system to control yaw rate and side slip angle.

Schematic diagram below 1.2 summarizes the **Vehicle Stability System (VSC)**. Main function of this system is to prevent skidding of vehicle in lateral plane. Although all the parameters shown in the diagram are not taken into consideration while carrying out this study, important factors and their functional importance are,

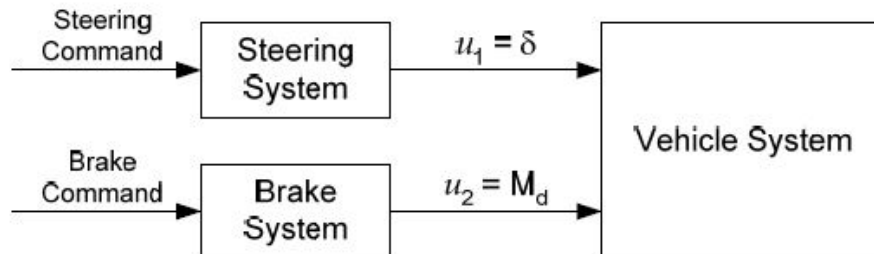


Figure 1.1: Schematic for application of active systems

1. Brake actuator for differential braking
2. Propelling force is controlled by throttle actuator
3. Sensors for yaw, wheel speed, steer angle
4. Sensor to sense longitudinal and lateral acceleration
5. Pressure sensor for master cylinder
6. Electronic control unit computational program

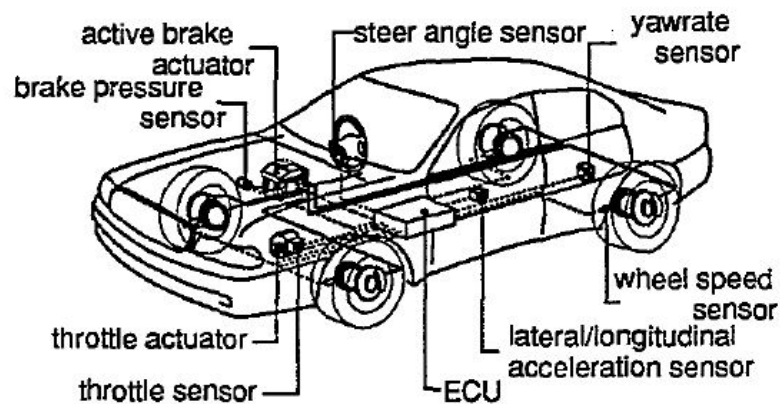


Figure 1.2: Schematic for VSC[1]

### Differential Braking

Under various vehicle stability systems, the yaw stability has got distinguished attention by researchers. In extreme driving conditions, yaw stability control system generates corrective yaw moment with the help of active steering and differential braking to compensate for driver's imperfect inputs.

As far as differential braking is concerned, the usage of existing ABS in cars, is the most economically and functionally preferred option. There are some major factors for ABS[4],

- The saturation effect in which brake pressure to wheel is limited to prescribed wheel slip and acceleration.
- Overall (brake) gain from hydraulic pressure to brake force.
- Lag in the system to react to input.

The saturation effect is the result of seeking a control performance where the maximum longitudinal brake force is imparted to the road without excessive longitudinal acceleration and slip. Overall brake gain is a scalar value based on physical dimension of hydraulic system assuming that disc brakes are used[4].

Hydraulic system response is modeled as[4]

$$\dot{P}_{hyd} + \frac{1}{0.2}\bar{P}_{hyd} = \frac{1}{0.2}P_{hyd} \quad (1.1)$$

where 0.2 is time lag,  $P_{hyd}$  is hydraulic pressure input command,  $\bar{P}_{hyd}$  is the resulting braking pressure. The braking force on each tire is[4],

$$F_B = k_B\bar{P}_{hyd} \quad (1.2)$$

Where  $k_B$  is the brake scale factor.

The details of ABS are not discussed in this study because the focus is on yaw stability. Hence using sliding mode controller, the required corrective moment that ABS should produce by differentially operating the brakes, is directly fed to the non linear vehicle model without taking ABS in consideration.

### Steering Assistance System

The steering assistance system, AFS, introduces additional steering angle correction to the driver's input, in order to track the ideal yaw rate. Various factors such as vehicle mass, speed, road condition are changing from time to time. The sliding mode controller provides AFS the robustness required against such varying parameters. It has also been shown that the implementation of AFS also increases the threshold limit for the rollover[13]. As already stated above, the combine implementation of DYC and AFS ensures superior performance over wide spectrum of driving conditions. Activating DYC based on differential braking, could alter the vehicle speed, which is not favorable, especially during obstacle avoiding maneuver. Moreover, application of DYC alone could lead to high level of annoyance



to driver because of frequent braking[14]. It is reported in the literature that the effective performance of standalone AFS could only be experienced in low to moderate lateral acceleration[14].

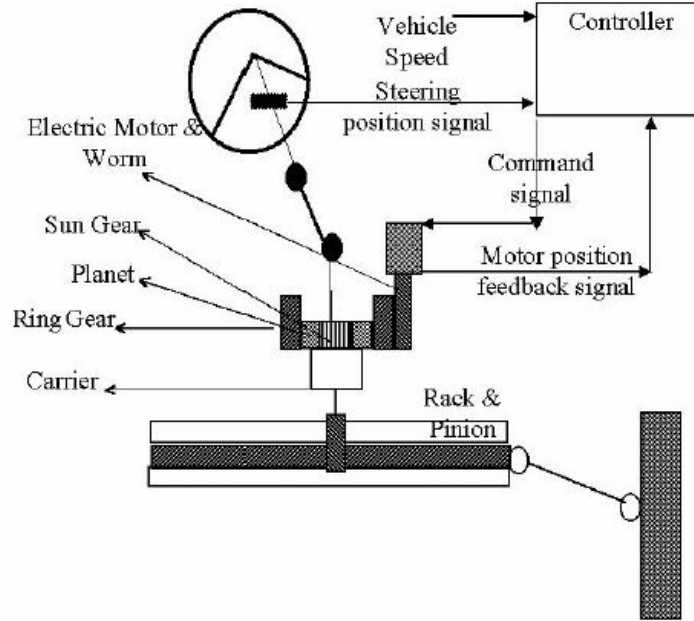


Figure 1.3: Schematic for AFS[2]

The schematic diagram of AFS is shown in figure 1.3. The system shown in the diagram can easily be integrated with vehicle stability control system. The detailed function of system shown, is not the part of this study, interested readers can refer [2] for the details, we will try to understand this system on broader scale.

Planetary gear arrangement is the key component of active steering system and is fixed between steering wheel and rack and pinion arrangement. The sun gear receives its input from the steering wheel i.e driver. An electric motor, via worm gear arrangement, transfers motion to the ring gear. Hence, the planetary gears receives motion from two inputs one being sun gear and other as ring. Three planetary gears mesh with sun gear on one side and ring gear on other, rides on the spider/carrier. The Spider is directly connected to the pinion of the rack and pinion arrangement. It can be inferred that the velocity of pinion can directly be changed by altering the velocities of sun and ring gear. The pinion angular velocity is given by [2],

$$\omega_p = k_1\omega_s + k_2 * \omega_m \quad (1.3)$$

where,

$$k_1 = \frac{k_r}{1 + k_r} \quad k_2 = \frac{1}{k_{mr}} \frac{1}{1 + k_r} \quad (1.4)$$

$k_r$  = Number of teeth on sun gear / Number of teeth on ring gear.

$k_{mr}$  = Number of teeth on ring / Number of teeth on worm.

With varying the motor speed, steering ratio can be changed in order to maintain desired steering gain. On integration of AFS to the above system, the input to the DC motor becomes the dependent parameter of controller. The difference between desired yaw rate and actual yaw rate and instantaneous longitudinal velocity of vehicle works as an input parameters to the robust AFS controller. Based on the various constants, which are appropriately assigned, controller calculates the desired steering angle. Hence angle thus obtained, triggers the DC electric motor appropriately to achieve the desired steering gain. On subtracting the input steering angle from the one obtained from AFS, we get the corrective steering angle.

### 1.1.2 Vehicle Model

Vehicle model used in this study is similar to the one explained in [3] with minor modifications. Figure

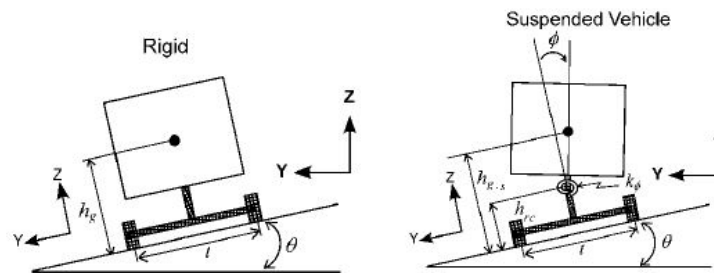


Figure 1.4: Schematic of rigid and suspended vehicle[3]

1.4 shows the roll plane model of rigid and suspended vehicle. The suspended vehicle model have a roll degree of freedom because of suspension springs and dampers which attach sprung mass with unsprung mass. Sprung mass is considered to rotate about kinematic roll center axis, which is a straight line joining front roll center and rear roll center. The position of these roll centers changes with the change in the geometry of corresponding suspension system, but for computational simplicity, we have constrained them to remain fixed. The mass of chassis is higher than that of unsprung mass by substantially. The 14 DOF model has following advantages,

- 14 DOF model has similar dynamic response as 8 DOF model with additional advantage of tracking pitch and heave motion.
- Functional/mathematical model of each suspension corner can be set separately.
- This model can predict the behavior of vehicle even if wheel lifts-off .

Despite of the fact that 14 DOF model covers lesser degrees of freedom as compared to multi-body dynamic model, it captures all important motions which are necessary in view of stability and handling.

In this study, we have modeled 14 DOF car model [3] with fixed roll centers, and validated it with ADAMS/CAR [15] . If we consider only the vehicle model, the non-linear effects due to roll, pitch, unsprung mass inertia, makes it non suitable to develop control systems. Hence to provide the compatible passage for plugging the controls, we have used some assumptions to omit the non linear terms.

### 1.1.3 Tire modeling

The input to all the dynamic equations is directly or indirectly dependent on the forces generated at tire ground interface. These forces i.e longitudinal and lateral, are the function of longitudinal and lateral slip respectively. To calculate these forces, we have used Magic formula as described in [5].

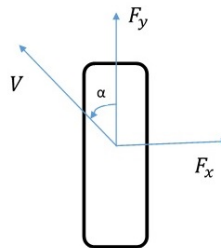


Figure 1.5: Schematic for direction of tire forces

The figure 1.5 above shows the positive directions to calculate the tire forces based on the tire slips.  $F_y$  is the lateral force which is dependent on the slip angle  $\alpha$ , where as  $F_x$  is the longitudinal force which is dependent on longitudinal slip ratio. The representation shown above in figure1.5 is the adapted Society of Automotive Engineer (SAE) representation. Since this study is regarding the stability during cornering when adhesion coefficient of road is suddenly dropped and raised again, each tire may undergo from combine slip condition (slip angle and longitudinal slip ratio together). Hence we need to use the Magic Formula in which the magnitude of forces due to combine presence of both the slips is discussed.

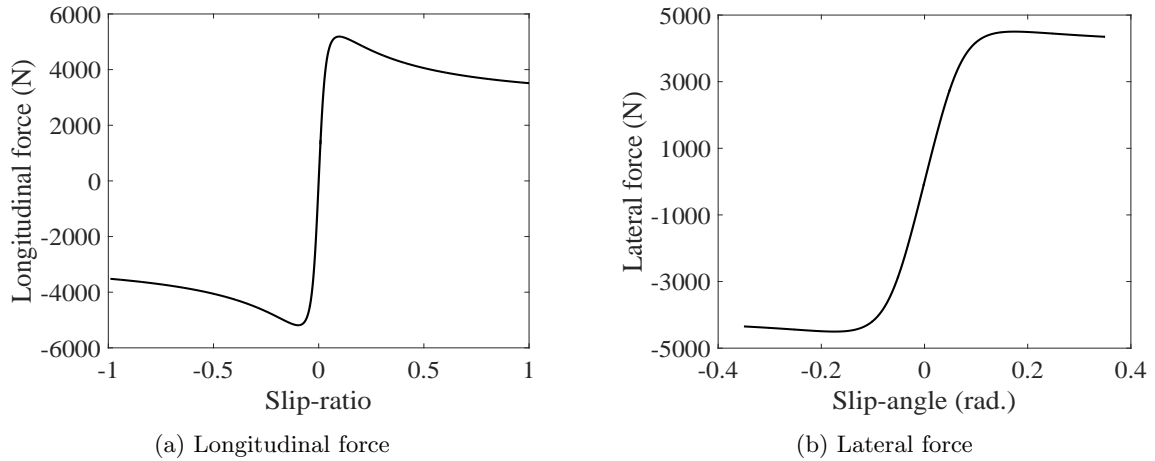


Figure 1.6: Tire forces

The figure 1.6 shows the behavior of forces with respect to change in corresponding slip when the 5000 N force is put on the tire. Note that these graphs shows the nature of curve in pure conditions. As we can observe, the nature of this graph is acceptably linear till threshold value of slip ratio/angle, beyond which, it no longer remains the linear, but starts to vary according to the Magic formula. Tire brush model is another model which use the side slip angle and slip ratio to calculate the tire forces[6]. Along with these two inputs, Brush model also requires some constants which defines the nature of manufacturing process been used for the tire. Such as vertical stiffness, lateral stiffness per unit length of contact patch etc. The word bristle is basically used for the tread elements of a tire. When the tire is freely rolling on the surface, without accelerating or braking, the first element comes in the contact with ground, enters perpendicular to the carcass. Additionally, if tire is not turning hence not producing any side slip angle and if camber angle is zero too, then these bristles do not deflect in any direction and hence do not produce any force.

## 1.2 Literature Review

This section explains about

1. Various vehicle models developed and utilized to implement active control systems.
2. Active stability systems which works on regulating the yaw rate and side slip angle of a vehicle using DYC and AFS

Ghike et al.[3] reviewed the 14 DOF vehicle modeling using non multi-body dynamic approach. In the present paper, sprung mass is considered as body in space and hence modeled for six independent

motions. Unsprung mass (tires) are constrained to have motions of rolling and translational (vertical). Hence each tire has two independent motions which adds another eight to previous six which sums to 14 DOF. The roll center height in this model is assumed constant and so as the inertia matrix. Various models, with increasing linearity in the equations are proposed and simulated. The results of these simplified models are validated with ADAMS/CAR[15] and CARSIM. As a part of linearizing the non linear equations, the terms of inertia forces of unsprung masses are also omitted in simplified models. To calculate the tire forces, Magic formula[5] has been used. Since the compression of each tire has modeled separately, the rollover prediction algorithm can be applied more effectively.

Cooper et al.[16] has discussed the stability of vehicle based on variable torque distribution and active suspension systems. The basics of variable torque distribution lies in the functioning of active differential gear box. Active gear box distributes torque in such a way that it is supplied to the corner which can perform maximize utilization. When lateral forces generated are higher, the steering controller become ineffective. In the situation like this, active suspension plays an important role for stabilization. The variable torque distribution system has Internal Model Controller which works to improve the yaw rate. But because of inefficient control, 'roll moment distribution PID controller' replaced the existing controller. Roll moment distribution controller adjusts the stiffness of active roll bars, hence changing cornering stiffness of front or rear axles. To implement these systems, a 8 DOF non linear vehicle model is used, which excludes heave and pitch motion of sprung mass as in 14 DOF model. Along with this, the vertical translational motion of wheels with respect to ground is also omitted, hence wheels have only the rotational DOF.

Mashadi B. et al.[17] analyzed the stability of electric vehicle using integrated AFS and DYC sliding model controller. A multilayer controlling method has been used to carry out the study. In multi layered control structure, the higher layer, based on driver's input of steering angle, speed of vehicle, yaw rate, reference yaw rate, reference side slip angle, feedback signal from vehicle, calculates the corrective steering angle and yaw moment signal. The exact function of high layer controller is to track the desired yaw rate and absolute value of side slip angle, close to desired one and that of low level controller is to apply the correcting yaw moment to the vehicle using electric motors, wheel slip controller and motor torque controller. It triggers electric motor to act in such a way that difference between reference and actual yaw rate is minimized. The model used is assumed to be four wheel driven and defined with 9 DOF. The 8 DOF are same as described by [16] above. In addition to this, the steering angle input from driver is also considered as an additional DOF to sum to 9 DOF.

He et al.[18] has worked on developing the stability system using AFS and Dynamic Stability Control (DSC). DSC comprise of standalone and combine effect of active braking and active driveline

control. The 8 DOF vehicle model has been used to implement control strategy. To calculate the tire forces, the non linear Magic formula has been used. The sliding surface used for this AFS controller is

$$s = r - r_d \quad (1.5)$$

$$\dot{s} = -k_1 s - k_2 \text{sgn}(s) \quad (1.6)$$

where  $k_1$  and  $k_2$  are positive constants and  $r_d$  is the desired yaw rate.

Fu Chunyun[19] has analyzed the stability of non linear vehicle model of 8 DOF using DYC. The tire forces generated are calculated using Magic formula. Firstly, the stability of vehicle is aimed at maintaining the neutral steering by tracking the reference yaw rate, secondly, the DYC works to maintain desired side slip angle, which is in this case is zero. The above two controlling techniques do not use sliding mode controller to define the control law. But to achieve enhanced stability performance, the sliding mode based DYC is proposed which uses novel switching function. This function ensures the simultaneous convergence of yaw rate and side slip angle to their respective reference values. The novel switching function used is,

$$s = \frac{\rho}{|\Delta r|_{max}} |r - r^*| + \frac{1 - \rho}{|\Delta \beta|_{max}} |\beta - \beta^*| \quad (1.7)$$

where  $\rho \in [0, 1]$  is a design parameter.  $|\Delta r|_{max}$  and  $|\Delta \beta|_{max}$  are the maximum values of difference between actual yaw rate and side slip angle with respect to their corresponding reference values respectively.

Bakker E et al.[5] has discussed the details of Magic formula to calculate the tire forces. The experimental results obtained from the particular class of tire by varying slip ratio and slip angle. All the experimental result data points are fitted in a curve. Magic formula provides the longitudinal force and lateral force for pure as well as combined slip condition. By changing the independent variables, the same formula calculates the longitudinal as well as lateral force. The nature of self aligning moment with respect to slip angle of tire is also been discussed.

Lee et al.[4] has discussed the stability of vehicle using integrated active front steering and differential braking. To implement the control strategies, a simplified linear 4 DOF vehicle model has been used. The effectiveness of these controllers in standalone mode and in integrated mode on non linear vehicle model is discussed. To calculate the tire forces, the linearized tire model is used in which the lateral tire force is assumed to be linear function cornering stiffness and slip angle. The stability of vehicle has been discussed against yaw rate and rollover coefficient. Rollover coefficient is indicator for rollover risk. Rollover coefficient is given by,

$$R_c = \frac{F_{z,r} - F_{z,l}}{F_{z,r} + F_{z,l}} \quad (1.8)$$

where  $F_{z,r}$  and  $F_{z,l}$  are normal forces on right and left tire respectively. For rollover stability,  $|R_c|$  should be less than 1. The control structure for yaw stability and rollover avoidance is,

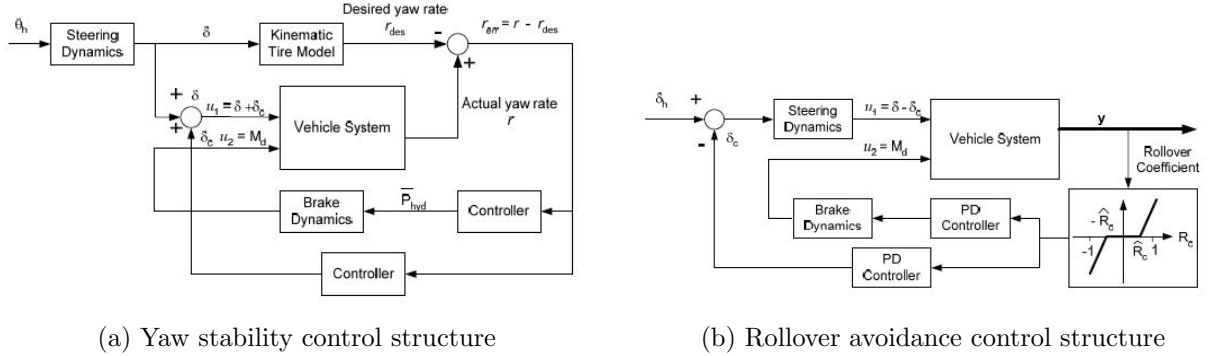


Figure 1.7: Integrated yaw rate controller and rollover avoidance controller[4]

### 1.3 Motivation, scope and objectives

The safety on the road has become prime important issue considering the number of accidents per day. Many times, fatalities occur due to misjudgments from the driver. Considering Indian traffic scenario, the fully autonomous cars seems to be nonviable option. Ever expanding cities has reached till countryside where the road conditions are irregular. During the night time with average intensity of headlights, it becomes difficult for the driver to identify spilled oil on the road or blackened ice patch or any laid material making it slippery. Situation becomes even critical when such a slippery patch happens to be on blind turns where drivers has no vision on account of darkness and non-adaptive headlights. In the situation like these, the vehicle shall be smart enough to understand the sudden change in its directionality and should help the driver to stabilize as soon as possible without fatal incidence to happen.

The objective of this research is to analyze the vehicle model which closely resembles to the medium price range vehicle dynamic model. Implementing the active control systems which is robust against varying parameters and uses existing setup of the car. These systems shall improve the stability and handling characteristics of the vehicle by maintaining the directionality. The design of these system should be such that they could be switched on or off at driver's wish. The effectiveness of these systems should be robust against dry, slippery or sudden slippery road surfaces.

This research extends from analyzing the appropriate vehicle model which closely defines the real vehicle model to implementing the yaw rate and side slip angle robust controllers. The direct yaw

moment is controlled by differential braking the rear wheels, which also controls the side slip angle. The active front wheel steering system controls the yaw rate only by working with existing steer-by-wire system in the vehicle. The effectiveness of these controllers has been checked on different road conditions and input variables from driver.

## 1.4 Thesis layout

This thesis consists of five chapters. Chapter 1 is the introduction of the research work with brief information about various active control system. It also consist of literature review of vehicle model, tire model and DYC and AFS system. A brief paragraph covers the motivation and scope.

Chapter 2 introduces the 14 DOF vehicle model and various equations of motions for sprung and unsprung masses. The sprung mass equations of motions describes its longitudinal, lateral , heave, roll, pitch and yaw motions. The two tire models *Magic formula* and *Tire-brush* model are also discussed. The vehicle model is scripted in MATLAB and the simulation results are validated using ADAMS/Car [15]. The initial conditions required for .m file of MATLAB are calculated by building a static model in ADAMS/View [15] environment.

In Chapter 3 robust controller based on sliding mode to directly control the yaw moment by altering the longitudinal tire forces of rear tires is introduced. The control law for differential braking system is derived, which decides the magnitude of braking torque to be applied to each one of rear wheels. The robust sliding mode based AFS to control the yaw moment is introduced in this chapter. The simultaneous application of these control systems to the vehicle model discussed in chapter 2, is carried out in MATLAB/Simulink environment.

Chapter 4 discusses the effectiveness of simultaneously applied controllers on vehicle model running of the road with different surface conditions. The results with continuously dry and continuously slippery surface are discussed. The performance of the controllers when the adhesion coefficient,  $\mu$ , of road suddenly drops on the corner, is also discussed. The results for two different adhesion coefficients are discussed in order to have the comparative study.

chapter 5 summarizes the conclusion of all the research steps and the recommendations for the future work.



## Chapter 2

# 14 DOF Vehicle Model

To implement the DYC and AFS, a full vehicle model which closely resembles to the vehicle dynamics is required. Using this vehicle model, the active control systems are simulated in MATLAB/Simulink environment. The mathematical structure of plant of this control circuit is nothing but the equations of motions of full vehicle model. The vehicle model which acceptably defines the real vehicle, should perfectly track its lateral, longitudinal, heave, roll, yaw and pitching motions. This chapter explains the 14 DOF vehicle model[3] in detail. Key points while analyzing the model are,

- Six equations of motion sprung mass.
- Dynamics response of suspension system and tires.
- Calculation of tire forces using Magic formula.
- Rotational equation of motion of wheel.

### 2.1 Equivalent Vehicle Model

The schematic diagram 2.1 shows the vehicle model having 14 DOF. Six DOF of chassis are accounted for the object in space and remaining eight describes the rolling and translational (vertical) motion for four tires. As can be seen from the diagram, the chassis is been supported on suspension system at four corners. The another spring in series with the suspension is the vertical stiffness of tires. Note that this model does not consider the damping property possessed by the tires. As can be seen from the figure, there are two coordinate frames defined.

**coordinate frame 1** Coordinate frame 1 is fixed to the **C**enter of **G**ravity (CG) of chassis. Hence the equations of motion of chassis are expressed in the same coordinate frame (Body coordinate

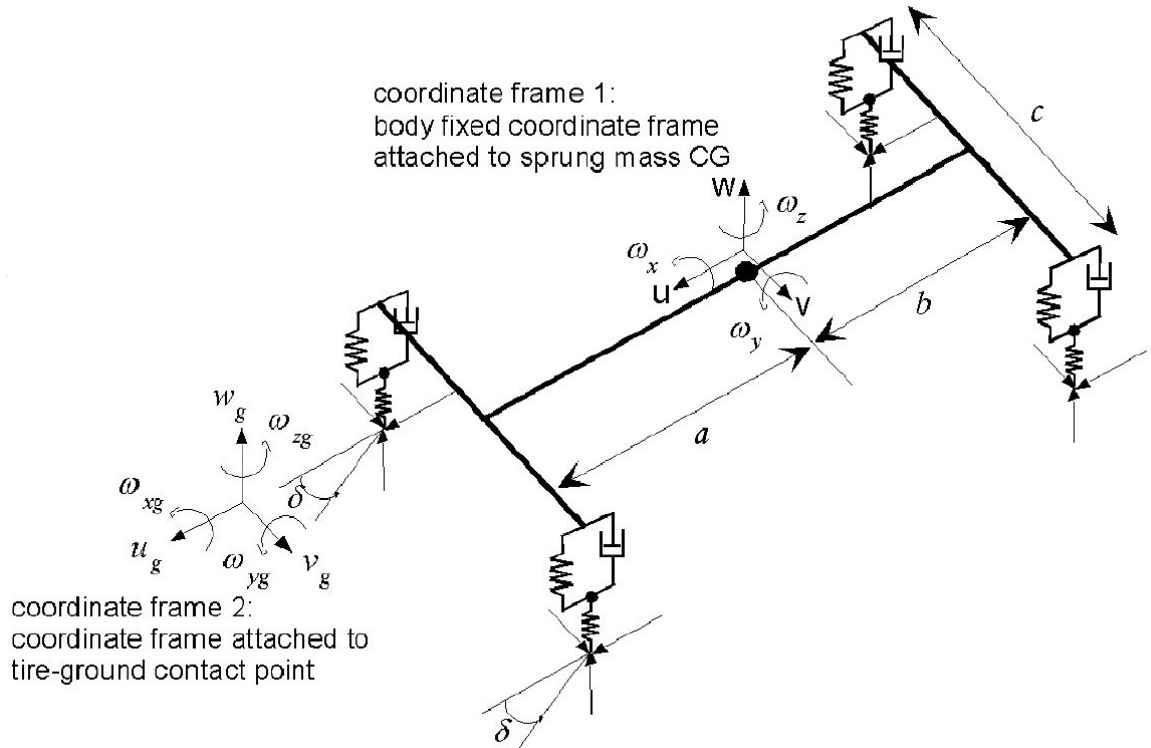


Figure 2.1: Equivalent vehicle model and co-ordinate systems[3]

frame). As shown in the figure 2.1, longitudinal, lateral, and heave motion of chassis are represented by  $u$ ,  $v$  and  $w$  respectively. Whereas roll, pitch and yaw velocities are represented by  $\omega_x$ ,  $\omega_y$  and  $\omega_z$  respectively. The roll, pitch and yaw angles are represented by  $\phi$ ,  $\theta$  and  $\psi$  respectively. Reorientation of the inertial frame (XYZ) by instantaneous yaw angle followed by pitch and then roll angle would give the orientation of chassis and hence coordinate frame 1.

**coordinate frame 2** As can be seen from figure 2.1, the coordinate frame 2 is fixed at the tire ground contact point. The longitudinal direction of coordinate frame 2 is oriented along the longitudinal direction of coordinate frame 1, Hence at any instant of time, both the frame will have same yaw angle. But coordinate frame 2 does not change its orientation with pitch and roll of the chassis. In other words, coordinate frame 2 is obtained by rotating inertial frame by yaw angle only. The velocities  $u_g$  and  $v_g$  are longitudinal and lateral velocities of contact patch of tires, expressed in coordinate frame 2

The position of center of gravity of chassis is unsymmetrical along longitudinal direction. It is at a distance of  $am$  from front axle and  $bm$  from the rear. The position of CG is evenly situated along the track of the vehicle,  $c$  is the track width of the vehicle model. For mathematical simplicity, the steering angle  $\delta$ , for road wheels is considered to be the same for inner as well as outer wheel in case of cornering. For the observer positioned at CG of chassis, facing in longitudinal direction of progression, the right corner of front axle appears **right-front**( $rf$ ) corner of the suspension system similarly the other corner as the **left-front** ( $lf$ ). Same direction sense follows for rear axle to objectify **right-back** ( $rb$ ) and **left-back** ( $lb$ ) corners of rear axle suspension.

Since the integration of longitudinal and lateral motions in coordinate frame 1 would not give conclusive results, we need to express the translational motions of the chassis in the inertial coordinate frame first and then should integrate them in time domain to understand the trajectory traced by the vehicle.

## 2.2 Vehicle Equations Of Motion

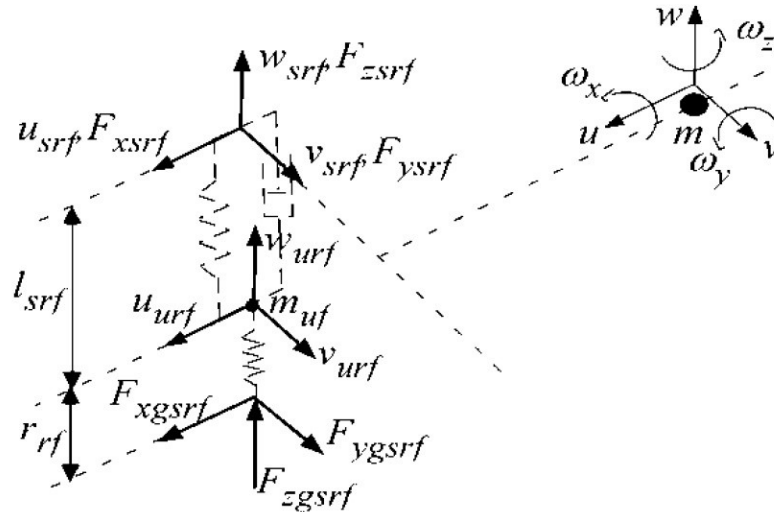


Figure 2.2: Various force and velocity components at right-front ( $rf$ ) corner of suspension system[3]

Figure 2.2 depicts the schematic of enlarge view of right front corner of vehicle model. Since the mathematical representation of dynamics of suspension and tire is same in all four corners of chassis, elaborating any one is sufficient to understand the dynamics of vehicle model. Hence we will analyze right-front ( $rf$ ) corner of vehicle model. It is important to understand the mechanics of transfer of

forces from tire to chassis via suspension system. Since we are expressing equations of motions of chassis in coordinate reference frame 1, we need to express each component of force in the same reference frame. In order to maintain the force components in frame 1, it is necessary to express all the velocity components in the same reference frame.

**Velocity Components at Right-Front Corner** Considering vehicle is moving with some velocity whose components are given by  $u$ ,  $v$  and  $w$ . Along with translational initial velocities, lets assume that it has some rotational initial velocities i.e.  $\omega_x$ ,  $\omega_y$  and  $\omega_z$ . Note that these all components of velocities are expressed in reference frame 1.

$$\begin{bmatrix} u_{srf} \\ v_{srf} \\ w_{srf} \end{bmatrix} = \begin{bmatrix} 0 & 0 & c/2 \\ 0 & 0 & a \\ -c/2 & -a & 0 \end{bmatrix} \begin{bmatrix} \omega_x \\ \omega_y \\ \omega_z \end{bmatrix} + \begin{bmatrix} u \\ v \\ w \end{bmatrix} \quad (2.1)$$

Where  $u_{srf}$ ,  $v_{srf}$  and  $w_{srf}$  are the velocities of point at which strut connects to chassis, expressed in coordinate frame 1.

**Instantaneous Radius of Tire** A tire rolling on the surface, undergoes deformation due to self weight of vehicle and dynamics load transfer of during cornering. Because of this compression of tire, the free rolling radius of tire reduces to instantaneous radius which is given by,

$$R_{rf} = R_0 - \frac{x_{trf}}{\cos \theta \cos \phi} \quad (2.2)$$

where  $R_{rf}$  is the instantaneous radius of tire,  $R_0$  is free rolling radius of tire and  $x_{trf}$  is instantaneous deformation of the tire. Note that  $x_{trf}$  is measured in coordinate frame 2, whereas  $R_{rf}$  is required in frame 1, hence we have expressed  $x_{trf}$  in coordinate frame 1 first and then subtracted it from free rolling radius to obtain instantaneous radius  $R_{rf}$ .

**Instantaneous Strut Length** As can be seen from figure 2.2, instantaneous strut length,  $l_{srf}$ , is the distance between wheel center and upper strut point. It is given by,

$$l_{srf} = l_{sif} - x_{srf} + x_{sif} \quad (2.3)$$

where  $x_{sif}$  is initial compression in right-front corner suspension spring on account of its contribution to balance the weight of chassis. Whereas  $l_{sif}$  is the initial length of strut, given by  $l_{sif} = h - R_0 + x_{tiff}$ . Where  $h$  is the height of CG from the ground and  $x_{tiff}$  is the initial compression in right front tire.

**Velocities Of Unsprung Mass** The velocity of unsprung mass i.e. wheel at right front corner, can be defined using three components, which are

$$u_{urf} = u_{srf} - l_{srf}\omega_y \quad (2.4)$$

$$v_{urf} = v_{srf} + l_{srf}\omega_x \quad (2.5)$$

Note that the third component of velocity i.e.  $w_{urf}$  has been discussed later. All three components of velocities are expressed in reference frame 1.

The vertical force arising due to compression of tire spring can be modeled as,

$$F_{zgrf} = F_{ztrf} = x_{trf}k_t \quad (2.6)$$

In equation 2.6,  $k_t$  is the vertical stiffness of tire. The vertical force  $F_{zgrf}$  calculated above is expressed in frame 2.

**Tire and Suspension Compression** The rate at which the deflection of tire varies is given by,

$$\dot{x}_{trf} = -\cos\theta(w_{urf}\cos\phi + v_{urf}\sin\phi) + u_{urf}\sin\theta \quad (2.7)$$

integrating above equation would yield the deflection of tire in coordinate reference frame 2. If this compression becomes equal to zero, the normal force on tire,  $F_{zgrf}$ , becomes zero i.e the wheel lifts off from the ground. The continuous information regarding compression of tire proves to be useful to avoid the impending rollover by providing active rollover avoidance system.

The rate of change of instantaneous deflection of suspension at right front corner is difference between the velocities of wheel and upper strut point,

$$\dot{x}_{srf} = -w_{srf} + w_{urf} \quad (2.8)$$

The deflection of suspension spring after integrating above equation is expressed in coordinate frame 1.

The vertical force transmitted to chassis through strut because of compression of suspension spring is given by

$$F_{zsrf} = x_{srf}k_{sf} + b_{sf}\dot{x}_{srf} \quad (2.9)$$

Where  $k_{sf}$  is the stiffness of suspension spring and  $b_{sf}$  is the damping coefficient. Note that  $F_{zsrf}$  is calculated in body coordinate frame

**Velocities at Tire Ground Contact Patch** We have assumed that the vehicle is traveling on a smooth road, hence the vertical component of velocity of tire-ground contact patch becomes zero. Longitudinal and lateral velocities are given by,

$$u_{grf} = \cos \theta (u_{urf} - \omega_y R_{rf}) + \sin \theta (w_{urf} \cos \phi + \sin \phi (\omega_x R_{rf} + v_{urf})) \quad (2.10)$$

$$v_{grf} = \cos \phi (v_{urf} + \omega_x R_{rf}) - w_{urf} \sin \phi \cos \phi \quad (2.11)$$

The longitudinal and lateral velocities calculated above decides the slip present between the tire and ground. Based on the slip, using Magic Formula, we have calculated the tire forces.

**Tire Slip Angle and Slip Ratio** Longitudinal slip ratio is generally denoted by  $\kappa$  and is denoted as the ratio of longitudinal slip velocity and forward speed of wheel center. As can be seen from figure 1.6, slip ratio is the independent variable to calculate the longitudinal force. Mathematical formulation for the slip ratio can be written as,

$$\kappa_{rf} = \frac{(R_{rf} \omega_{rf} - (u_{grf} \cos \delta + v_{grf} \sin \delta))}{|u_{grf} \cos \delta + v_{grf} \sin \delta|} \quad (2.12)$$

Where  $\omega_{rf}$  is the angular velocity of a wheel, and  $\delta$  is the steering angle at wheel. The lateral slip is the ratio of lateral velocity of contact center and longitudinal running speed of wheel [6]. From figure 1.6, we can see that, in Magic Formula, slip angle is the independent parameter to calculate lateral force generated. In terms of slip angle  $\alpha$ ,

$$\tan \alpha = \frac{(v_{grf} \cos \delta - u_{grf} \sin \delta)}{(u_{grf} \cos \delta + v_{grf} \sin \delta)} \quad (2.13)$$

The Magic Formula based tire model has been discussed in subsequent section. Based on this tire model, with slip ratio and slip angle as independent parameters, longitudinal and lateral tire forces are calculated which are denoted as  $F_{xtrf}$  and  $F_{ytrf}$  respectively.

**Wheel Dynamics** In order to calculate the longitudinal slip ratio as shown in equation 2.12, we require the angular velocity of wheel. In order to calculate that, we need to consider the moment equilibrium equation of wheel about its center of rotation. Figure 2.3 shows the force and moment acting on wheel about its center of rotation. The moment equilibrium about center of rotation can be written as,

$$J \frac{d\omega}{dt} = T - F_{xtrf} R_{rf} \quad (2.14)$$

where  $J$  is the mass moment of inertia of wheel assembly, and  $T$  is the external torque applied to the wheel and  $\omega$  is the angular velocity of the wheel. Note that while understanding the dynamics of

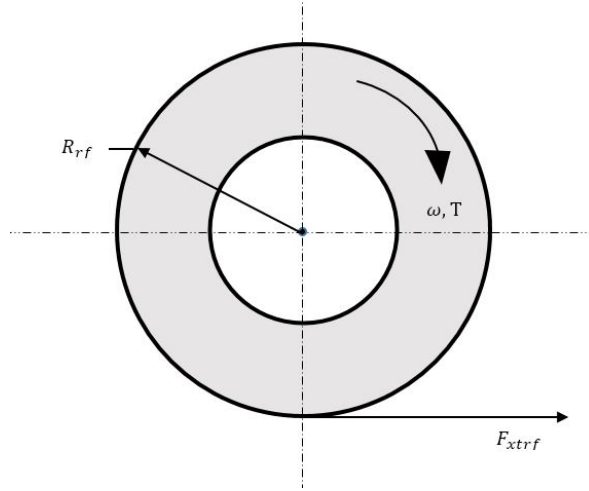


Figure 2.3: Schematic of wheel

wheel, we have neglected the effect of pneumatic trail. The consideration of  $T$  is based on the wheels which are powered by drive-line. Since we are discussing a model which is rear wheel driven, the term signifying the external torque applied should not be considered for right-front corner analysis. Hence equation 2.14 is modified to

$$J \frac{d\omega}{dt} = -F_{xtrf} R_{rf} \quad (2.15)$$

and while writing the equation for rear tires, the term  $T$  shall be considered.

**Forces at Tire Ground Contact Patch** The tire forces calculated using the Magic Formula  $F_{xtrf}$  and  $F_{ytrf}$  are in longitudinal and lateral direction of steered wheel as shown in the figure 2.4. The components of these forces along the longitudinal and lateral direction of coordinate frame 2 are denoted by  $F_{xgrf}$  and  $F_{ygrf}$  respectively and can be written as,

$$F_{xgrf} = F_{xtrf} \cos \delta - F_{ytrf} \sin \delta \quad (2.16)$$

$$F_{ygrf} = F_{ytrf} \cos \delta + F_{xtrf} \sin \delta \quad (2.17)$$

From equation 2.6, we have calculated the value of  $F_{zgrf}$ .

All the three components of forces mentioned above are expressed in coordinate frame 2, since these forces are transferred to chassis via strut, we need to express them in coordinate frame 1.

$$\begin{bmatrix} F_{xgsrf} \\ F_{ygsrf} \\ F_{zgsrf} \end{bmatrix}_{frame1} = \begin{bmatrix} 1 & 0 & 0 \\ 0 & \cos \phi & \sin \phi \\ 0 & -\sin \phi & \cos \phi \end{bmatrix} \begin{bmatrix} \cos \theta & 0 & -\sin \theta \\ 0 & 1 & 0 \\ \sin \theta & 0 & \cos \theta \end{bmatrix} \begin{bmatrix} F_{xgrf} \\ F_{ygrf} \\ F_{zgrf} \end{bmatrix}_{frame2} \quad (2.18)$$

The rotation matrix in the equation above follows YX convention while transforming from frame 2 to frame 1.

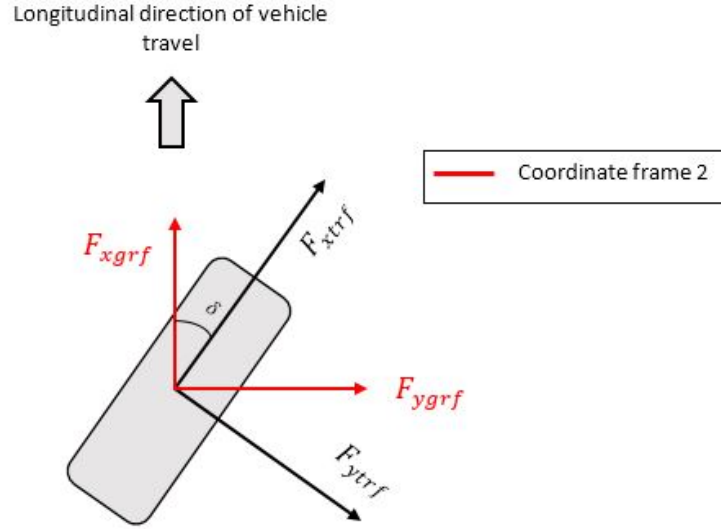


Figure 2.4: Plan of steered wheel

**Forces at Upper Strut Point** The component forces which is calculated from equation 2.18, with the effect of gyroscopic action and self weight of unsprung mass i.e. wheel, gets transferred to the sprung mass through strut. The figure 2.5 helps to better visualize the directions of various forces and velocities. The forces at upper strut point where the strut is attached to the chassis can be written as,

$$F_{xsrf} = F_{xgsrf} + m_u g \sin \theta + m_u \omega_z v_{urf} - m_u \omega_y w_{urf} \quad (2.19)$$

$$F_{ysrf} = F_{ygsrf} - m_u g \sin \phi \cos \theta + m_u \omega_x w_{urf} - m_u \omega_z u_{urf} \quad (2.20)$$

The vertical component of force at upper strut point has already been calculated from equation 2.9. Hence all the three component forces at chassis are obtained.

**Dynamic Load Transfer** As we have assumed that the vehicle is traveling on the smooth road, hence the pitching motion of chassis can be neglected. Therefore chassis and all the wheel can be assumed to make same motion along x-direction. By taking moment about CG and force equilibrium in z-direction, the dynamics force transfer due to longitudinal acceleration or deceleration can be understood from figure 2.6, equation 2.21 and 2.22

$$F_{frf} = F_{flf} = \frac{1}{2l} (mgb - h (F_{xgsrf} + F_{xgslf} + F_{xgsrb} + F_{xgslb})) \quad (2.21)$$

$$F_{brb} = F_{blb} = \frac{1}{2l} (mga + h (F_{xgsrf} + F_{xgslf} + F_{xgsrb} + F_{xgslb})) \quad (2.22)$$



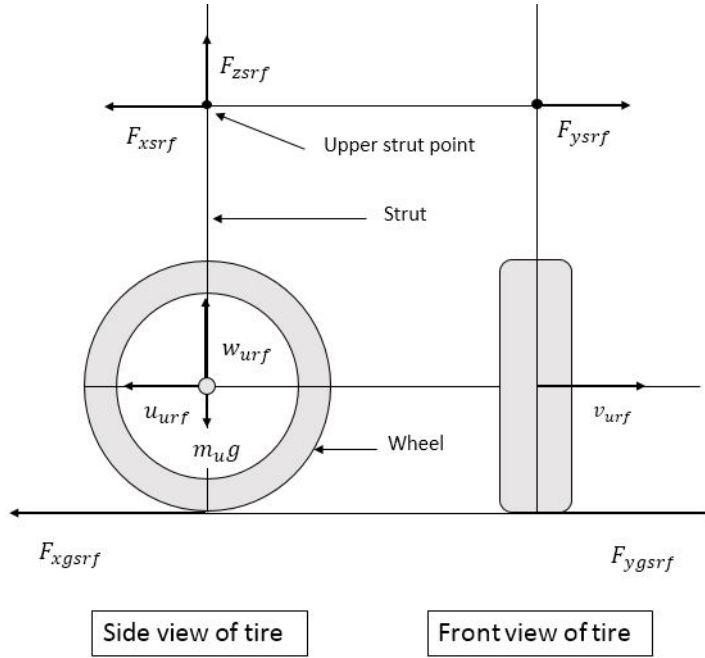


Figure 2.5: Schematic showing various velocities and forces at right-front corner

Where  $F_{fij}$  and  $F_{bij}$  are the forces generated due to load transfer because of accelerating or braking. Also, the effect of roll motion on load transfer is considered. Figure 2.7 shows the front view of vehicle model where  $R$  denotes the front roll centre. In the absence of roll centre, the roll moment transferred to the sprung mass at right-front corner is,

$$M_{xrf} = F_{ygsrf}R_{rf} + F_{ysrf}l_{srf} \quad (2.23)$$

and when roll centre is present, the roll moment transferred to the sprung mass is,

$$M_{xrf} = F_{ysrf}H_{rcf} \quad (2.24)$$

Hence when roll centre is considered, the roll moment transferred to sprung mass by front suspension is reduced, the difference between above two roll moment produces jacking forces i.e. lateral force transfer, which is given by,

$$F_{dzrf} = -F_{dzlf} = \frac{(F_{ygsrf}R_{rf} + F_{ysrf}l_{srf} + F_{ygsrf}R_{lf} + F_{ysrf}l_{srf} - (F_{ysrf} + F_{ysrf})H_{rcf})}{c} \quad (2.25)$$

Since while cornering, the roll centres acquire the position which is offset to the ground plane, the moment transferred to chassis around x-axis should be taken as proposed in equation 2.24 and that around y axis is given by,

$$M_{yrf} = -(F_{xgsrf}R_{rf} + F_{xsrfl_{srf}}) \quad (2.26)$$

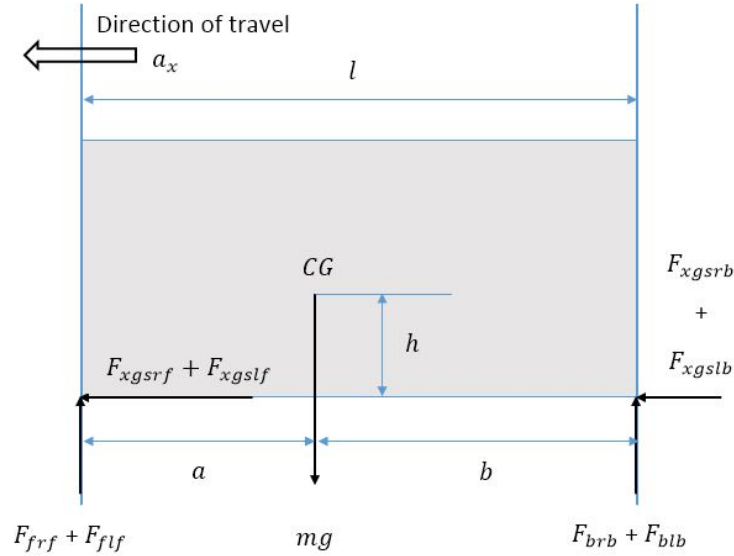


Figure 2.6: Longitudinal motion

**Equations of Motion for Chassis** The motion of sprung mass of vehicle model can be described by six equations. Out of which three are for rotational degrees of freedom and three are for translational. The rotational equations of motion is given by,

$$J_x \dot{\omega}_x = \sum M_{xij} + (F_{zslf} + F_{zslb} - F_{zsr_f} - F_{zsr_b}) \frac{c}{2} \quad (2.27)$$

$$J_y \dot{\omega}_y = \sum M_{yij} + (F_{zslb} + F_{zsr_b}) b - (F_{zslf} + F_{zsr_f}) a \quad (2.28)$$

$$J_z \dot{\omega}_z = (F_{yslf} + F_{ysrf}) a - (F_{ysl_b} + F_{ysr_b}) b + (-F_{xslf} + F_{xsr_f} - F_{xsl_b} + F_{xsr_b}) \frac{c}{2} \quad (2.29)$$

and the translational equations of motions are given by,

$$m (\dot{u} + \omega_y w - \omega_z v) = \sum F_{xsi_j} + mg \sin \theta \quad (2.30)$$

$$m (\dot{v} + \omega_z u - \omega_x w) = \sum F_{ysi_j} - mg \sin \phi \cos \theta \quad (2.31)$$

$$m (\dot{w} + \omega_x v - \omega_y u) = \sum (F_{zsi_j} + F_{dzi_j}) - mg \cos \phi \cos \theta \quad (2.32)$$

where  $m$  is sprung mass and  $ij$  represents right-front ( $rf$ ), left-front ( $lf$ ), right-back ( $rb$ ) and left-back ( $lb$ ). Detailed steps of equations of motions are given in [19].

**Equations for Cardan Angles** This paragraph focuses on the detail procedure by which the equations of Cardan angles obtained. Details of cardan angles from standpoint of biomechanics has been explained by [20] and the concept of rotation matrix, disadvantages of using Cardan angle i.e.

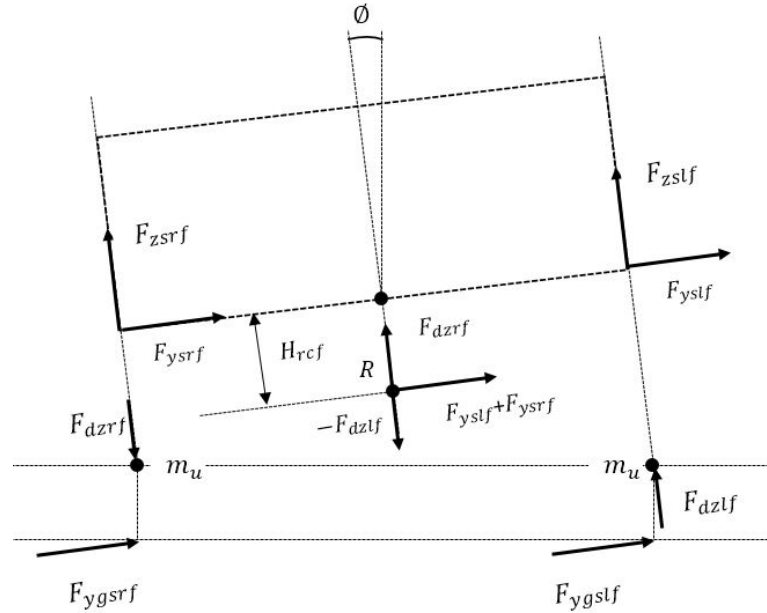


Figure 2.7: Front view of vehicle model

gimbal lock, Euler's parameters, kinematics and dynamics of rigid body in 3D space has been worked out in the work of [21]. As in this particular study, we have applied the concept of Cardan angle to vehicle dynamics, and vehicle can never pitch or roll to the angle  $\frac{\pi}{2}$ , it is safe to use the Cardan angles without facing the consequence of gimbal lock. If at all vehicle pitch or roll to the angle  $\frac{\pi}{2}$ , it is already very late to apply any control measures. Figure 2.8 represents different coordinate axes system obtained on successively rotating inertial reference frame  $XYZ$  by Cardan angles, to finally obtain coordinate axes  $xyz$  whereas, figure 2.9 depicts the sequence in which inertial frame is rotated to obtain body reference frame. Before continuing the derivation, we need to understand the meaning of some symbolic representations.  ${}^A R_B$  is the rotation matrix which transforms any vector expressed in frame B to a representation in frame A whereas  ${}^A \omega_{AB}$  is the representation of angular velocity, in which **A** is the frame of reference in which vector is defined, *A* is the frame at which rate of change is calculated and *B* is the frame of interest. Mathematically, Cardan angles are given as [21],

$${}^A \vec{\omega}_{AB'} = \begin{bmatrix} 0 \\ 0 \\ \dot{\psi} \end{bmatrix} \quad {}^{B'} \vec{\omega}_{B'B''} = \begin{bmatrix} 0 \\ \dot{\theta} \\ 0 \end{bmatrix} \quad {}^{B''} \vec{\omega}_{B''B} = \begin{bmatrix} \dot{\phi} \\ 0 \\ 0 \end{bmatrix}$$

$${}^A \vec{\omega}_{AB} = {}^A \vec{\omega}_{AB'} + {}^A R_{B'} \cdot {}^{B'} \vec{\omega}_{B'B''} + {}^A R_{B''} \cdot {}^{B''} \vec{\omega}_{B''B}$$

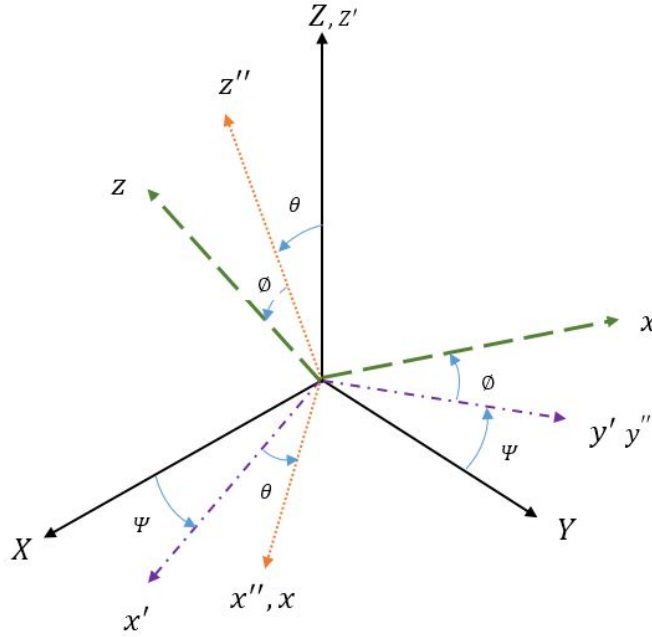


Figure 2.8: Coordinate axes system on rotating by Cardan angles

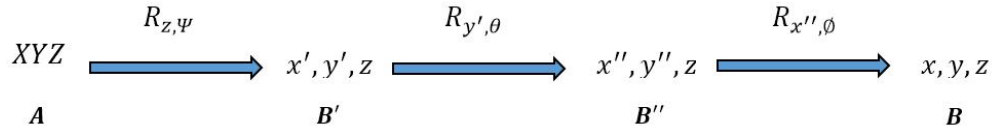


Figure 2.9: Sequence of rotation of inertial frame

$${}^A\vec{\omega}_{AB} = \begin{Bmatrix} 0 \\ 0 \\ \dot{\psi} \end{Bmatrix} + R_{Z,\psi} \begin{Bmatrix} 0 \\ \dot{\theta} \\ 0 \end{Bmatrix} + R_{Z,\psi} R_{y',\theta} \begin{Bmatrix} \dot{\phi} \\ 0 \\ 0 \end{Bmatrix}$$

$${}^A\vec{\omega}_{AB} = {}^A R_B \cdot {}^B\vec{\omega}_{AB}$$

where  ${}^A R_B = R_{Z,\psi} R_{y',\theta} R_{x'',\phi}$

Angular velocity vector  ${}^B\vec{\omega}$  is available in body frame. Let  $\dot{\phi}, \dot{\theta}$  and  $\dot{\psi}$  be the Cardan angle rates in ZYX system. Then

$${}^B\vec{\omega} = \begin{bmatrix} \dot{\phi} \\ 0 \\ 0 \end{bmatrix} + R_{x'',\phi}^{-1} \begin{bmatrix} 0 \\ \dot{\theta} \\ 0 \end{bmatrix} + R_{x'',\phi}^{-1} R_{y',\theta}^{-1} \begin{bmatrix} 0 \\ 0 \\ \dot{\psi} \end{bmatrix}$$

$${}^B\vec{\omega} = \begin{bmatrix} \dot{\phi} \\ 0 \\ 0 \end{bmatrix} + \begin{bmatrix} 1 & 0 & 0 \\ 0 & \cos \phi & \sin \phi \\ 0 & -\sin \phi & \cos \phi \end{bmatrix} \begin{bmatrix} 0 \\ \dot{\theta} \\ 0 \end{bmatrix} + \begin{bmatrix} \cos \theta & 0 & -\sin \theta \\ \sin \theta \sin \phi & \cos \phi & \sin \phi \cos \theta \\ \cos \phi \sin \theta & -\sin \phi & \cos \theta \cos \phi \end{bmatrix} \begin{bmatrix} 0 \\ 0 \\ \dot{\psi} \end{bmatrix}$$

Solving above matrix equation gives,

$${}^B\vec{\omega} = \begin{bmatrix} 1 & 0 & -\sin \theta \\ 0 & \cos \phi & \sin \phi \cos \theta \\ 0 & -\sin \phi & \cos \phi \cos \theta \end{bmatrix} \begin{bmatrix} \dot{\phi} \\ \dot{\theta} \\ \dot{\psi} \end{bmatrix}$$

${}^B\vec{\omega}$  is angular velocity vector expressed in body coordinate form, therefore

$${}^B\vec{\omega} = \begin{bmatrix} \omega_x \\ \omega_y \\ \omega_z \end{bmatrix}$$

$$\begin{bmatrix} \dot{\phi} \\ \dot{\theta} \\ \dot{\psi} \end{bmatrix} = \begin{bmatrix} 1 & \sin \phi \tan \theta & \cos \phi \tan \theta \\ 0 & \cos \phi & -\sin \phi \\ 0 & \frac{\sin \phi}{\cos \theta} & \frac{\cos \phi}{\cos \theta} \end{bmatrix} \begin{bmatrix} \omega_x \\ \omega_y \\ \omega_z \end{bmatrix}$$

Simplifying above equation we get,

$$\dot{\theta} = \omega_y \cos \phi - \omega_z \sin \phi \quad (2.33)$$

$$\dot{\psi} = \omega_y \frac{\sin \phi}{\cos \theta} + \omega_z \frac{\cos \phi}{\cos \theta} \quad (2.34)$$

$$\dot{\phi} = \omega_x + \omega_y \sin \theta \tan \theta + \omega_z \cos \phi \tan \theta \quad (2.35)$$

Cardan angles needed for simulation are obtained by integrating equations 2.33, 2.34 and 2.35.

**Vertical Velocity of Unsprung Mass** The translational degree of freedom of unsprung mass is mathematically modeled by equation 2.37. Its rate of change is defined as,

$$\begin{aligned} m_u \dot{w}_{urf} &= \cos \phi (\cos \theta (F_{zgrf} - m_u g) + F_{xgrf} \sin \theta) - F_{ygrf} \sin \phi - F_{dzrf} \\ &\quad - x_{srf} \cdot k_{sf} - \dot{x}_{srf} \cdot b_{sf} - m_u (v_{urf} \cdot \omega_x - u_{urf} \cdot \omega_y) \end{aligned} \quad (2.36)$$

where  $k_{sf}$  is front suspension spring stiffness,  $b_{sf}$  is its damping coefficient,  $x_{srf}$  is its compression at particular instant and  $m_u$  is the mass of unsprung mass i.e wheel. As discussed above,  $F_{dzrf}$  is the dynamic load transfer on account of cornering.

**Vehicle Trajectory** As we have already seen above that the translational velocities of sprung mass  $u$ ,  $v$  and  $w$  are in body coordinate frame. If we need to capture the trajectory traced by the vehicle, we must represent these velocity in inertial frame of reference which can be written as,

$$\begin{bmatrix} U \\ V \\ W \end{bmatrix} = \begin{bmatrix} \cos \psi & -\sin \psi & 0 \\ \sin \psi & \cos \psi & 0 \\ 0 & 0 & 1 \end{bmatrix} \begin{bmatrix} \cos \theta & 0 & \sin \theta \\ 0 & 1 & 0 \\ -\sin \theta & 0 & \cos \theta \end{bmatrix} \begin{bmatrix} 1 & 0 & 0 \\ 0 & \cos \phi & -\sin \phi \\ 0 & \sin \phi & \cos \phi \end{bmatrix} \begin{bmatrix} u \\ v \\ w \end{bmatrix} \quad (2.37)$$

In the above matrix equation  $U$ ,  $V$  and  $W$  are the translational velocities of body expressed in inertial coordinate frame. After integrating, we can obtain the displacement of vehicle with respect to stationary observer.

## 2.3 Tire Model

### 2.3.1 Magic Formula

As already discussed above, the well-known Magic Formula tire model by Pacejka et al. [5] has been used to calculate the tire forces. Forces calculated using the Magic Formula fairly matches with the actual tire forces. The basic Equation is given by,

$$Y = D \sin(C \arctan(B\Phi)) \quad (2.38)$$

with

$$\Phi = (1 - E)X + \left(\frac{E}{B}\right) \arctan(BX) \quad (2.39)$$

In the above equation,  $B$  is the stiffness factor,  $C$  is the shape factor,  $D$  is the peak factor and  $E$  is the curvature factor. The same Magic Formula can give the value of longitudinal force  $F_{xtrf}$ , the lateral force  $F_{ytrf}$  and aligning moment  $M_z$  in place of  $Y$  if we respectively submit slip ratio  $\kappa$ , slip angle  $\alpha$  and slip angle  $\alpha$  in place of  $X$ . The above formulation is valid only when the tire is experiencing pure condition i.e. either cornering without braking or only braking without cornering.

Magic Formula also facilitates the calculation of longitudinal and lateral force simultaneously when the tire is experiencing combine slip condition i.e. braking accelerating while cornering. The vertical adjustment  $S_v$  to the value  $Y$  i.e.  $(Y + S_v)$  and the horizontal adjustment  $S_h$  to the value of  $X$  i.e.  $(X + S_h)$  is to account for ply steer, conicity and rolling resistance. With variable vertical load on tire, the values of  $B, C, D$  and  $E$  changes which can be written by table 2.1, while calculating the constants using table 2.1, the value of  $F_z$  shall be in  $kN$ .

### Combine Slip condition

As shown in figure 2.10,  $F_x$  and  $F_y$  are total force component in longitudinal and lateral direction respectively,  $\vec{V}$  is the speed in the direction of travel.  $\vec{V}_s$  is slip speed vector and  $\vec{V}_r$  is rolling speed vector. The theoretical longitudinal  $\sigma_x$  and lateral  $\sigma_y$  slip is given by,

$$\sigma_x = \frac{V_{sx}}{V_r} \quad (2.40)$$

$$\sigma_y = \frac{V_{sy}}{V_r} \quad (2.41)$$

Longitudinal force	Lateral force
$D = a_1 F_z^2 + a_2 F_z$	$D = a_1 F_z^2 + a_2 F_z$
$BCD = \frac{(a_3 F_z^2 + a_4 F_z)}{e^{a_5 F_z}}$	$BCD = a_3 \sin(a_4 \arctan(a_5 F_z))$
$C = 1.65$	$C = 1.3$
$E = a_6 F_z^2 + a_7 F_z + a_8$	$E = a_6 F_z^2 + a_7 F_z + a_8$

Table 2.1: Magic Formula constants [5]

	$a_1$	$a_2$	$a_3$	$a_4$	$a_5$	$a_6$	$a_7$	$a_8$	$a_9$	$a_{10}$	$a_{11}$	$a_{12}$	$a_{13}$
$F_y$	-22.1	1011	1078	1.82	0.208	0	-0.354	0.707	0.028	0	14.8	0.022	0
$F_x$	-21.3	1144	49.6	226	0.069	-0.006	0.056	0.486	0.015	-0.066	0.945	0.03	0.07

Table 2.2: Various constants in Magic Formula,  $F_z$  in  $kN$  [5]

$$\sigma = \sqrt{\sigma_x^2 + \sigma_y^2}$$

$\vec{\sigma}$  is oriented in the same direction as  $\vec{V}_s$

$$F_x = -\left(\frac{\sigma_x}{\sigma}\right) F_{x0}(\sigma) \quad (2.42)$$

$$F_y = -\left(\frac{\sigma_y}{\sigma}\right) F_{y0}(\sigma) \quad (2.43)$$

where  $F_{x0}(\sigma)$  and  $F_{y0}(\sigma)$  are the longitudinal and lateral forces for pure conditions respectively. Another way of representing theoretical slips are given by [5],

$$\sigma_x = \frac{V_r - V_x}{V_r} = 1 - \frac{V_x}{V_r} = 1 - \frac{1}{1 + \kappa} = \frac{\kappa}{1 + \kappa} \quad (2.44)$$

$$\sigma_y = \frac{V_{sy}}{V_r} = \frac{\frac{V_{sy}}{V_x}}{1 + \frac{V_r - V_x}{V_x}} = \frac{\tan \alpha}{1 + \kappa} \quad (2.45)$$

We have already seen from equation 2.12 and 2.13 that  $\kappa$  is the practical longitudinal slip and  $\alpha$  is the practical slip angle.

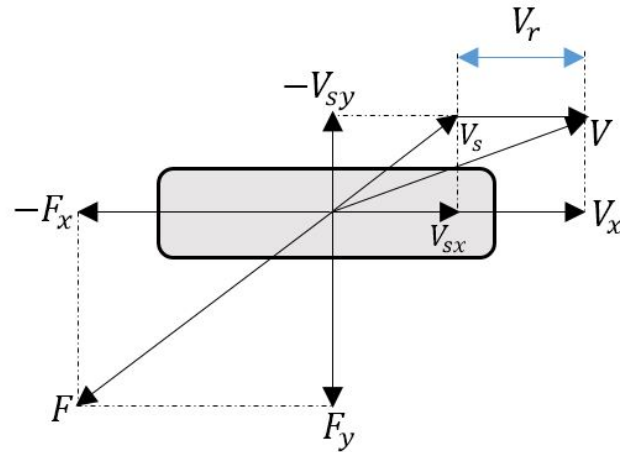


Figure 2.10: Plan view of tire during combine slip condition [5]

### 2.3.2 Tire Brush Model

#### Pure Side Slip

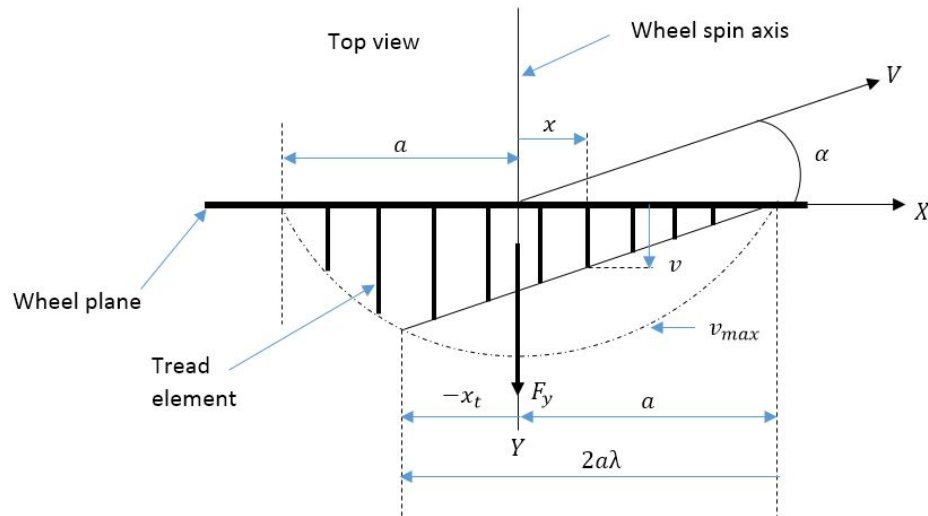


Figure 2.11: Brush model with constant slip angle [6]

In tire brush model, bristles stands for tread element of the tire. The tire brush model having constant slip angle has been shown in figure 2.11. The straight line runs parallel to the velocity vector  $V$  in adhesion region and continued by curved profile later in sliding region where available friction force is insufficient to hold the tips of bristles to the road surface. If  $\mu = \infty$  or  $\alpha = 0$ , the straight line continue till the end of contact patch. Lateral stretch of tread elements at any distance  $x$  as shown



in figure 2.11 is given by [6],

$$v = (a - x) \tan \alpha \quad (2.46)$$

if  $c_{py}$  is stiffness per unit length of a tread element, then lateral force produced by continuous tread elements throughout contact patch is,

$$F_y = c_{py} \int_{-a}^a v dx = 2c_{py} a^2 \alpha \quad (2.47)$$

and cornering stiffness as,

$$C_{F\alpha} = \left( \frac{\partial F_y}{\partial \alpha} \right)_{\alpha=0} = 2c_{py} a^2 \quad (2.48)$$

but while cornering on asphalt road,  $\mu \neq \infty$  and  $\alpha \neq 0$  hence above mathematical model is not of much use. Let force per unit length in contact patch varies with parabolic variation with zero values at beginning and end of contact patch. It is given by

$$q_z = \frac{3F_z}{4a} \left\{ 1 - \left( \frac{x}{a} \right)^2 \right\} \quad (2.49)$$

$F_z$  is vertical force on the tire. The maximum side force per unit length is given by,

$$|q_{y,max}| = \mu q_z = \frac{3}{4} \mu F_z \frac{a^2 - x^2}{a^3} \quad (2.50)$$

As can be seen from figure 2.11,  $x_t$  is the distance from center of contact patch from where the adhesion region ends and sliding region starts. It can lie either on left or right side of center of contact patch. At  $x = x_t$ , stretch of an element due to adhesion becomes equal to that because of sliding region. i.e. adhesion force per unit length is equal to sliding force per unit length. Mathematically,

$$c_{py} (a - x_t) \tan \alpha = \frac{3}{4} \mu F_z \frac{a^2 - x_t^2}{a^3}$$

simplifying above equation gives,

$$\frac{2a^2 c_{py}}{3\mu F_z} = \frac{a + x_t}{2a \tan \alpha}$$

A parameter  $\theta_y$  is defined as,

$$\theta_y = \frac{2a^2 c_{py}}{3\mu F_z}$$

therefore,

$$x_t = 2a\theta_y \tan \alpha - a \quad (2.51)$$

From equation 2.51, The angle  $\alpha_{sl}$  at which only sliding region exists and no tread element adheres to road surface at all, is give by substituting  $x_t = a$ ,

$$\tan \alpha_{sl} = \frac{1}{\theta_y} \quad (2.52)$$

Now with the knowledge of  $x_t$ , one can identify the sliding and adhesion region distinctively. Hence the total force  $F_y$  can be calculated by separate integration over adhesion region ( $x_t < x < a$ ) and sliding region ( $-a < x < x_t$ ).

If  $|\alpha| \leq \alpha_{sl}$ ,

$$F_y = 3\mu F_z \theta_y \sigma_y \left\{ 1 - |\theta_y \sigma_y| + \frac{1}{3} (\theta_y \sigma_y)^2 \right\} \quad (2.53)$$

where  $\sigma_y = \tan \alpha$ .

If  $\alpha_{sl} < \alpha < \frac{\pi}{2}$ ,

$$F_y = \mu F_z \operatorname{sgn}(\alpha) \quad (2.54)$$

### Pure Longitudinal Slip

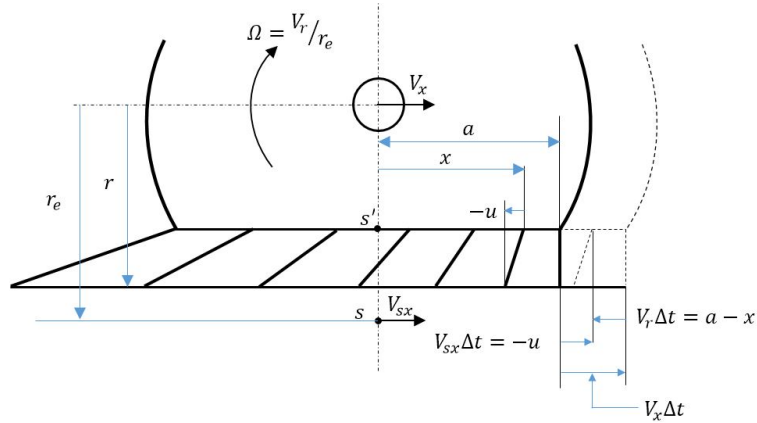


Figure 2.12: Braked Tire Brush model without sliding [6]

The tire brush model with flexible tread elements, the mechanism of generation of longitudinal force is similar to that of pure lateral slip. Figure 2.12 shows the side view of tire. Point  $S$  is the slip point at the radius of  $r_e$  from center of rotation and is assumed to be firmly attached to the rim.  $r_e$  is effective rolling radius. When wheel freely rolling on the road, the point  $s$  is assumed to have no relative velocity but for a braked wheel, point  $s$  gains longitudinal slip velocity  $V_{sx}$  in forward direction while, when driven, it gains it in backward direction. It can be seen from figure 2.12, point  $s'$  is attached to base line. Point  $s$  and  $s'$  have equal slip velocities during braking or accelerating. At free rolling  $s$  and  $s'$  both possess no slip velocity. Longitudinal slip velocity is given by,

$$V_{sx} = V_x - V_r \quad (2.55)$$

Consider an element which enters the contact patch, the tip of which is adhered to the ground and base is attached to carcass. In time  $\Delta t$ , base moves to rear by the distance of  $(a - x)$ , hence  $\Delta t = \frac{(a-x)}{V_r}$ .

During this time, tip of the element travels by

$$u = -V_{sx} \frac{(a-x)}{V_r} \quad (2.56)$$

The equation 2.56 can also be written as,

$$u = (a-x) \frac{(V_r - V_x)}{V_r} = (a-x) \left(1 - \frac{V_x}{V_r}\right) = (a-x) \left(1 - \frac{1}{1+\kappa}\right) = (a-x) \left(\frac{\kappa}{1+\kappa}\right) \quad (2.57)$$

From equation 2.44 and 2.57,

$$u = (a-x) \sigma_x \quad (2.58)$$

From the similar steps from equation 2.49 to 2.51,

$$\theta_x = \frac{(a+x_t)}{2a\sigma_x} \quad (2.59)$$

The condition of total sliding would occur when  $a = x_t$ ,

$$\theta_x = \frac{1}{\sigma_{x,sl}} = \frac{1}{\frac{\kappa_{sl}}{1+\kappa_{sl}}} \quad (2.60)$$

Therefore,

$$\kappa_{sl} = \frac{-1}{(1-\theta_x)} \quad (2.61)$$

where

$$\theta_x = \frac{2 c_{px} a^2}{3 \mu F_z}$$

### Combine Slip Condition

For the sake of mathematical simplicity, It is assumed that the tire has isotropic stiffness per unit length.

$$c_p = c_{px} = c_{py} \quad (2.62)$$

Note that the value of  $c_p$  has been assumed, since tire manufacturer generally do not reveal its value. The coefficient of friction of road is also considered as isotropic in nature.

$$\mu = \mu_x = \mu_y \quad (2.63)$$

The process of calculation of tire forces is similar to that described for pure conditions above. Deflection of element in adhesion region is given by,

$$e = \begin{pmatrix} u \\ v \end{pmatrix} \quad (2.64)$$

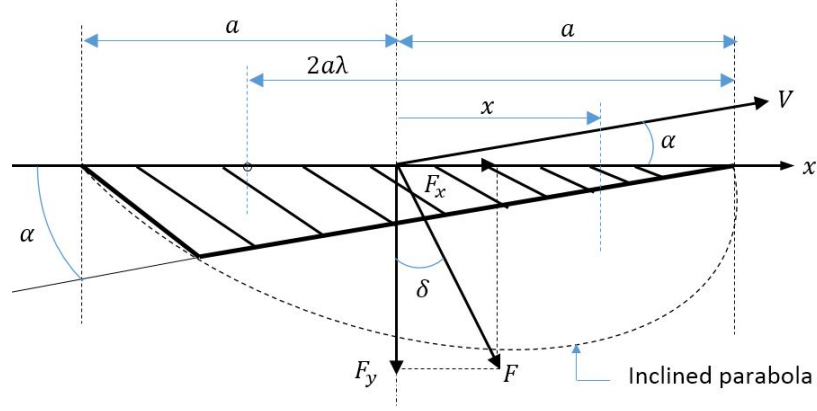


Figure 2.13: Plan view of contact patch when the tire has constant slip angle and is braked. [6]

Theoretical slip vector is given by,

$$\sigma = \begin{pmatrix} \sigma_x \\ \sigma_y \end{pmatrix} \quad (2.65)$$

in adhesive patch, the element deforms by,

$$e = (a - x) \sigma \quad (2.66)$$

the force per unit length of contact patch is

$$q = c_p (a - x) \sigma \quad (2.67)$$

where  $q$  is a vector written as  $\begin{pmatrix} q_x \\ q_y \end{pmatrix}$ . in sliding contact patch, The friction force per unit length is given by,

$$q_x = \frac{\sigma_x}{\sqrt{\sigma_x^2 + \sigma_y^2}} \mu q_z \quad (2.68)$$

$$q_y = \frac{\sigma_y}{\sqrt{\sigma_x^2 + \sigma_y^2}} \mu q_z \quad (2.69)$$

the distance from center of contact patch at which adhesion region ends and sliding region starts, can be found out by,

$$c_p (a - x_t) \sqrt{\sigma_x^2 + \sigma_y^2} = \frac{3}{4} \mu F_z \frac{a^2 - x_t^2}{a^3} \quad (2.70)$$

simplifying above equation gives,

$$x_t = \frac{4}{3} \frac{c_p a^3 \sqrt{\sigma_x^2 + \sigma_y^2}}{\mu F_z} - a \quad (2.71)$$

The parameter  $\theta$  is defined as,

$$\theta = \frac{2}{3} \frac{c_p a^2}{\mu F_z}$$

From equation 2.71, we can define the condition for  $\sigma$  when total sliding occur without adhesion by putting  $x_t=a$ ,

$$\sigma_{sl} = \frac{1}{\theta} \tag{2.72}$$

The parameter  $\lambda$  is defined as,

$$\lambda = 1 - \theta \sqrt{\sigma_x^2 + \sigma_y^2}$$

now magnitudes of tire forces is calculated by,

for  $\sigma \leq \sigma_{sl}$

$$F = \mu F_z (1 - \lambda^3) \tag{2.73}$$

for  $\sigma > \sigma_{sl}$

$$F = \mu F_z \tag{2.74}$$

the components of forces are given as,

$$F_x = F \frac{\sigma_x}{\sigma} \tag{2.75}$$

$$F_y = F \frac{\sigma_y}{\sigma} \tag{2.76}$$

## 2.4 Validation of 14 DOF Vehicle Model Using ADAMS/View and ADAMS/Car

### 2.4.1 Initial Condition Calculation for MATLAB Model Using Static ADAMS Model

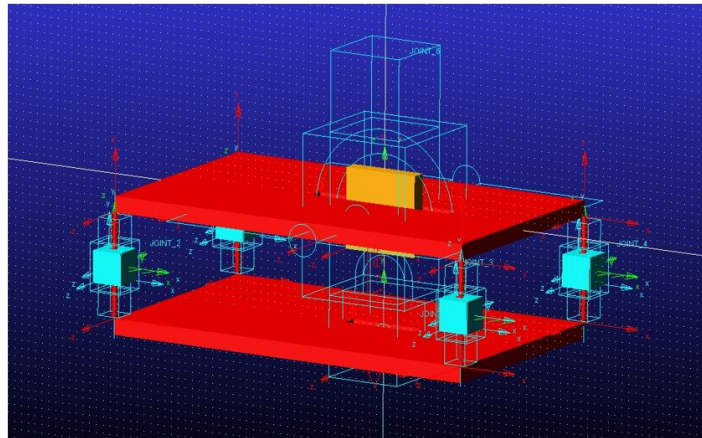


Figure 2.14: Static vehicle model in ADAMS/View

The 14 DOF vehicle model discussed above has been simulated using MATLAB script file as well as MATLAB/Simulink. The present model is complex and requires the solution for many differential

equations. The initial condition required for the solution of differential equations has been calculated by using ADAMS/View [15]. Model shown in 2.14 shows four masses having vertical translational degree of freedom and upper red cube represents body having three degrees of freedom. Shown assembly is allowed to deform under the force of gravity and the deformations of various springs are noted. These values are given to MATLAB model as the initial conditions for various differential equations. Various deformations of springs as well as the initial guess values for various differential equations has been noted in Appendix.

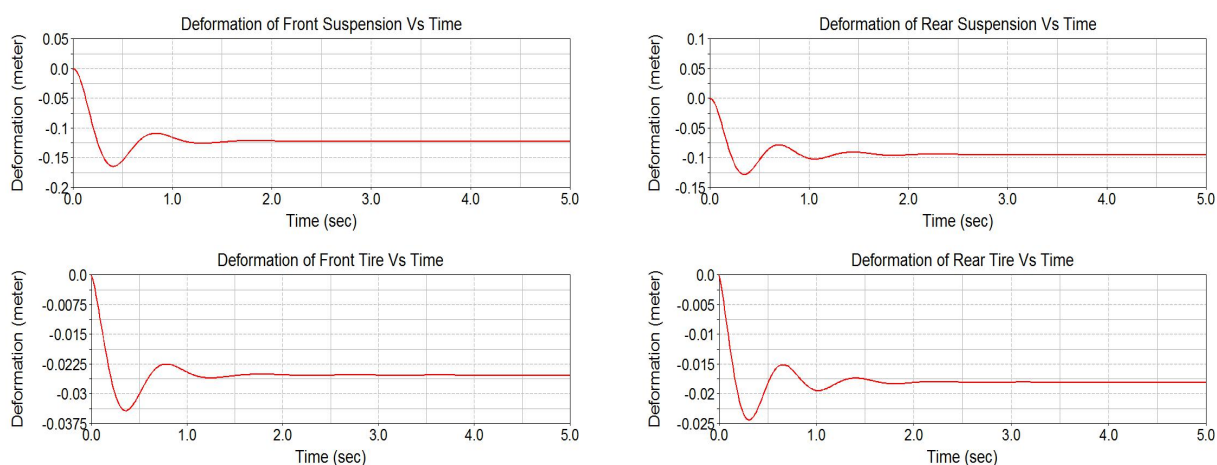


Figure 2.15: Compression of various springs in ADAMS for initial conditions

Figure 2.15 above shows the strip chart from post-processing environment of ADAMS/View. The titles of strip graph informs the spring for which the initial condition has been calculated.

### 2.4.2 Validation Using ADAMS/Car

The figures 2.16 shows the degree to which the results of vehicle model matches with the model prepared in ADAMS/Car. The parameters for which the MATLAB model been tested against the ADAMS model are,

- Vertical load on front tires.
- Vertical load on rear tires.
- Roll angle.

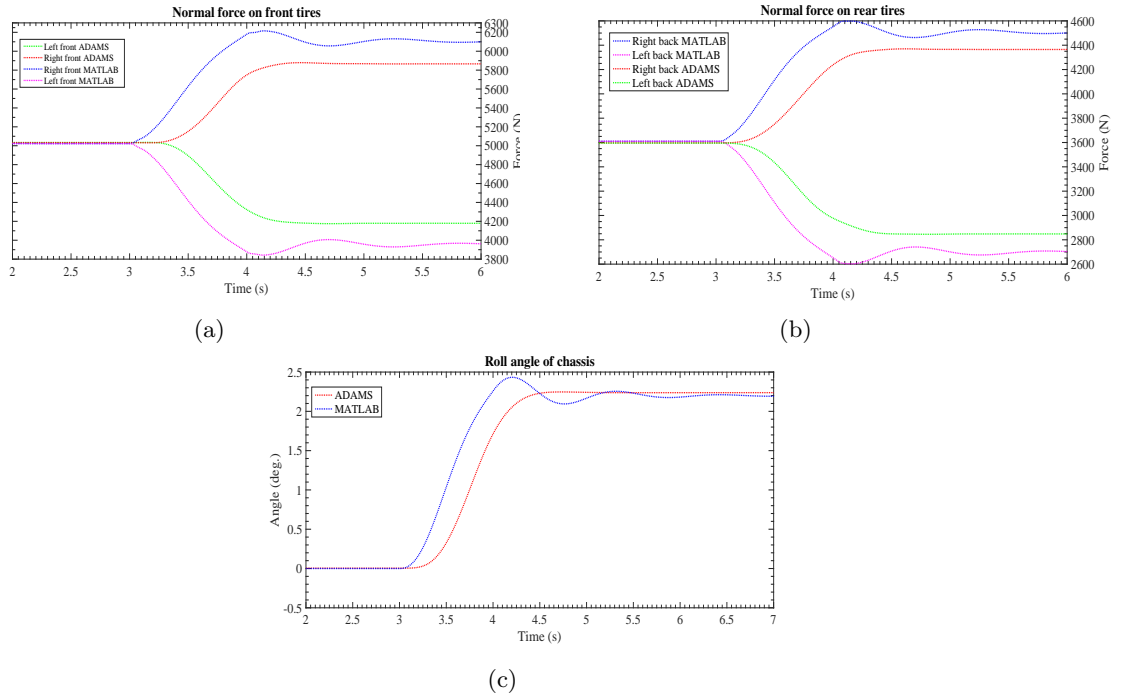


Figure 2.16: Validation of MATLAB model with ADAMS/Car Model

From the results obtained we can see that the MATLAB model well agrees with that of ADAMS model with minor difference of around  $150(N)$  to  $200(N)$  in the vertical load. From equation 2.6, we know that the vertical force on the tire,  $F_{ztrf}$ , is the function of vertical deformation of tire  $x_{trf}$ . Note that the stiffness of tires  $k_t$  we have assumed is  $200000 \frac{N}{m}$ . Hence the difference of  $200N$  is the error of  $1mm$  of tire deformation between ADAMS and MATLAB model. The reason for this difference has been discussed later in this section.

The nature of maneuverability given to the vehicle model which is initially running at  $54 \frac{km}{hr}$  is depicted in figure 2.17

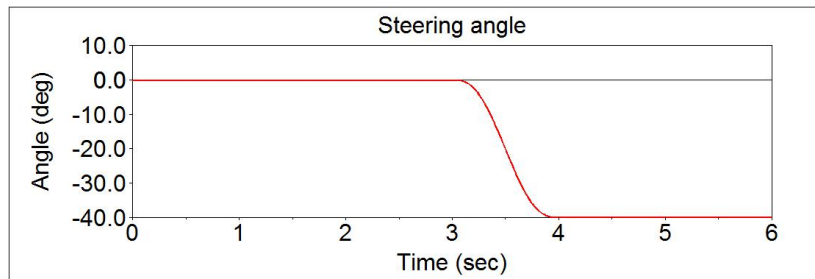
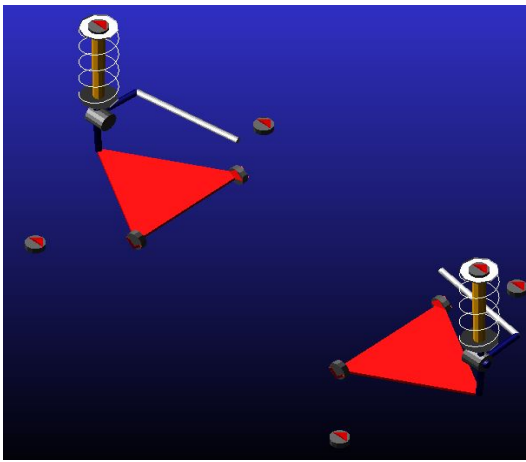
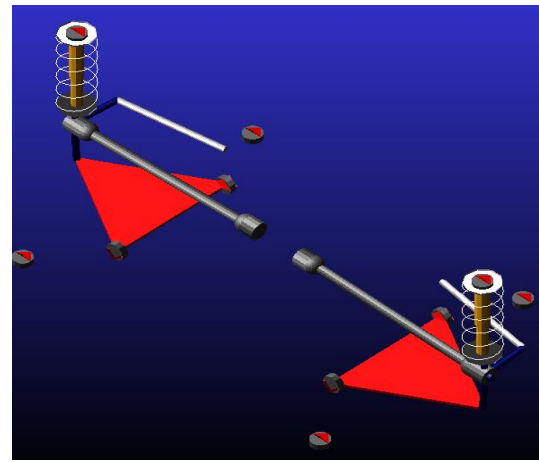


Figure 2.17: Steering angle given to vehicle model in ADAMS/Car

The overall steering ratio i.e. the ratio of steering wheel angle to that of ground wheel angle is maintained as 27.6. In ADAMS/Car, while preparing the vehicle model, the suspension plays an important role. We have modeled and prepared our own separate Mcpherson type suspension system without sourcing from available database of MSC ADAMS [15]. The figure 2.18a and 2.18b shows the same.



(a) Front suspension in ADAMS/Car



(b) Rear suspension in ADAMS/Car

Whereas the other vehicle systems such as steering, tires, chassis, driveline and brakes, has been imported from available database of MSC ADAMS/Car with appropriate modifications in order to align with the MATLAB vehicle model. From the results shown in figures 2.16, we observe a small error in vertical force on tires, the reason for this error can be accounted for following reasons,

1. As per the 14 DOF vehicle model described in the section of equivalent vehicle modeling, the wheel is constrained to have only rotational and translational degrees of freedom. Hence while calculating the vertical deformation of tire  $x_{trf}$ , we have not considered the effect which may arise if the wheel shows out of paper angular deflection around x axis i.e. we have not considered the effect of camber angle on normal deformation of tire. The tire Forces by the Magic formula [5] has an effect of camber influence. Since we have assume that wheel always keeps vertical with respect to ground, the influence of camber of camber angle is neglected while building the model in MATLAB as well as while calculating tire forces. While in the model of ADAMS/Car, during cornering, the tire has shown the camber angle shift of almost 4 degree as shown in figure 2.19.



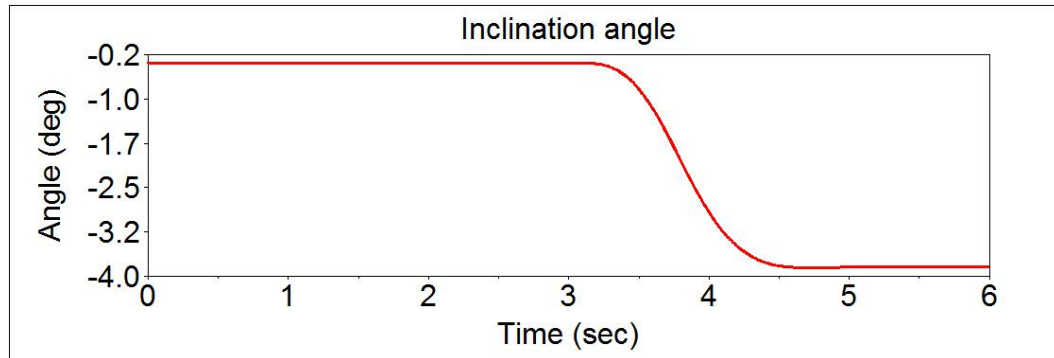


Figure 2.19: Inclination of wheel

On account of this, the compression of tire is influenced and so the vertical force on tire.

- From the figure 2.16, it may be observed that the nature of both the graphs vary from each other at the beginning of the cornering. The reason behind that is the tire model being used. As discussed above, MATLAB model uses Pac87 model [5] while ADAMS/Car uses the Pac89 tire model. Various coefficients as shown in table 2.2 are different for both the tire model. Therefore the resultant roll motion of chassis varies in ADAMS/Car from that of MATLAB.

On the similar lines, from figure 2.16a and 2.16b, one may conclude the delay in the response for the ADAMS/Car model based on its sluggish behavior to respond the steering angle. It appears that the ADAMS model has started cornering after 3.3 sec even when the input of steering started on the 3<sup>rd</sup> sec exactly. From figure 2.20, it can be seen that the ADAMS/Car model reacted to the steering almost instantly, but because of same reason discussed above, the nature of response did not match with that of MATLAB model.

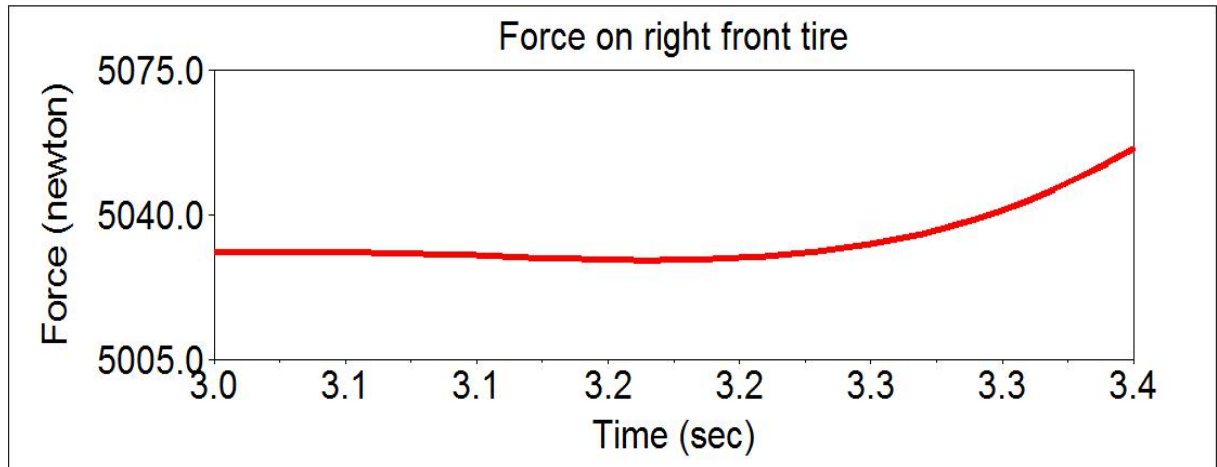


Figure 2.20: Reaction time for ADAMS/Car model to the steering input

## 2.5 Summary

This chapter has dealt with non-linear mathematical 14 DOF vehicle model. The non-linear equation for right-front corner (*rf*) of the vehicle model has been explained in detail. Similarly, the equations for other three remaining corners could be formulated. The Magic Formula tire model and Tire brush model, which are used to calculate the tire forces, are also explained in detail. Note that, for the validation purpose of 14 DOF non linear vehicle model, we have used the Magic formula tire model since ADAMS/Car does not offer Tire Brush model in its shared database. However the control strategies for yaw rate and side slip angle need the tire model which express the tire forces which are function of friction coefficient of road,  $\mu$ . Hence in MATLAB/Simulink environment where we have established the control structure, Tire Brush model has been used to calculate tire forces. The mathematical model simulated in MATLAB environment has been validated by ADAMS/Car. The result shows that both the models shows the similar characteristics on an acceptable level.

## Chapter 3

# Control of Yaw Rate and Side-Slip by SMC Based DYC and AFS

### 3.1 Introduction

This chapter focuses on the application of simultaneous control of yaw rate and side slip angle using differential braking and active steering. Hence for DYC and AFS, yaw rate and side slip errors work as control variables. The linear normalized novel switching function of errors between the actual and desired values of yaw rate and slip angle is fed to control system. The sliding model control based DYC and AFS try to converge these error values to minimum. In control system design, we have used non-linear vehicle model to make the model more accurate. Vehicle model often face many uncertainties such as variable mass of passengers, external aerodynamic force, variable adhesion condition of road. As sliding mode controller provides robust control over such variable quantities, it is vastly used in the automotive industries.

The sole function of any SMC is to close the state of the non-linear function to control surface  $s = 0$ , and then try to maintain it. During cornering at high speed, the magnitude of lateral acceleration produced is also high, as a result of which vehicle shows high roll angle shift and hence dynamic load transfer. Because of which it is not safe to use linearized vehicle and tire model. The Tire Brush model incorporated in this study is non-linear in nature. In this chapter, the complete nonlinear vehicle model derived in Chapter 2 is used to derive sliding mode DYC and AFS method. As in contrast to that of DYC technique, where the switching function try to converge the yaw rate error as well as side slip error to zero simultaneously, the switching function for AFS try to improve steerability control by minimizing the yaw rate error alone. In other words, AFS controller in this study, try to track reference yaw rate only. The functional nature of AFS in this study is driver assisting system by which it provides the correction to the demanded steering angle by the driver so that the

vehicle can track the desired yaw rate. On account of uncertain nature of vehicle model stated above, the SMC based AFS technique has been used to provide robustness warranted by the stability. The switching function used for the AFS is the linear function of yaw rate error.

### 3.2 Necessity to Control Yaw Rate and Side slip Angle

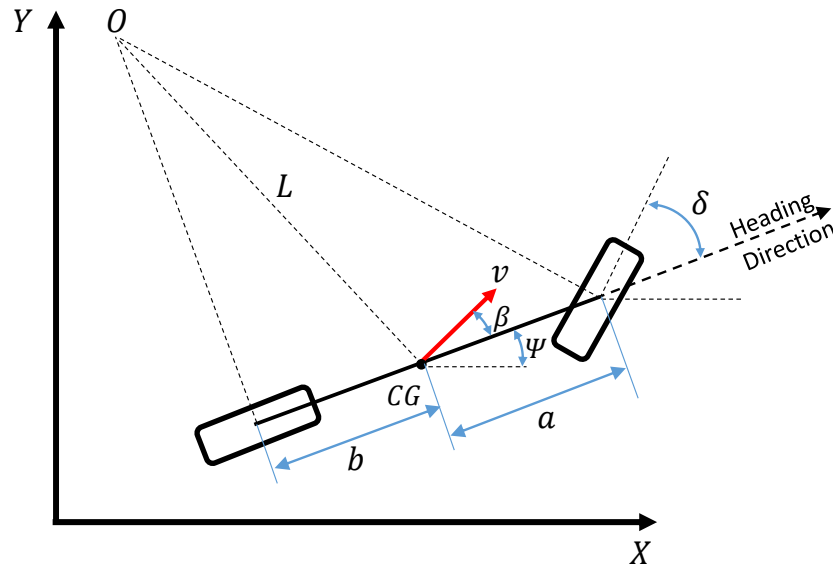


Figure 3.1: Bicycle model

Figure 3.1 shows the bicycle model of 2 DOF. Based on the vehicle longitudinal velocity and steering angle, the reference yaw rate can be calculated. The detailed expression for the desired yaw rate based on the bicycle model is given by [22, 23].

$$\omega_{z,desired} = \frac{v_x \delta}{(a+b)(1+Kv_x^2)} \quad (3.1)$$

where  $K$  is stability factor,

$$K = \frac{m}{(a+b)^2} \left( \frac{b}{C_{\alpha f}} - \frac{a}{C_{\alpha b}} \right) \quad (3.2)$$

where  $C_{\alpha}$  is the cornering stiffness of the tire. The turning radius of vehicle  $L$  is given as,

$$L = \frac{v}{\omega_z} \quad (3.3)$$

since  $v \sim v_x$  as  $v_y \sim 0$ ,

$$L = \frac{v_x}{\omega_z} \quad (3.4)$$

From equation 3.1, turning radius can be written as,

$$L = \frac{(a+b)(1+Kv_x^2)}{\delta} \quad (3.5)$$

Based on the positive, negative and zero value of stability factor  $K$ , the vehicle is said to have *understeer*, *oversteer* and *neutralsteer* characteristic respectively. The vehicle having *oversteer* characteristic is considered to be risky to drive, as when the velocity  $v_x$  reaches to the critical value [22], vehicle spins about itself. The *neutralsteer* characteristic is the ideal one in which turning radius becomes independent of longitudinal speed of vehicle, and hence this condition is most ideal to calculate the desired yaw rate of the vehicle. But since the cornering stiffness of tires  $C_\alpha$ , continuously changes while cornering, it is practically impossible for driver to keep  $K = 0$  throughout the cornering. Hence we need the assistance of the of active systems such as DYC and AFS etc. Based on  $K = 0$ , we write,

$$L = \frac{(a+b)}{\delta} \quad (3.6)$$

Hence from equation 3.1, desired yaw rate is given by

$$\omega_{z,desired} = \frac{v_x \delta}{(a+b)} \quad (3.7)$$

The side slip angle is the angle between the direction in which vehicle is heading and the direction of resultant velocity  $v$  of the CG. The necessity of controlling the side slip angle to desired value is for the reason mentioned below.

With excessive side slip angle, on account of non linear behavior of tires, the cornering stiffness decreases and hence yaw moment generated by tire lateral forces i.e. from equation 2.29,

$\{(F_{y_{slf}} + F_{y_{srf}})a - (F_{y_{slb}} + F_{y_{srb}})b\}$ , also decrease such that even excessive steering input by driver does not help in maintaining the stability. Secondly, an unskilled driver assumes that the heading direction of the vehicle is the direction in which the vehicle is proceeding, which is poor and misleading judgment which makes him/her to excessively or insufficiently turn the steering wheel. A small side slip angle helps giving better sense of actual direction of heading as the direction of heading and the direction of  $v$ , are almost same.

### 3.3 Control law for DYC

In this section, a sliding mode based yaw and side slip angle control technique is applied to the 14 DOF model discussed in chapter 2. The objective of DYC is to track desire yaw rate and side slip angle. From equation 3.7, the desired yaw rate  $\omega_z^*$  is,

$$\omega_z^* = \frac{v_x \delta}{l} \quad (3.8)$$

where  $l = a + b$ . And desired side slip angle is taken as,

$$\beta^* = 0 \quad (3.9)$$

The detailed procedure about designing the sliding model controller is given in [24]. One of the most important step in SMC is the switching function. As our aim is to simultaneously control the yaw rate and side slip angle, we choose to use the function given by [19] which is,

$$s = \frac{\rho}{|\Delta r|_{max}} |r - r^*| + \frac{1 - \rho}{|\Delta \beta|_{max}} |\beta - \beta^*| \quad (3.10)$$

where  $\rho \in [0, 1]$  is a design parameter.  $|\Delta r|_{max}$  and  $|\Delta \beta|_{max}$  are the maximum values of difference between actual yaw rate and side slip angle with respect to their corresponding reference values respectively.

Also  $\omega_z^* = r^*$  and  $\omega_z = r$ .

We know that the objective of any sliding mode controller is to bring the state trajectories of system in the control surface i.e.  $s = 0$ , and once this is been achieved, the later step is to keep them on the control surface  $s = 0$ .

From equation 3.10, we see that the value to  $s$  becomes zero only when the error in yaw rate i.e.  $|r - r^*|$  and the error in side slip angle i.e.  $|\beta - \beta^*|$  both reaches to zero. Hence on application of this switching function, the controller will perform control action until both, the yaw rate error and side slip error reaches zero, which is the aim of this study. Therefore we choose to use the switching function mentioned in equation 3.10. From equation 3.9, the reference value of  $\beta$  is zero, hence equation 3.10 is re-written as ,

$$s = \frac{\rho}{|\Delta r|_{max}} |r - r^*| + \frac{1 - \rho}{|\beta|_{max}} |\beta| \quad (3.11)$$

Taking derivative of equation 3.11, and re-substituting the values of  $r$  and  $r^*$ .

$$\dot{s} = \frac{\rho}{|\Delta \omega_z|_{max}} (\dot{\omega}_z - \dot{\omega}_z^*) \text{sgn}(\omega_z - \omega_z^*) + \frac{(1 - \rho)}{|\beta|_{max}} \dot{\beta} \text{sgn}(\beta) \quad (3.12)$$

According to the process described by [24], to drive the state equations of the system to the control surface, the sliding condition is written as,

$$\frac{1}{2} \frac{d}{dt} s^2 = s \dot{s} \leq -\eta |s| \quad (3.13)$$

Where  $\eta$  is positive constant. When trajectories of system are outside the control surface, i.e.  $s > 0$ ,

$$\dot{s} \leq -\eta \quad (3.14)$$

From equation 2.29, we can write as,

$$\dot{\omega}_z = \frac{1}{J_z} \left\{ (F_{y_{slf}} + F_{y_{srf}}) a - (F_{y_{slb}} + F_{y_{srb}}) b + (F_{x_{srf}} - F_{x_{slf}}) \frac{c}{2} + \Delta M \right\} \quad (3.15)$$

where  $\Delta M = (F_{xsrb} - F_{xslb}) \frac{c}{2}$ . Note that, because of different values of  $F_{xsrb}$  and  $F_{xslb}$  the yaw moment  $\Delta M$  is generated. Our aim for DYC in this study, is to achieve such values of  $F_{xsrb}$  and  $F_{xslb}$  by differentially operating the rear brakes/motors that, the yaw moment thus so generated, corrects the yaw rate of the vehicle. The motion of the system while plying on the sliding surface is known as an 'average' of the system on both sides. While on the siding surface we can write,

$$\dot{s} = 0 \quad (3.16)$$

On solving this equation, we get the mathematical model for  $\Delta M$ , called equivalent control,  $\Delta M_{eq}$  which can be interpreted as the continuous control law that would assure  $\dot{s} = 0$  if the dynamics were exactly known.

Substituting equation 3.15 in equation 3.12 and using the condition of equation 3.16

$$\begin{aligned} 0 = & \frac{\rho}{|\Delta\omega_z|_{max}} \frac{1}{J_z} \left\{ (F_{yf})a - (F_{yb})b + (F_{xsrf} - F_{xslf}) \frac{c}{2} + \Delta M_{eq} \right\} \text{sgn}(\omega_z - \omega_z^*) \\ & + \frac{(1-\rho)}{|\dot{\beta}|_{max}} \dot{\beta} \text{sgn}(\beta) - \frac{\rho}{|\Delta\omega_z|_{max}} \dot{\omega}_z^* \text{sgn}(\omega_z - \omega_z^*) \end{aligned}$$

where,  $F_{yf} = (F_{ysrf} + F_{ysl f})$  and  $F_{yb} = (F_{ysrb} + F_{ysl b})$ .

On solving the above equation for  $\Delta M_{eq}$ ,

$$\begin{aligned} \Delta M_{eq} = & J_z \left( -\frac{1-\rho}{\rho} \frac{|\Delta\omega_z|_{max}}{|\Delta\beta|_{max}} \dot{\beta} \text{sgn}(\beta) \frac{1}{\text{sgn}(\omega_z - \omega_z^*)} + \dot{\omega}_z^* \right) - F_{yf}a + bF_{yb} \\ & - \frac{c}{2} (F_{xsrf} - F_{xslf}) \end{aligned} \quad (3.17)$$

The expression obtained above for  $\Delta M_{eq}$  defines itself as a continuous control law that would satisfy the condition of equation 3.16. We add to  $\Delta M_{eq}$ , a discontinuous function [24],

$$\Delta M = \Delta M_{eq} - k \text{sgn}(\omega_z - \omega_z^*) \quad (3.18)$$

Where  $k$  is a large value and as we know  $\text{sgn}$  i.e.  $\text{sign}$  is a discontinuous function.

$$\begin{aligned} \text{sgn}(a) &= 1 & a > 0 \\ \text{sgn}(a) &= -1 & a < 0 \end{aligned}$$

From equation 3.18 and 3.17,

$$\begin{aligned} \Delta M = & J_z \left( -\frac{1-\rho}{\rho} \frac{|\Delta\omega_z|_{max}}{|\Delta\beta|_{max}} \dot{\beta} \operatorname{sgn}(\beta) \frac{1}{\operatorname{sgn}(\omega_z - \omega_z^*)} + \dot{\omega}_z^* \right) - F_{yfa} + bF_{yfb} \\ & -k \operatorname{sgn}(\omega_z - \omega_z^*) - \frac{c}{2} (F_{xsr} - F_{xsl}) \end{aligned} \quad (3.19)$$

substituting the value of  $\Delta M$  from equation 3.19 in the equation 3.15 would give,

$$\dot{\omega}_z = -\frac{1-\rho}{\rho} \frac{|\Delta\omega_z|_{max}}{|\Delta\beta|_{max}} \dot{\beta} \operatorname{sgn}(\beta) \frac{1}{\operatorname{sgn}(\omega_z - \omega_z^*)} + \dot{\omega}_z^* - \frac{k}{J_z} \operatorname{sgn}(\omega_z - \omega_z^*) \quad (3.20)$$

substituting equation 3.20 in the equation 3.12 gives,

$$\dot{s} = -\frac{k\rho}{J_z |\Delta\omega_z|_{max}} \quad (3.21)$$

comparing equation 3.14 and 3.21 we get,

$$\eta = \frac{k\rho}{J_z |\Delta\omega_z|_{max}} \quad (3.22)$$

therefore from equation 3.22,  $k$  can be written as,

$$k = \frac{\eta |\Delta\omega_z|_{max} J_z}{\rho} \quad (3.23)$$

From equation 3.18, the discontinuous term  $\operatorname{sgn}(\omega_z - \omega_z^*)$  has been introduced to account the disturbances and imprecision in the model [24]. Discontinuous functions introduces chattering in the control system which is undesirable since it initiates continuous control activity [24].

$$\begin{aligned} \Delta M = & J_z \left( -\frac{1-\rho}{\rho} \frac{|\Delta\omega_z|_{max}}{|\Delta\beta|_{max}} \dot{\beta} \operatorname{sat} \left( \frac{\beta(\omega_z - \omega_z^*)}{\Phi_1} \right) + \dot{\omega}_z^* \right) - F_{yfa} + bF_{yfb} \\ & -k \operatorname{sat} \left( \frac{(\omega_z - \omega_z^*)}{\Phi_2} \right) - \frac{c}{2} (F_{xsr} - F_{xsl}) \end{aligned} \quad (3.24)$$

Where  $\operatorname{sat}$  is the saturation function and  $\Phi$  is the boundary thickness [24].

$$\Delta T_{rb} = \frac{\Delta M}{c} R_{rb} \quad (3.25)$$

$$\Delta T_{lb} = \frac{\Delta M}{c} R_{lb} \quad (3.26)$$

If  $T$  is the torque being supplied to the particular wheel, the corresponding appropriate  $\Delta T$  should be added to it to form  $T_{new}$ . The altering of  $T$  by  $\Delta T$  is accomplished by differential braking.



### 3.4 Control Law for AFS

Function of active steering is to improve the linear handling region. Control law used for the active steering control has been explained in detail by [18], which is developed for the linear bicycle model. We have used the same control structure with minor modifications and implemented it as the combined/parallel control to the DYC structure. The sliding surface used is,

$$s = \omega_z - \omega_z^* \quad (3.27)$$

$$\dot{s} = -k_1 s - k_2 \operatorname{sgn}(s) \quad (3.28)$$

Where  $k_1$  and  $k_2$  are positive constants. The value of yaw rate  $\omega_z$ , which is the linearized form of equation 2.29, is given in [18],

$$\dot{\omega}_z = v \left( \frac{(bC_b - aC_f)}{J_z u} \right) - \left( \frac{(a^2 C_f + b^2 C_b)}{J_z u} \right) \omega_z + \delta_f \frac{aC_f}{J_z} \quad (3.29)$$

where  $u$  and  $v$  are the longitudinal and lateral velocities of CG respectively.  $\delta_f$  is steering angle which will be added to the steering angle, demanded by the driver.  $J_z$  is moment of inertia about  $z$  axis. Note that  $C_{\alpha,f}$  and  $C_{\alpha,b}$  are the cornering stiffness of front and rear axles, which varies continuously while cornering. For the sake of mathematical simplicity, we consider them as constant with values given in [18]. Using similar steps as explained in the design of control law of DYC, the final control law for AFS given by [18] is,

$$\begin{aligned} \delta_f = & \frac{bC_f}{J_z} \left\{ -v \left( \frac{(bC_b - aC_f)}{J_z u} \right) + \left( \frac{(a^2 C_f + b^2 C_b)}{J_z u} \right) \omega_z + \dot{\omega}_z^* \right\} \\ & + \frac{bC_f}{J_z} \left\{ -k_1 (\omega_z - \omega_z^*) - k_2 \operatorname{sat} \left( \frac{\omega_z - \omega_z^*}{\Phi_1} \right) \right\} \end{aligned} \quad (3.30)$$

where  $\Phi_1$  is the boundary layer thickness.

The control law input given in equation 3.30,  $\delta_f$ , can be directly applied to front wheels as steering angle. However the corrective steering angle is given by,

$$\delta_{corrected} = \delta_f - \delta_{fd} \quad (3.31)$$

where  $\delta_{fd}$  is the steering angle given by the driver to the front wheels.

### 3.5 Yaw Stability Controller Structure

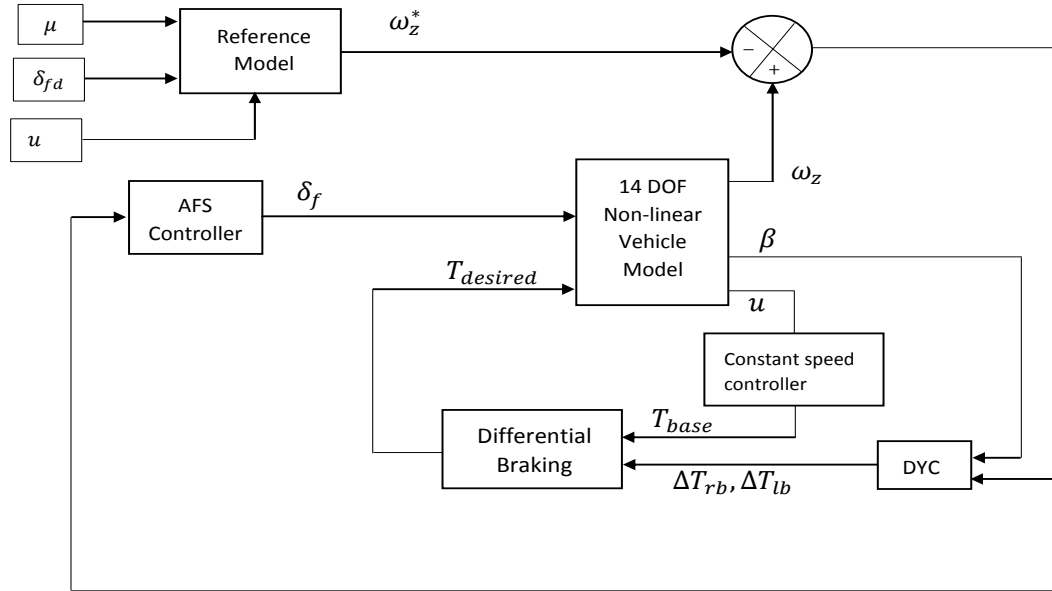


Figure 3.2: Controller structure

Fig. 3.2 shows the combine controller structure for yaw stability. As can be seen, the yaw rate error,  $e = \omega_z^* - \omega_z$ , and the side slip angle  $\beta$  has been given as an input to the sliding mode DYC which gives out corrective braking torque to be, applied to rear wheels. In order to keep longitudinal the velocity  $u$  constant, the proportional controller has been implemented. The Proportional controller produces the output torque signal  $T_{base}$  to be given to wheels. The corrective braking torques  $\Delta T_{rb}$  and  $\Delta T_{lb}$  are given to the differential braking arrangement, which controls the torque of each wheel in such a way that desired yaw moment is tracked. Active steering control system receives the same yaw rate error as an input signal. Using the control law modeled in equation 3.30, it produces the corrected the steering angle which is given to the steer-by-wire system, which is already installed in the vehicle.

### 3.6 Summary

This chapter focuses on the implementation of active control systems to the vehicle model derived in chapter 2. The necessity of these active system is because of *understeer* or *oversteer* characteristics of the vehicle during the cornering, which affects the side slip angle and non compliance with reference yaw rate, hence the active control systems and their corresponding control laws discussed. Since the sliding mode controller provides the robustness against variable parameters, the vehicle model is made

---

precise to track the reference conditions by implementing robust yaw rate and side slip controllers. The sliding surface for DYC is the linear and normalized sum of absolute side slip and yaw rate error and that for AFS, it is the error in yaw rate. The yaw rate equation 2.29 is not linearized to derive the control law. The mathematical formulation for ideal yaw rate has been taken from [22] where as the limit conditions for this model has been referenced from [25].

## Chapter 4

# Effectiveness of Controllers

### 4.1 Introduction

This chapter shows the performance of sliding mode controllers in extreme driving conditions. The comparative effectiveness of standalone active steering control and differential braking control has been discussed with the help of simulation results.

This chapter also discusses the trajectory control while on corner, when the adhesion coefficient of road suddenly drops i.e. vehicle passes over an ice or oil patch for very small time span. All the simulations in this chapter are performed for initial longitudinal velocity of  $45 \frac{km}{hr}$ . In the event of cornering, once the driver gives the final steering angle, he/she does not change it for the rest of the time.

### 4.2 Performance on the Dry Road

Figure below depicts the maneuverability of the vehicle on the dry road with constant adhesion coefficient. The input angle from the driver  $\delta_{fd}$  is shown in figure 4.1a where we can see that the stepped input angle increases from 0 to  $0.03 \text{ rad}$  in the span of 1 second i.e. driver starts turning steering wheel at  $4^{th}$  second from the start of analysis period and at constant rate of  $0.03 \frac{\text{radian}}{\text{s}}$ , he/she finishes it at  $5^{th}$  second and keeps it  $0.03 \text{ rad}$  for the rest of the time. The coefficient of friction of road has been kept constant to the value of 0.9, which can be considered as dry asphalt road.

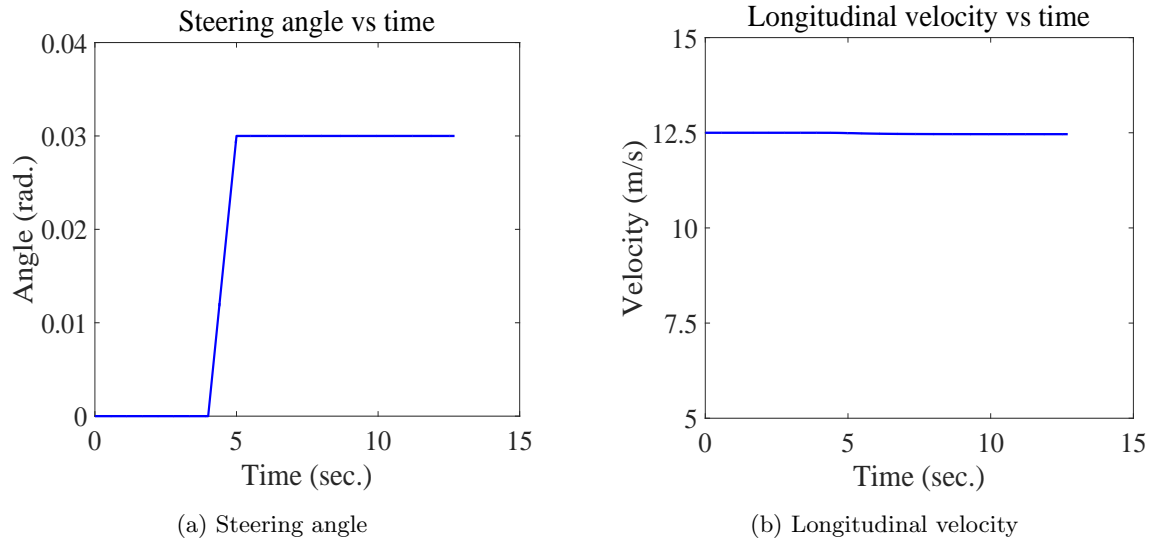


Figure 4.1: Driver input condition during maneuverability

### 4.2.1 Comparison by Parameters

The performance of vehicle with and without controller on the dry asphalt road, has been shown in figure 4.2 and 4.3.

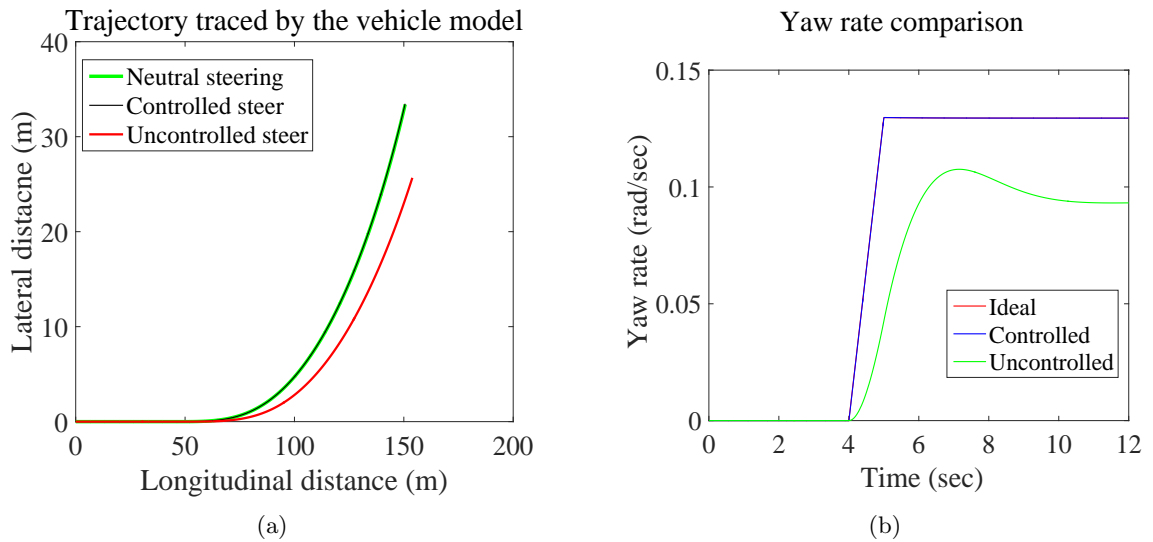


Figure 4.2: Trajectories and yaw rate comparison

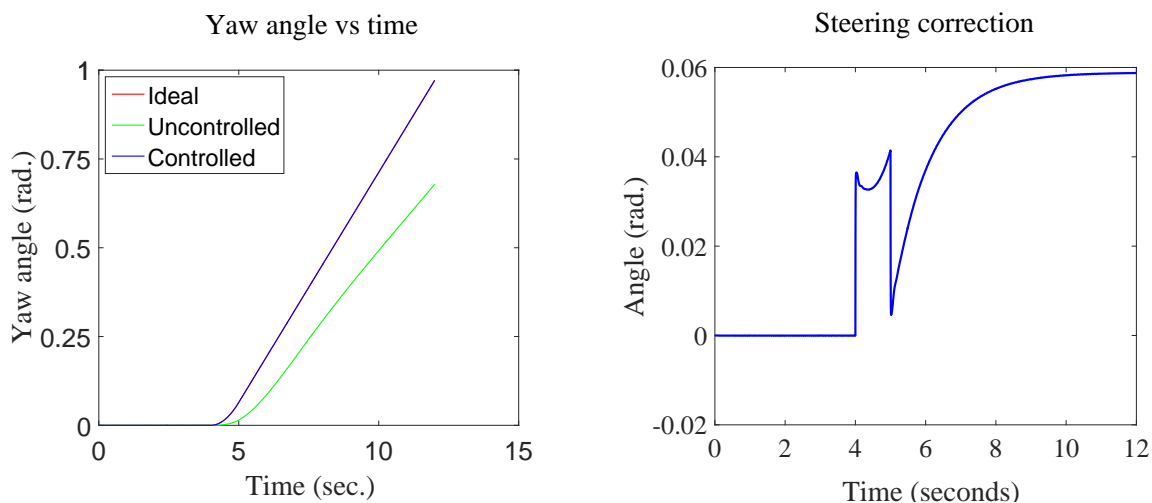


Figure 4.3: Heading angle comparison and correction angle by AFS

Without controllers, the reference yaw rate has not been tracked by the vehicle, which can be seen from figure 4.2b. As an effect of which, the yaw angle which is calculated by integrating the yaw rate, shows the deviation from the reference value. Note that the performance of the controller to track the reference model is vastly affected by the value of  $c_p$ , used in equation 2.67. Since the exact value of this parameter could not be found for the tire-brush model being used, we have assumed for it an appropriate value.

### 4.3 Performance on Slippery Road

This section focuses on the effectiveness of combined/parallel controllers on the road which is slippery continuously. To analyze the performance on slippery road, the coefficient of adhesion of road is kept 0.23 throughout the simulation. The longitudinal velocity kept constant as  $45 \frac{km}{hr}$ . All other parameters kept constant as that of above analysis.

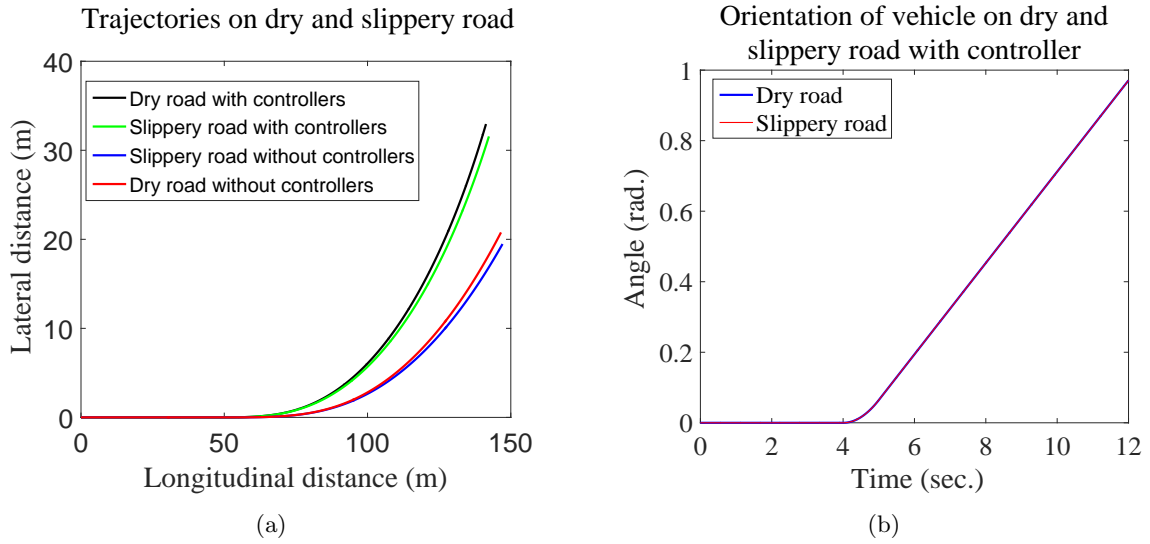


Figure 4.4: Trajectories and orientation comparison on dry and slippery road

From figure 4.4a, it can be seen that the coefficient of friction of 0.23 is sufficient to drift the vehicle off from its existing trajectory. When the vehicle is traveling on the slippery road without controllers, it negotiates with turn of radius which is comparatively more than that on dry asphalt road. From figure 4.4b we can observe that, when both the controllers controls the yaw rate, the angle made by vehicle about  $z$  axis of the inertial coordinate frame i.e. yaw angle, is almost same as it would make on dry road. Figure 4.5a is the enlarge view of figure 4.4a towards the end of simulation time. From figure 4.5a, we can observe that the vehicle, traveling on slippery road and under the effect of controllers, would trace almost same trajectory as it would do on the dry road with minor shift of  $1m$  in longitudinal and lateral displacement. Figure 4.5b is also the enlarge view of figure 4.4a towards the end of simulation time. From figure 4.5b, we can observe the noticeable difference in longitudinal displacement over  $4.75m$ , if the vehicle is traveling on slippery road without controllers and the lateral distance traveled in two cases, shows the considerable difference of over  $11m$ .

Hence in summary, the vehicle traveling on the continuously slippery road with coefficient of friction 0.23, may drive off the road, if the driver do not intervene in speed or braking, but the vehicle with controllers on-board, drives similar as to maneuver on dry asphalt road, with neutral steering condition, without seeking for driver's intervention.

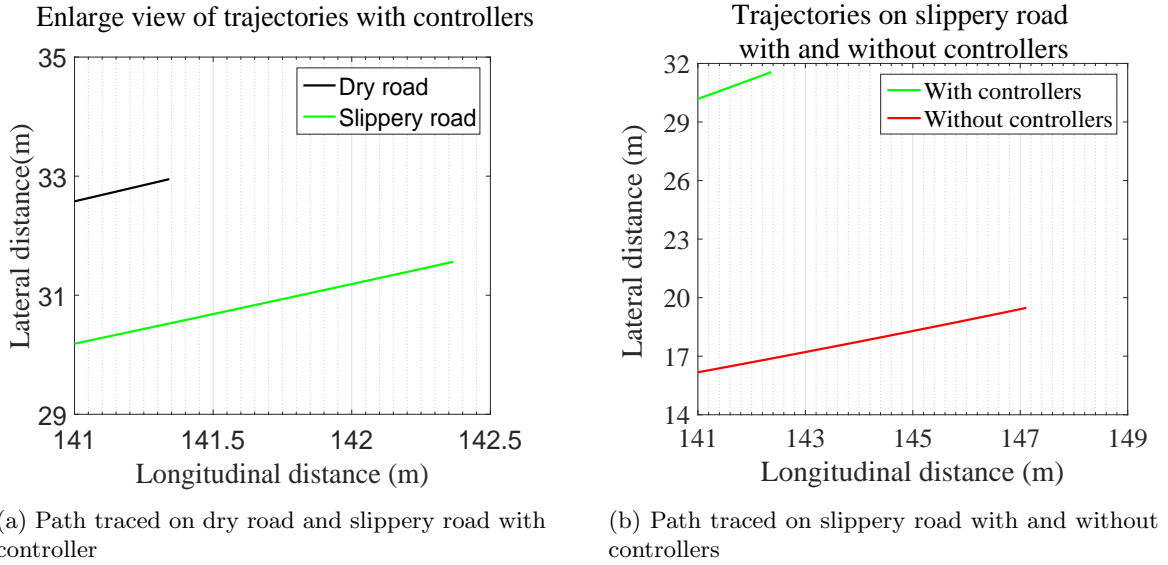


Figure 4.5: Enlarged view of trajectories traced on slippery surface

**Robustness of DYC**

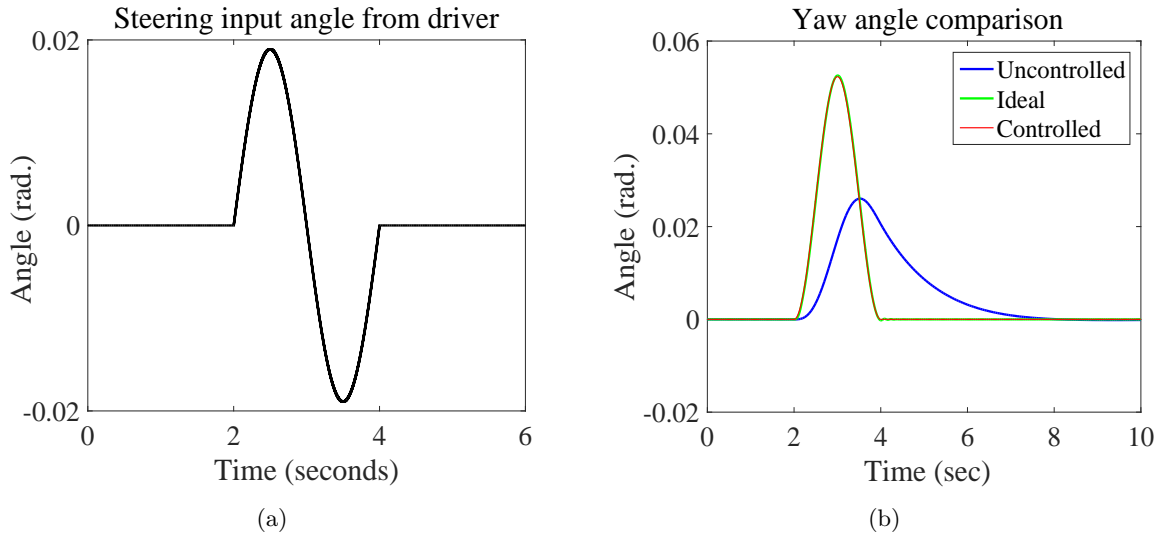


Figure 4.6: Tracking performance of DYC for sinusoidal steering input on slippery road

The more challenging driving scenario could be made by changing the steering input from the driver and worsening the road condition by deteriorating the adhesion coefficient to the value of 0.13. Note that since this subsection focuses on robustness of DYC only, we have deactivated the AFS control. As we can see from figure 4.6a, we assume that a sinusoidal steering input with peak value of 0.019



has been given by the driver with the frequency of  $1/2\text{hz}$ . It can be seen from figure 4.6b that vehicle orientation about inertial  $z$  axis (yaw angle) is almost same as that of reference yaw angle while the uncontrolled vehicle model shows noticeable difference from reference yaw angle

From figure 4.6b, we can infer that even when the implementation of DYC technique has improved the handling characteristic of vehicle, the figure 4.7 shows the poor tracking performance of DYC for side slip angle. The value of side slip angle seems to vary from its reference value of 0 with more margin than that for the uncontrolled vehicle model.

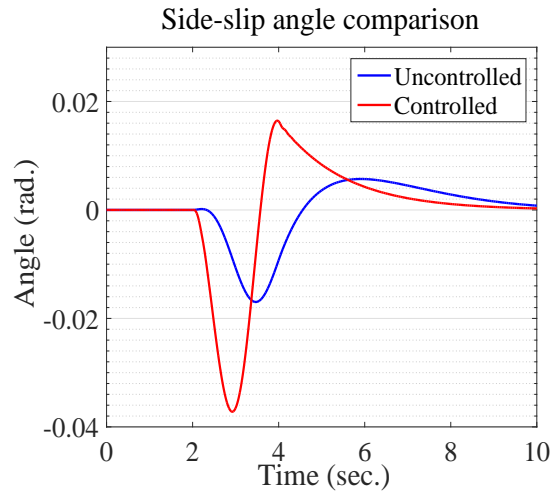


Figure 4.7: Side-slip angle on slippery road with sinusoidal steering input

But from section 3.2, we have seen that the sole purpose of tracking the side-slip angle  $\beta$  is to give the driver better sense of direction of heading so that he/she can alter the steering wheel input to achieve neutral steering condition. From figure 4.6b, we see that the vehicle is already tracking a reference heading angle even when  $\beta$  is not exactly tracking its reference value of  $\beta^* = 0$ . Therefore this can be considered as an acceptable condition in view on ideal handling characteristic of the vehicle.

## 4.4 Performance on Sudden Loss of Adhesion Coefficient of Road

### 4.4.1 Introduction of the Case

We have seen from equation 2.63, that for the Tire-Brush model, the adhesion coefficient is isotropic in nature. As seen in section 4.3, when the vehicle is continuously travelling of slippery surface and is prone to skid, the mental condition of driver would obviously be alert to adjust all the input parameters on which he/she is holding the controls. Hence in the alert mental condition, driver would keep keen

observation on the road surface. Hence the response time of driver would be tremendously low than usual conditions. When the driving conditions are not extreme like slippery road surface i.e. vehicle cornering on newly made asphalt road of friction coefficient 0.9, the alertness level of the driver would be lesser and hence his/her response time to the sudden change in any external parameter would be comparatively high.

Consider the scenario when the vehicle suddenly loses its grip from the road and starts sliding while traveling on the asphalt road. The severity would be even worse when the loss of friction coefficient happens during cornering. When one such an incidence happen, the driver can efficiently adjust the controls like steering wheel, brakes, throttle after 1 or 1.5 seconds after the incidence but the parameters of vehicle immediately after 0.5sec to 0.7sec once it completely pass over the ice patch will decide the future course of actions the driver is to take. In this regards, the instantaneous yaw angle i.e. heading direction will be one of the influential factors. If vehicle is still facing in the scope of the curvature, it will be easy for the driver to decide the corrective actions. The another influencing factor would be the distance it covers while on the ice patch. Lesser the distance, more is the chance that vehicle is not off the road. Table 4.1 shows the adhesion coefficient for different road conditions.

Description of road surfaces	Dry		Wet	
	Less than 30 mph	More than 30 mph	Less than 30 mph	More than 30 mph
New asphalt road	0.8 to 1.2	0.65 to 1	0.5 to 0.8	0.45 to 0.75
Traveled asphalt road	0.6 to 0.8	0.55 to 0.7	0.45 to 0.7	0.4 to 0.65
Smooth Ice	0.1 to 0.25	0.07 to 0.2	0.05 to 0.1	0.05 to 0.1
Packed snow	0.3 to 0.55	0.35 to 0.55	0.3 to 0.6	0.3 to 0.6
Loose snow	0.1 to 0.25	0.1 to 0.25	0.3 to 0.6	0.3 to 0.6

Table 4.1: Adhesion Coefficient for different road surfaces [7]

It can be observe that the adhesion coefficient for the ice covered road for the vehicle traveling at the speed less than 30 mph ranges from 0.1 to 0.25. A vehicle being given same maneuver condition as shown in figure 4.1a but instead of continuous dry or slippery road conditions, if we provide a sudden drop in the adhesion coefficient of road by introducing an ice patch, we can assess the performance of the controllers in the extreme driving conditions. The steering angle has been increased to the

final value of 0.08 for sharper cornering thereby increasing the critical nature of the curve. Some parameters of the DYC based system are slightly changed to increase the accuracy. The coefficient of friction of an ice patch is fixed to be 0.1. The length of ice patch is such that each pair of front and rear tires of the vehicle has to pass over it for exact 2sec. As already discussed above in this section, the parameters of the vehicle immediately after the passing over the ice patch, influence the further course of actions of driver. Figure 4.8a shows the location of ice patch on the curvature.

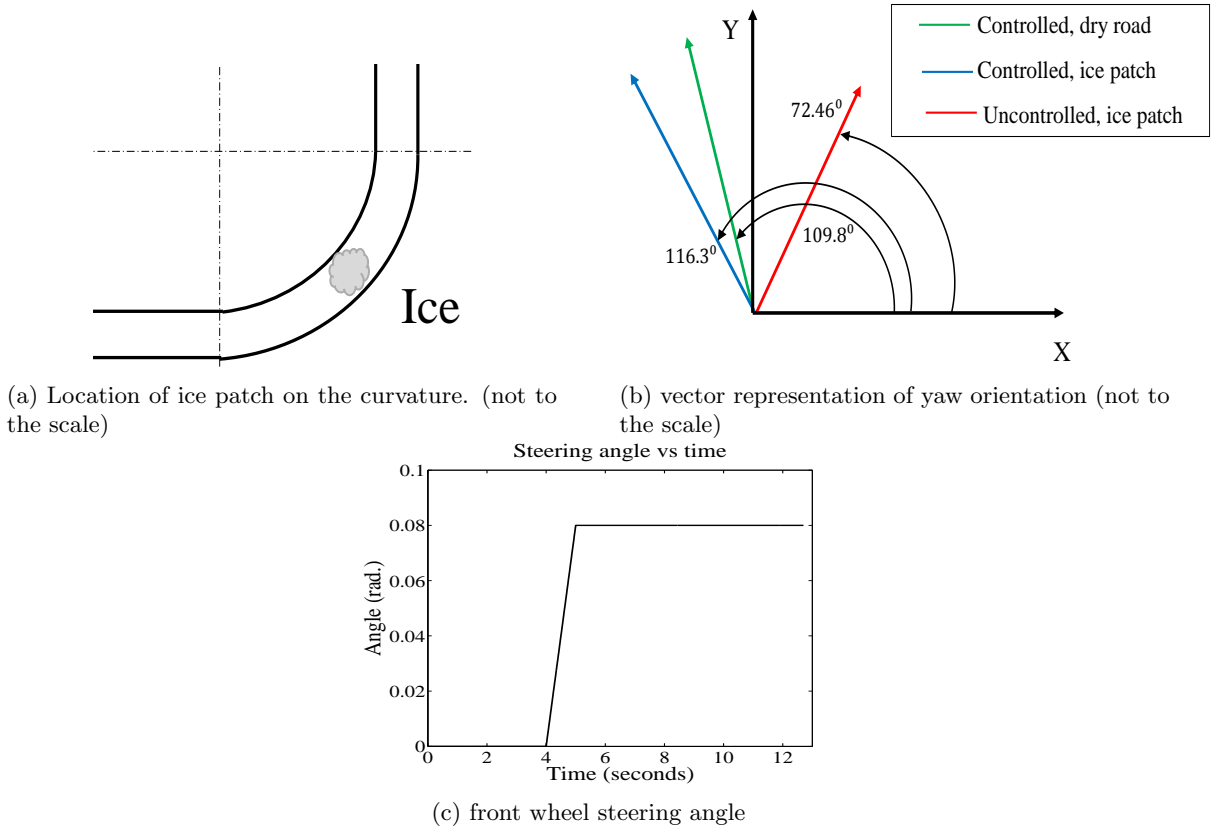


Figure 4.8: Topography of road and vector diagram of yaw orientation at the end of simulation

### 4.4.2 Parameters Comparison

For the simulation results discussed here, the complete vehicle passes over the ice patch after 12<sup>th</sup> second from the beginning of simulation. The nature of change in friction coefficient for rear and front tires has been shown in figure 4.9a. Simulation results shows the values of various parameters till 12.7<sup>th</sup> second, because after which driver can adjust the input parameters. Note that the value of adhesion coefficient of ice taken for parametric study is 0.1, which is very low as compared to other parallel studies on stability and handling. Figure 4.9b shows the yaw orientation of the vehicle. As

can be seen from the same figure, the vehicle traversing on the road with coefficient of friction 0.9, would make the yaw angle of  $2.03 \text{ rad}$ . i.e  $116.31 \text{ deg}$ . with respect to inertial longitudinal direction, where as the angle of orientation for the vehicle under the effect of controllers shows the yaw angle orientation of  $109.81 \text{ deg}$ . which almost equal to the orientation of vehicle on the dry road. Hence with the controllers in effect, the vehicle passed over sudden patch of ice would still be facing the road which helps the driver to judge the steering input to be given to the vehicle so that it can either realign with proper lane or stop at safe location,

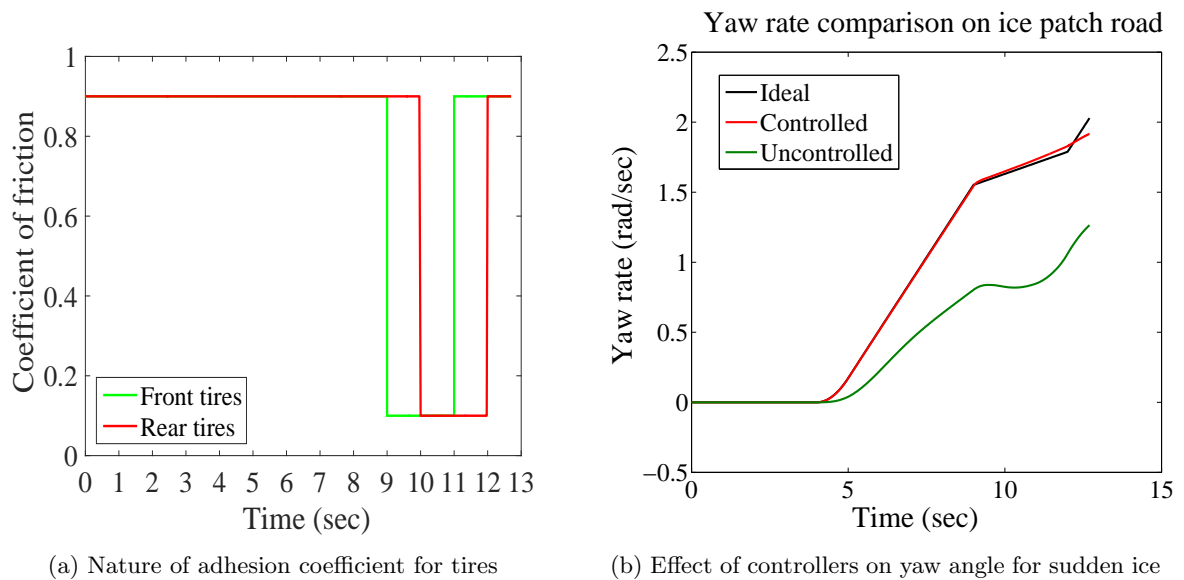


Figure 4.9: Friction coefficients for different tires and yaw angle comparison

whereas from the same figure 4.9b, it is observed that the vehicle with no controllers would skid off its curvature and loose its orientation to the value of  $72.46 \text{ deg}$ . which is  $43.85 \text{ deg}$ . less than the ideal yaw angle. As an effect of which, vehicle may not be facing the road which may pose difficulty for the driver to judge the situation. Figure 4.8b shows the orientation for each case in vector form at the end of  $12.7^{\text{th}}$  second.

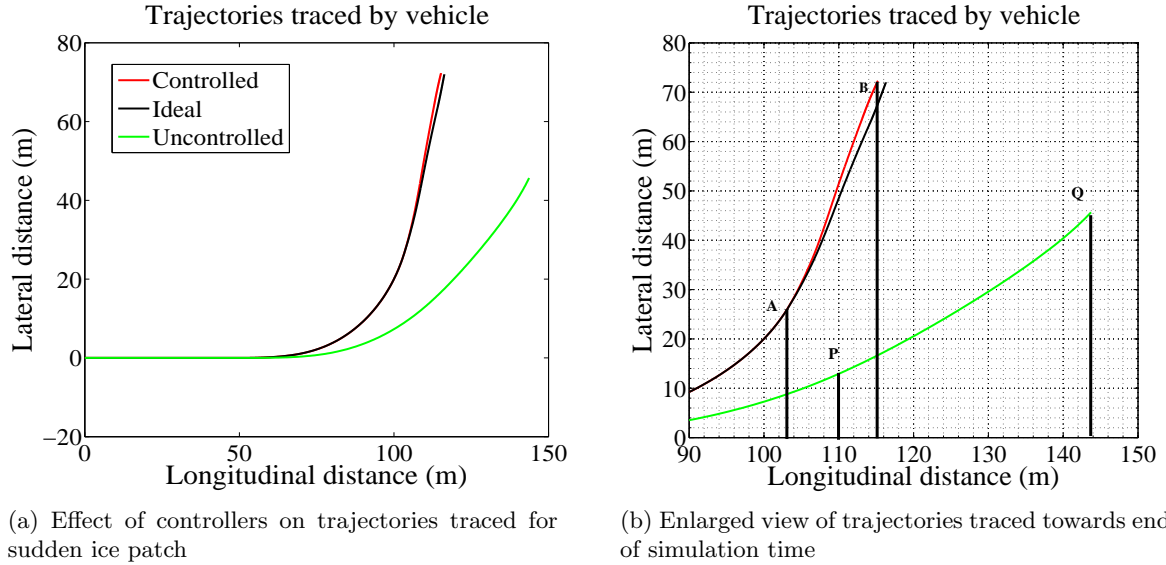


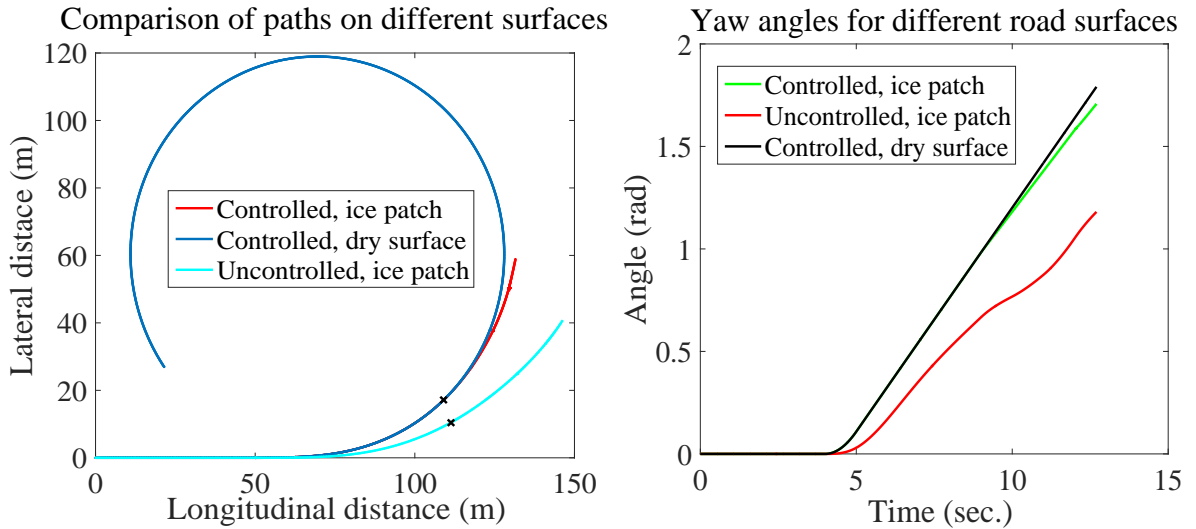
Figure 4.10: Path traced by vehicle over the sudden ice patch and dry road

Figure 4.10a shows the path, a vehicle would follow if it is made to travel on the road with ice patch on the corner with and without controllers. The same figure also shows the path it takes on the dry asphalt road under the effect of controllers, which we consider as the reference condition. Figure 4.10b is the enlarged view of 4.10a, focusing on the end time position of the vehicle. From figure 4.10b, the vertical lines intersecting different curves at points *A* and *P* shows the location at which the front tires of the vehicle touches the ice patch, where as *B* and *Q* shows the location where rear tires completely pass over the ice patch. From the same figure, following observations could be identified.

The horizontal distance covered by vehicle with no controllers is  $21.875m$  more than the vehicle with the controllers. The lateral distance traveled by the uncontrolled vehicle is  $26m$  less than that of controlled one. Hence we can infer that, the uncontrolled vehicle skids to cover larger horizontal and lateral distance which increases the probability skidding off the road.

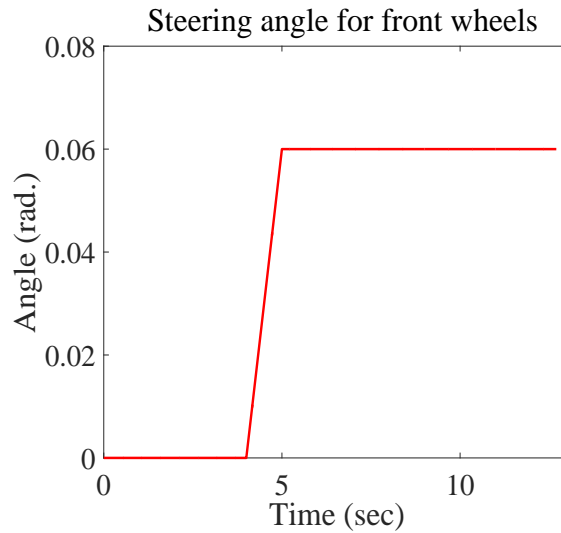
It is to be noted that, with the longitudinal velocity of  $12.5 \frac{m}{s}$ , the front tires pass over an ice patch for  $2sec$ . i.e. for the approximate distance of  $25m$ . Also the coefficient of friction of ice patch is only  $0.1$  which is a meager value. From figure 4.9a we can see that, from  $10^{th}$  second to  $12^{th}$  second, the whole vehicle travels ice patch without any intervention from the driver.

If we increase the coefficient of friction marginally to the value of  $0.16$ , The vehicle shows much controlled performance with different parameters obtained as follows,



(a) Path traced by a vehicle of sudden ice patch of friction coefficient 0.25

(b) Yaw angles for various conditions of road and controllers



(c) Steering angle for the front wheels

Figure 4.11: Parameters of vehicle which passed over a sudden ice patch of friction coefficient 0.25

From the figure 4.11 we see that when the coefficient of friction is slightly increased to the value of 0.25, which is still a smooth ice, the path traced by the vehicle almost matches with the reference, if the controllers are active. Whereas, with disabled controllers, vehicle corners with higher turning radius with skidding over an ice patch. The yaw angle traced by the controlled vehicle tracks the desired one. Note that the final steering angle of the stepped input is reduced to 0.06.

## 4.5 Summary

This chapter focuses on the effectiveness of the controllers on the vehicle which travels on different types of road surfaces. From first two sections, we can infer that the vehicle equipped with controllers, performs well according to neutral steering condition. The effect of controllers could be distinctively observed while on the corner. Even when the road surface is dry asphalt of friction coefficient of 0.9 or slippery of 0.23, the controllers effectively works to keep the path traced by the vehicle close to reference path.

The effectiveness of the controllers on cornering while an ice patch/oil patch is laid on the corner becomes more important to avoid fatalities. The simulation results for smooth ice patch of friction coefficient 0.1 and 0.16, on the corner, are also discussed. The results obtained with friction coefficient 0.16 shows significant effect of controllers which could work out as lives saver system.

## Chapter 5

# Conclusion and Recommendations

### 5.1 Conclusion

More realistic vehicle dynamic model could be structured by increasing the number of DOF for the vehicle model. Since the model discussed in this study needs to produce the more accurate results like that of multi-body dynamic model, we have chosen the one with 14 DOF. To implement the control strategies to it, the validation of 14 DOF model was performed using ADAMS/Car. In the software package ADAMS, in Car environment, Macpherson strut type suspension system for the front and rear axle was developed, whereas the body and steering systems were directly sourced from the existing shared database of MSC ADAMS/Car with modifications needed to fit according to physical characteristics of 14 DOF model. The Magic Formula tire modeling has been used to calculate the tire forces while constructing the vehicle model. The tire model which ADAMS/Car uses is different than the one, which we have used while building the vehicle model. Since the aim of this study is to examine the stability on the road with variable friction coefficient, while building the control structure, we have used the Tire-Brush model to facilitate the use of variable  $\mu$  and hence dependent tire forces.

The key parameters which greatly affects the performance of the vehicle on corner are yaw rate and side slip angle since these parameters affects the yaw orientation and better sense of exact direction of heading respectively. Hence we have used the DYC system in parallel with AFS control technique to regulate the above parameters. Both the controllers are robust in nature with sliding mode. The control law for DYC system ensures the conversion of yaw rate as well as side slip angle to the reference value whereas the AFS system used, controls the yaw rate alone and derived based on the bicycle model. The reference value for the yaw rate i.e. desired yaw rate, has be calculated based on the neutral steering condition. The reference value for side slip angle in this study is zero. The DYC uses differential braking technique like ABS whereas AFS uses steer-by-wire system to control their



corresponding control parameters.

With the control system on-board, the performance of the these active systems for different road surface conditions like dry, slippery and sudden slippery, are checked and it has been observed that the control systems works efficiently on the continuous dry and slippery road. For the road on which a smooth ice patch of  $\mu = 0.1$  has been laid on the corner, the controllers worked satisfactorily to keep track of desired values. For the ice patch with  $\mu = 0.16$ , the controllers has worked in such a way that the fatalities could be saved.

## 5.2 Recommendations

While validating the 14 DOF model with ADAMS/Car, the steering system is used from the existing shared database, the template of which uses the "steering assist" function. This function saves the vehicle from taking sudden turns and hence the step input to vehicle with large step within short time is not possible. The steering template without steering assist function should be built. The tire model used by ADAMS/Car (Pac.89) is different than one used in MATLAB model. Both the tire models should be consistent to match the results exactly. The value of property of tire,  $c_p$ , is randomly assumed, which may introduce inconsistencies in the results. Precise value of this parameter should be acquired from the tire manufacturer. The current control structure for AFS has been based on bicycle model, it should be designed for 14 DOF model. Another controller should be integrated with DYC and AFS which will work to avoid the rollover propensity of the vehicle.



## Appendix A

# Support .m file for MATLAB/Simulink Model

### 14 DOF Vehicle Data

$$a = 1.016m$$

$$c = 1.5m$$

$$b = 1.524m$$

$$C1 = 0.8621m$$

$$C2 = 0.8621m$$

$$C3 = 0.8962m$$

$$C4 = 0.8962m$$

$$R_0 = 0.285m$$

$$K_t = 200000 \frac{N}{m}$$

$$B_{sb} = 2000 \frac{Ns}{m}$$

$$K_{sb} = 30000 \frac{Ns}{m}$$

$$J_w = 1kg \ m^2$$

$$K_{sf} = 35000 \frac{N}{m}$$

$$B_{sf} = 2500 \frac{Ns}{m}$$

$$H_{rcf} = 0.65m$$

$$H_{rcb} = 0.6m$$

$$C = 1.5m$$

$$M_u = 80kg$$

$$J_x = 900kg \, m^2$$

$$J_y = 2000kg \, m^2$$

$$M = 1440kg$$

$$L = 2.54m$$

$$V_{ini} = 12.5 \frac{m}{s}$$

$$J_z = 2000kg \, m^2$$

$$C_{\text{alphaf}} = 3.076e5 \frac{N}{rad}$$

$$C_{\text{alphaR}} = 2.9898e5 \frac{N}{rad}$$

$$cp = 3.5e5 \frac{N}{rad \cdot m}$$

$$K = M/L^2 \cdot ((b/C_{\text{alphaf}}) - (a/C_{\text{alphaR}}))$$

---

**DYC Controller Data**

$$boundary = 100$$

$$RHO = 0.25$$

$$eta = 4$$

$$xi = 1 - RHO/RHO$$

$$rho = eta * 2000 * 0.2 * /RHO$$

**AFS Controller**

$$b\_2 = b * 105058 / J\_z$$

$$a\_21 = (b * 105058 - a * 79030) / J\_z$$

$$a\_22 = -(105058 * a^2 + 79030 * b^2) / J\_z$$

$$boundary\_1 = 100$$

$$K\_1 = 17$$

$$K\_2 = 67$$

**Initial Angular Velocities of Wheels**

$$W\_rf = V\_ini / (R\_0 - 0.0251)$$

$$W\_lf = V\_ini / (R\_0 - 0.0251)$$

$$W\_rb = V\_ini / (R\_0 - 0.018)$$

$$W\_rb = V\_ini / (R\_0 - 0.018)$$

## A.1 .txt File of Initial Conditions for .m File

W_x	0	Roll Velocity
W_y	0	PITCH_ANGULAR_VELOCITY
W_z	0	YAW_ANGULAR_VELOCITY
THETA	0	PITCH_ANGLE
SIGH	0	YAW_ANGLE
PHI	0	ROLL_ANGLE
x_trf	0.02511275	TIRE_COMPRESSION_RIGHTFRONT
x_srf	0.121075	SPRING_COMPRESSION_RIGHTFRONT
x_tlf	0.02511275	
x_slf	0.121075	
x_trb	0.0180502	
x_srb	0.094175	
x_tlb	0.0180502	
x_slb	0.094175	
W_urf	0	WHEEL_VERTICAL_VELOCITY_BODYFRAME_RF
W_ulf	0	
W_urb	0	
W_ulb	0	

U	15	CHASSIS_LONGITUDINAL_VELOCITY_BODYFRAME
V	0	
W	0	
w_rf	57.8563	ANGULAR_VELOCITY_RIGHTFRONT
w_lf	57.8563	
w_rb	56.325622	
w_lb	56.325622	
X	0	LONGITUDINAL_DISTANCE_TRAVELLED_BY_CAR
Y	0	
Z	0	

## A.2 MATLAB Script File and Simulink Model

```

1 function Test_1
2 clc
3 clear all
4 close all
5 global m J_x J_y J_z a b h c K_sf B_sf K_sb B_sb M_u K_t R_0 H_rcf H_rcb
   g cp
6
7 %% vehicle parameter input and dynamic response output
8
9 m = 1440;      J_x = 900;      J_y = 2000;
10 J_z = 2000;   a = 1.016;      b = 1.524;
11 h = 0.75;    c = 1.5;      K_sf = 35000;
12 B_sf = 2500; K_sb = 30000;   B_sb = 2000;
13 M_u = 80;    K_t = 200000;   R_0 = 0.285;
14 H_rcf = 0.65; H_rcb = 0.6;   g = 9.81;
15 cp = 0.5e6;
16
17 fid = fopen( 'initial_conditions.txt' );
18 hdr = textscan( fid, '%s%f%s', 'Delimiter', '\t' );
19 q_ini = (cell2mat(hdr(:,2)))';
20
21 tic
22 options = odeset( 'Events', @eventfun, 'RelTol', 1e-8, 'AbsTol', 1e-14*ones
   (1,28) );
23 [T_out, Q_out] = ode45( @chassis_response, [0 10], q_ini, options );
24 toc
25
26 save ( 'matrix_2', 'Q_out', 'T_out' )
27 end

```

```

28
29 function dq = chassis_response(t,q)
30 %%
31 global m J_x J_y J_z a b h c K_sf B_sf K_sb B_sb M_u K_t R_0 H_rcf H_rcb
      g
32 if t < 3
33     dlt_outer = 0;
34     dlt_inner = 0;
35
36 elseif t >= 3 && t <= 4
37     dlt_outer = 0.025294*(t - 3);
38     dlt_inner = 0.025294*(t - 3);
39 else
40     dlt_outer = 0.025294;
41     dlt_inner = 0.025294;
42 end
43 %% analysis of front right corner of the model (RF)
44 U_srf = q(19) + 0.5*c*q(3);
45 V_srf = q(20) + a*q(3);
46 W_srf = q(21) - a*q(2) - 0.5*c*q(1);
47 R_rf = R_0 - (q(7)/(cos(q(6))*cos(q(4))));
48 L_srf = (h - R_rf + 0.0251 - q(8) + 0.1211);
49 U_urf = U_srf - L_srf*q(2);
50 V_urf = V_srf + L_srf*q(1);
51 F_zgrf = K_t*q(7);
52 F_ztrf = F_zgrf;
53 dq(7,1) = -q(15) - V_urf*q(6) + U_urf*q(4);
54 dq(8,1) = q(15) - W_srf;
55 F_zsrf = q(8)*K_sf + dq(8,1)*B_sf;
56 U_grf = U_urf - q(2)*R_rf + q(15)*q(4) + q(1)*q(6)*q(4)*R_rf + V_urf*q(4)
      *q(6);
57 V_grf = V_urf + q(1)*R_rf - q(15)*q(6);
58 K_rf = (q(22,1)*R_rf - (U_grf*cos(dlt_outer) + V_grf*sin(dlt_outer))) /
      abs(U_grf*cos(dlt_outer) + V_grf*sin(dlt_outer));
59 A_rf = atan( (V_grf*cos(dlt_outer) - U_grf*sin(dlt_outer)) / (U_grf*cos(
      dlt_outer) + V_grf*sin(dlt_outer)));
60 [F_xtrf, F_ytrf] = magic(F_ztrf*10^-3, K_rf, A_rf);
61 dq(22,1) = R_rf*F_xtrf;
62 F_xgrf = F_xtrf*cos(dlt_outer) - F_ytrf*sin(dlt_outer);
63 F_ygrf = F_ytrf*cos(dlt_outer) + F_xtrf*sin(dlt_outer);
64 M_rf = [1 0 0; 0 cos(q(6)) sin(q(6)); 0 -sin(q(6)) cos(q(6))] * [cos(q(4)) 0
      -sin(q(4)); 0 1 0; sin(q(4)) 0 cos(q(4))] * [F_xgrf; F_ygrf; F_zgrf];
65 F_xgsrf = M_rf(1,1);
66 F_ygsrf = M_rf(2,1);
67 %% analysis of left front corner of the model (LF)
68 U_slf = q(19) - 0.5*c*q(3);
69 V_slf = q(20) + a*q(3);
70 W_slf = q(21) + 0.5*c*q(1) - a*q(2);
71 R_lf = R_0 - (q(9)/(cos(q(6))*cos(q(4))));

```



```

72 L_slf = (h - R_lf + 0.0251 - q(10) + 0.1211);
73 U_ulf = U_slf - L_slf*q(2);
74 V_ulf = V_slf + L_slf*q(1);
75 F_zglf = K_t*q(9);
76 F_ztlf = F_zglf;
77 dq(9,1) = U_ulf*q(4) - q(16) - V_ulf*q(6);
78 dq(10,1) = q(16) - W_slf;
79 F_zslf = q(10)*K_sf + dq(10,1)*B_sf;
80 U_glf = U_ulf + V_ulf*q(6)*q(4) + q(16)*q(4) - q(2)*R_lf + q(1)*R_lf*q(4)
      *q(6);
81 V_glf = V_ulf - q(16)*q(6) + q(1)*R_lf;
82 K_lf = ((q(23,1)*R_lf) - (U_glf*cos(dlt_inner) + V_glf*sin(dlt_inner))) /
      abs(U_glf*cos(dlt_inner) + V_glf*sin(dlt_inner));
83 A_lf = atan((V_glf*cos(dlt_inner) - U_glf*sin(dlt_inner)) / (U_glf*cos(
      dlt_inner) + V_glf*sin(dlt_inner)));
84 [F_xtlf, F_ytlf] = magic(F_ztlf*10^-3, K_lf, A_lf);
85 dq(23,1) = R_lf*F_xtlf;
86 F_xglf = F_xtlf*cos(dlt_inner) - F_ytlf*sin(dlt_inner);
87 F_yglf = F_ytlf*cos(dlt_inner) + F_xtlf*sin(dlt_inner);
88 M_lf = [1 0 0; 0 cos(q(6)) sin(q(6)); 0 -sin(q(6)) cos(q(6))] * [cos(q(4)) 0
      -sin(q(4)); 0 1 0; sin(q(4)) 0 cos(q(4))] * [F_xglf; F_yglf; F_zglf];
89 F_xgslf = M_lf(1,1);
90 F_ygslf = M_lf(2,1);
91 %% analysis of right back corner of the model (RB)
92 U_srb = q(19) + 0.5*c*q(3);
93 V_srb = q(20) - b*q(3);
94 W_srb = q(21) - 0.5*c*q(1) + b*q(2);
95 R_rb = R_0 - (q(11)/(cos(q(6))*cos(q(4))));
96 L_srb = (h - R_rb + 0.018 - q(12) + 0.0941);
97 U_urb = U_srb - q(2)*L_srb;
98 V_urb = V_srb + q(1)*L_srb;
99 F_zgrb = K_t*q(11);
100 F_ztrb = F_zgrb;
101 dq(11,1) = - q(17) - V_urb*q(6) + U_urb*q(4);
102 dq(12,1) = q(17) - W_srb;
103 F_zsrb = q(12)*K_sb + dq(12,1)*B_sb;
104 U_grb = U_urb + V_urb*q(4)*q(6) + q(17)*q(4) + q(1)*R_rb*q(4)*q(6) - q
      (2)*R_rb;
105 V_grb = V_urb - q(17)*q(6) + q(1)*R_rb;
106 K_rb = (q(24,1)*R_rb - U_grb) / abs(U_grb);
107 A_rb = atan(V_grb / U_grb);
108 [F_xtrb, F_ytrb] = magic(F_ztrb*10^-3, K_rb, A_rb);
109 dq(24,1) = R_rb*F_xtrb;
110 F_xgrb = F_xtrb;
111 F_ygrb = F_ytrb;
112 M_rb = [1 0 0; 0 cos(q(6)) sin(q(6)); 0 -sin(q(6)) cos(q(6))] * [cos(q(4)) 0
      -sin(q(4)); 0 1 0; sin(q(4)) 0 cos(q(4))] * [F_xgrb; F_ygrb; F_zgrb];
113 F_xgsrb = M_rb(1,1);
114 F_ygsrb = M_rb(2,1);

```

```

115 %% analysis of the left back tire of the model (LB)
116 U_slb = q(19) - 0.5*c*q(3);
117 V_slb = q(20) - b*q(3);
118 W_slb = q(21) + b*q(2) + 0.5*c*q(1);
119 R_lb = R_0 - (q(13)/(cos(q(6))*cos(q(4))));
120 L_slb = (h - R_lb + 0.018 - q(14) + 0.0941);
121 U_ulb = U_slb - q(2)*L_slb;
122 V_ulb = V_slb + q(1)*L_slb;
123 F_zglb = K_t*q(13);
124 F_ztlb = F_zglb;
125 dq(13,1) = - q(18) - V_ulb*q(6) + U_ulb*q(4);
126 dq(14,1) = q(18) - W_slb;
127 F_zslb = q(14)*K_sb + dq(14,1)*B_sb;
128 U_glb = U_ulb + V_ulb*q(4)*q(6) + q(18)*q(4) - q(2)*R_lb + q(1)*R_lb*q
      (4)*q(6);
129 V_glb = V_ulb - q(18)*q(6) + q(1)*R_lb;
130 K_lb = (q(25,1)*R_lb - U_glb) / abs(U_glb);
131 A_lb = atan(V_glb / U_glb);
132 [F_xtlb, F_ytlb] = magic(F_ztlb*10^-3, K_lb, A_lb);
133 dq(25,1) = R_lb*F_xtlb;
134 F_xglb = F_xtlb;
135 F_yglb = F_ytlb;
136 M_lb = [1 0 0; 0 cos(q(6)) sin(q(6)); 0 -sin(q(6)) cos(q(6))] * [cos(q(4)) 0
      -sin(q(4)); 0 1 0; sin(q(4)) 0 cos(q(4))] * [F_xglb; F_yglb; F_zglb];
137 F_xgslb = M_lb(1,1);
138 F_ygslb = M_lb(2,1);
139 %% assembling equation for rigid body motion
140 F_xsrfl = F_xgsrfl + M_u*g*q(4) + M_u*V_urf*q(3) - M_u*q(15)*q(2);
141 F_xslfl = F_xgslfl + M_u*g*q(4) + M_u*V_ulf*q(3) - M_u*q(16)*q(2);
142 F_xsrbl = F_xgsrbl + M_u*g*q(4) + M_u*V_urb*q(3) - M_u*q(17)*q(2);
143 F_xslbl = F_xgslbl + M_u*g*q(4) + M_u*V_ulb*q(3) - M_u*q(18)*q(2);
144
145 F_ysrfl = F_ygsrfl - M_u*g*q(6) - M_u*U_urf*q(3) + M_u*q(15)*q(1);
146 F_yslfl = F_ygslfl - M_u*g*q(6) - M_u*U_ulf*q(3) + M_u*q(16)*q(1);
147 F_ysrbl = F_ygsrbl - M_u*g*q(6) - M_u*U_urb*q(3) + M_u*q(17)*q(1);
148 F_yslbl = F_ygslbl - M_u*g*q(6) - M_u*U_ulb*q(3) + M_u*q(18)*q(1);
149
150 F_dzrfl = ((F_ygsrfl*R_rfl + F_ygslfl*R_lfl + F_ysrfl*L_srfl + F_yslfl*L_slfl - (
      F_ysrfl + F_yslfl)*H_rcfl) / c) ;
151 F_dzrbl = ((F_ygsrbl*R_rbl + F_ygslbl*R_lbl + F_ysrbl*L_srbl + F_yslbl*L_slbl - (
      F_ysrbl + F_yslbl)*H_rcbl) / c) ;
152
153 F_dzlf = -F_dzrfl;
154 F_dzlb = -F_dzrbl;
155
156 M_xrfl = F_ysrfl*H_rcfl ;
157 M_xlfl = F_yslfl*H_rcfl;
158 M_xrbl = F_ysrbl*H_rcbl ;
159 M_xlbl = F_yslbl*H_rcbl ;

```

```

160
161 M_yrf = -(F_xgsrf*R_rf + F_xsrfl*L_srf);
162 M_ylf = -(F_xgslf*R_lf + F_xslfl*L_slf);
163 M_yrb = -(F_xgsrb*R_rb + F_xsrbl*L_srb);
164 M_ylb = -(F_xgslb*R_lb + F_xslbl*L_slb);
165
166 dq(1,1) = (1/J_x)*(M_xrf + M_xlf + M_xrb + M_xlb + (F_zslf + F_zslb -
    F_zsrf - F_zsrb)*0.5*c);
167 dq(2,1) = (1/J_y)*(M_yrf + M_ylf + M_yrb + M_ylb + (F_zsrb + F_zslb)*b -
    (F_zslf + F_zsrf)*a);
168 dq(3,1) = (1/J_z)*((F_yslf + F_ysrf)*a - (F_ysrb + F_yslb)*b + (F_xsrf -
    F_xslf + F_xsrb - F_xslb)*0.5*c);
169
170 dq(4,1) = q(2)*cos(q(6)) - q(3)*sin(q(6));
171 dq(5,1) = (q(2)*sin(q(6))/cos(q(4))) + (q(3)*cos(q(6))/cos(q(4)));
172 dq(6,1) = q(1) + q(2)*sin(q(6))*tan(q(4)) + q(3)*cos(q(6))*tan(q(4));
173
174 dq(15,1) = (1/M_u)*(F_zgrf - M_u*g + F_xgrf*q(4) - F_ygrf*q(6) - F_dzrf -
    q(8)*K_sf - dq(8,1)*B_sf - M_u*V_urf*q(1) + M_u*U_urf*q(2));
175 dq(16,1) = (1/M_u)*(F_zglf - M_u*g + F_xglf*q(4) - F_yglf*q(6) - F_dzlf -
    q(10)*K_sf - dq(10,1)*B_sf - M_u*V_ulf*q(1) + M_u*U_ulf*q(2));
176 dq(17,1) = (1/M_u)*(F_zgrb - M_u*g + F_xgrb*q(4) - F_ygrb*q(6) - F_dzrb -
    q(12)*K_sb - dq(12,1)*B_sb - M_u*V_urb*q(1) + M_u*U_urb*q(2));
177 dq(18,1) = (1/M_u)*(F_zglb - M_u*g + F_xglb*q(4) - F_yglb*q(6) - F_dzlb -
    q(14)*K_sb - dq(14,1)*B_sb - M_u*V_ulb*q(1) + M_u*U_ulb*q(2));
178
179 dq(19,1) = (1/m)*(F_xsrf + F_xslf + F_xsrb + F_xslb + m*g*sin(q(4)) + m*q
    (3)*q(20) - m*q(2)*q(21));
180 dq(20,1) = (1/m)*(F_ysrf + F_yslf + F_ysrb + F_yslb - m*g*q(6) - m*q(3)*q
    (19) + m*q(1)*q(21));
181 dq(21,1) = (1/m)*(F_zsrf + F_zslf + F_zsrb + F_zslb + F_dzrf + F_dzlf +
    F_dzrb + F_dzlb - m*g - m*q(1)*q(20) + m*q(2)*q(19));
182
183 Vel_IF = [cos(q(5)) -sin(q(5)) 0; sin(q(5)) cos(q(5)) 0; 0 0 1]*[cos(q(4))
    0 sin(q(4)); 0 1 0; -sin(q(4)) 0 cos(q(4))]*[1 0 0; 0 cos(q(6)) -sin(q(6))
    ]; 0 sin(q(6)) cos(q(6))]*[q(19); q(20); q(21)];
184 dq(26,1) = Vel_IF(1,1);
185 dq(27,1) = Vel_IF(2,1);
186 dq(28,1) = Vel_IF(3,1);
187
188 end
189
190 function [F_xt, F_yt] = magic(F_n, K, A)
191 %%
192 if K==0&&A ==0
193     F_xt = 0;
194     F_yt = 0;
195 else
196 if F_n <= 0

```

```

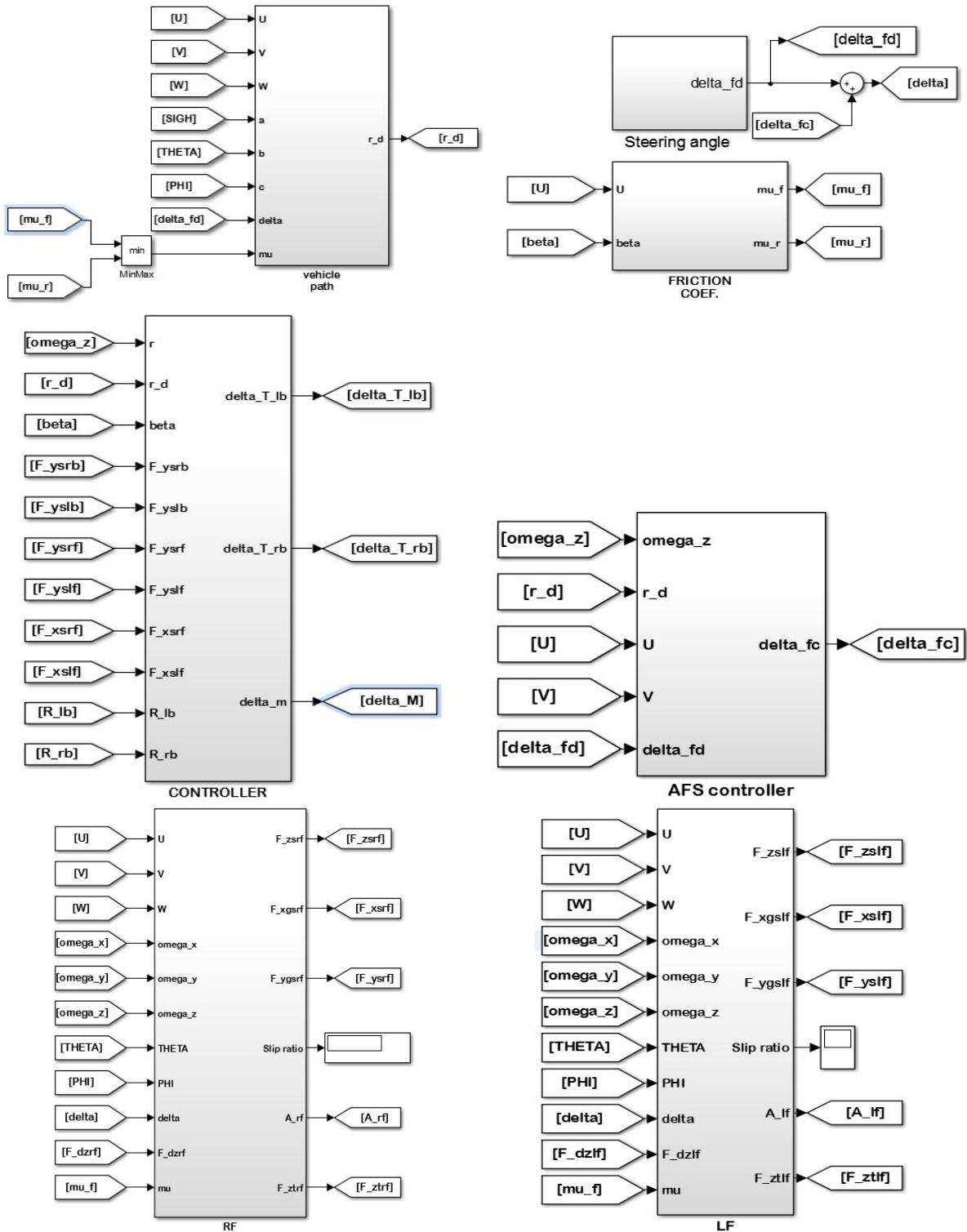
197     F_xt = 0;
198     F_yt = 0;
199     else
200     D_x = -21.3*(F_n)^2 + 1144*(F_n);
201     B_x = (49.6*(F_n)^2 + 226*(F_n)) / D_x * 1.65 * exp(0.069*F_n);
202     E_x = -0.006*(F_n)^2 + (0.056*F_n) + 0.486;
203     D_y = -22.1*(F_n)^2 + 1011*F_n;
204     B_y = 1078*sin(1.82*atan(0.208*F_n)) / (1.3 * D_y);
205     E_y = -0.354*F_n + 0.707;
206     Th = 0:0.1:1;
207     for i = 1:length(Th)
208         PHI_x = (1 - E_x) * Th(i)*100 + (E_x / B_x)*atan(B_x *Th(i)*100);
209         F_x(i) = D_x * sin(1.65*atan(B_x * PHI_x));
210         PHI_y = (1 - E_y)*(Th(i)*180/pi) + (E_y / B_y)*atan(B_y * (Th(i)*180/
                pi));
211         F_y(i) = D_y * sin(1.3*atan(B_y * PHI_y));
212     end
213     M = max(F_x);
214     N = max(F_y);
215     for i = 1:length(Th)
216         if F_x(i) == M
217             sigma_m_x = Th(i);
218         else
219             end
220             if F_y(i) == N
221                 sigma_m_y = Th(i);
222             else
223                 end
224         end
225     sigma_x_star = K / ((1 + K)*sigma_m_x);
226     sigma_y_star = tan(A) / ((1 + K)*sigma_m_y);
227     sigma_star = sqrt((sigma_x_star)^2 + (sigma_y_star)^2);
228     PHI_x0 = (1 - E_x) * sigma_star*100 + (E_x/B_x)*atan(B_x *sigma_star*100)
                ;
229     F_xt = -(sigma_x_star / sigma_star) * D_x * sin(1.65*atan(B_x *
                PHI_x0));
230     PHI_y0 = (1 - E_y) * (sigma_star*180/pi) + (E_y / B_y)*(atan(B_y * (
                sigma_star*180/pi)));
231     F_yt = -(sigma_y_star / sigma_star) * D_y * sin(1.3 *atan(B_y *
                PHI_y0));
232     end
233     end
234     end
235
236     function [value, isterminal, direction] = eventfun(t,q)
237     %%
238     value = q(13) ;
239     isterminal = 1;
240     direction = -1;

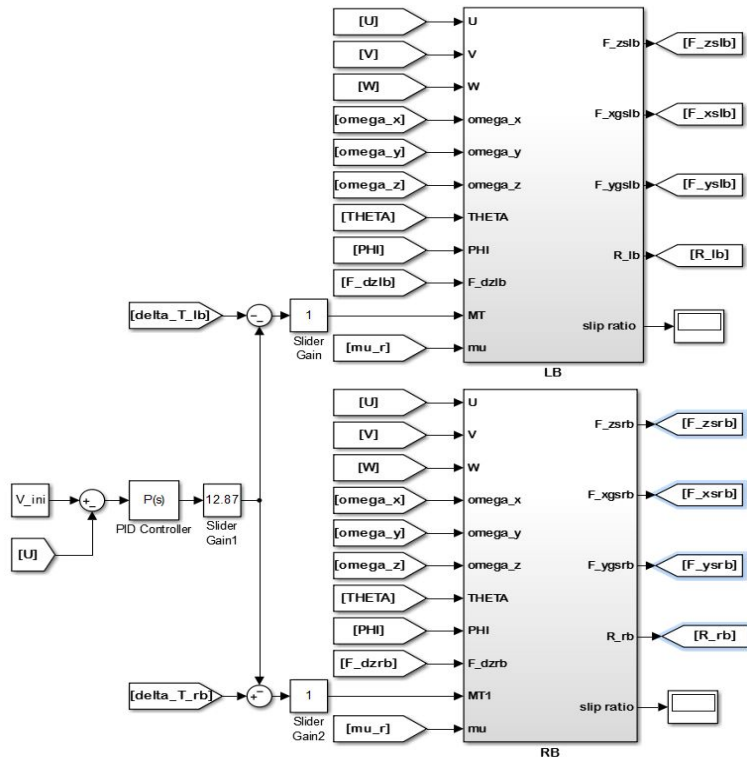
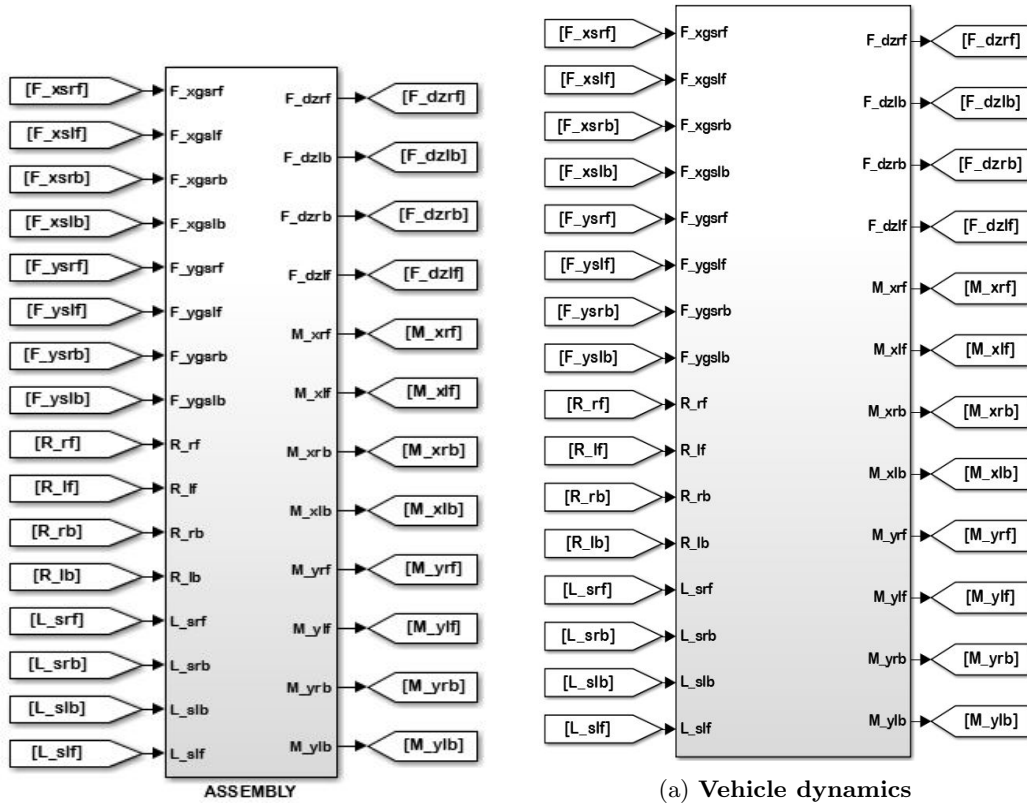
```

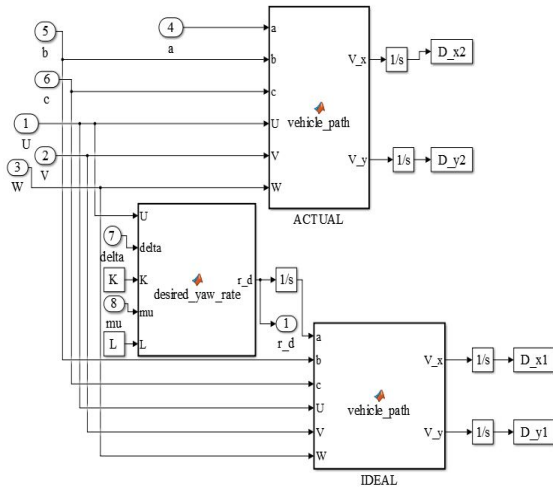
241 **end**

### Tire-Brush Model Code of MATLAB/Simulink model

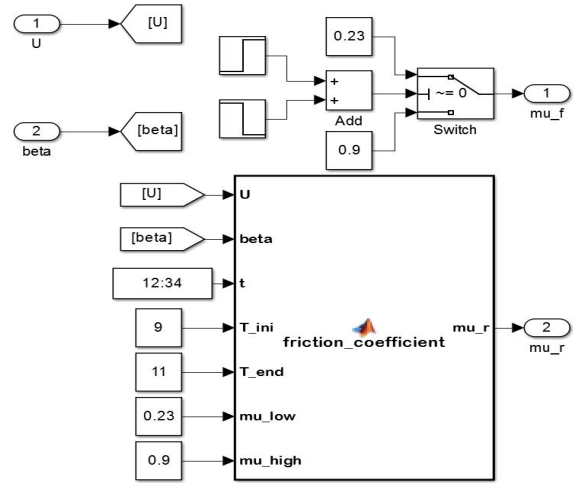
```
1     function [F_yt, F_xt] = brush_model(K,A,F_n, x_tr ,mu)
2     cp = 0.29898e6;
3     R_0 = 0.285;
4     sigma_x = K / (K + 1);
5     sigma_y = tan(A) / (K + 1);
6     sigma = sqrt(sigma_x^2 + sigma_y^2);
7     a = R_0 * (0.35 * (x_tr / R_0) + (0.79 * sqrt(x_tr / R_0)));
8     theta = (2 * cp * a^2) / (3 * mu * F_n);
9     lamda = 1 - (theta * sigma);
10    sigma_sl = 1 / theta;
11    if sigma <= sigma_sl
12        F = mu * F_n * (1 - lamda^3);
13    elseif sigma > sigma_sl && sigma < pi * 0.5
14        F = mu * F_n;
15    else
16        F = inf;
17    end
18    F_xt = -(sigma_x / sigma) * F;
19    F_yt = -(sigma_y / sigma) * F;
20    end
```



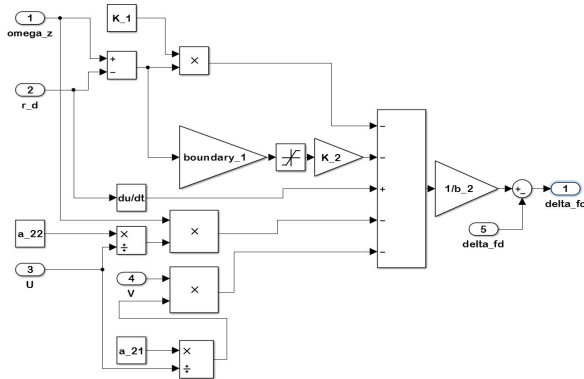




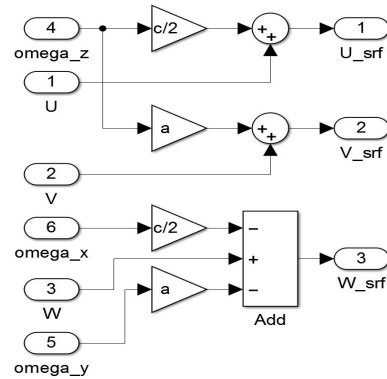
(a) Details of vehicle path



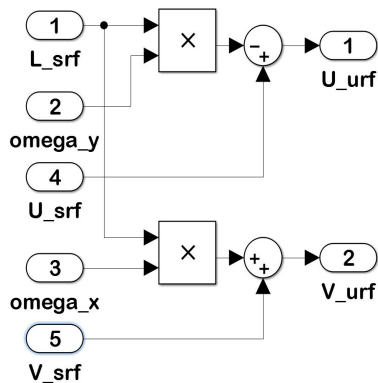
(b) Friction coefficient



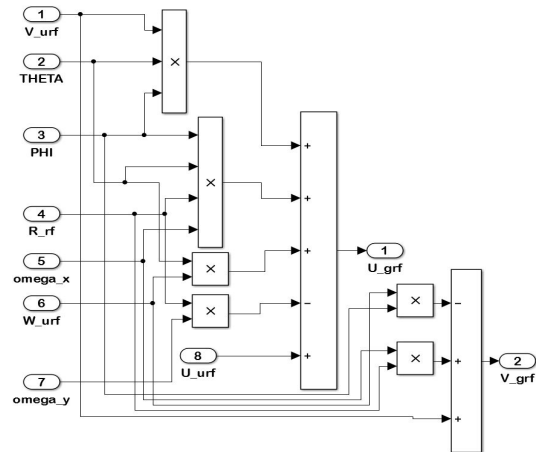
(c) AFS controller



(d) Sprung mass velocities

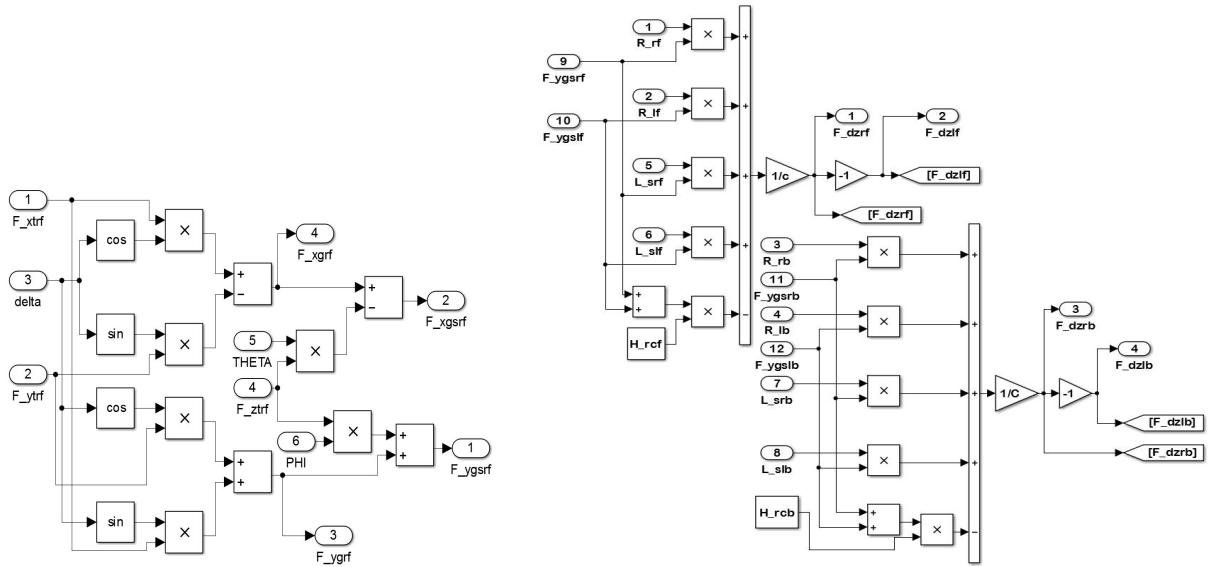


(e) Unsprung mass velocities



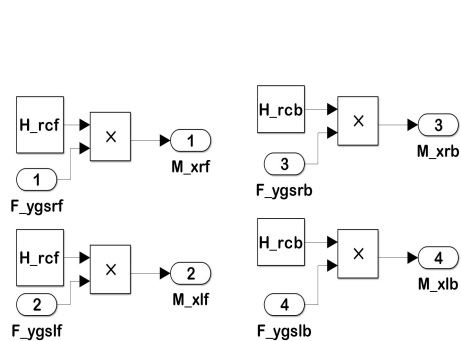
(f) Contact patch velocities



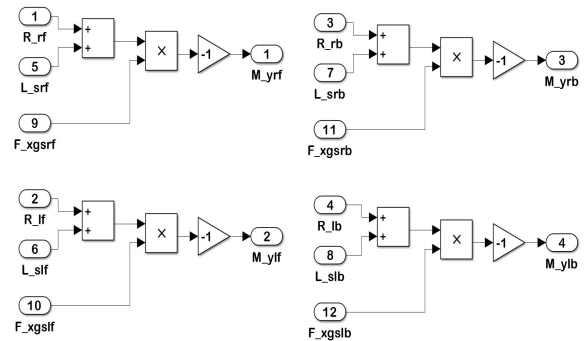


(a) Force at contact patch

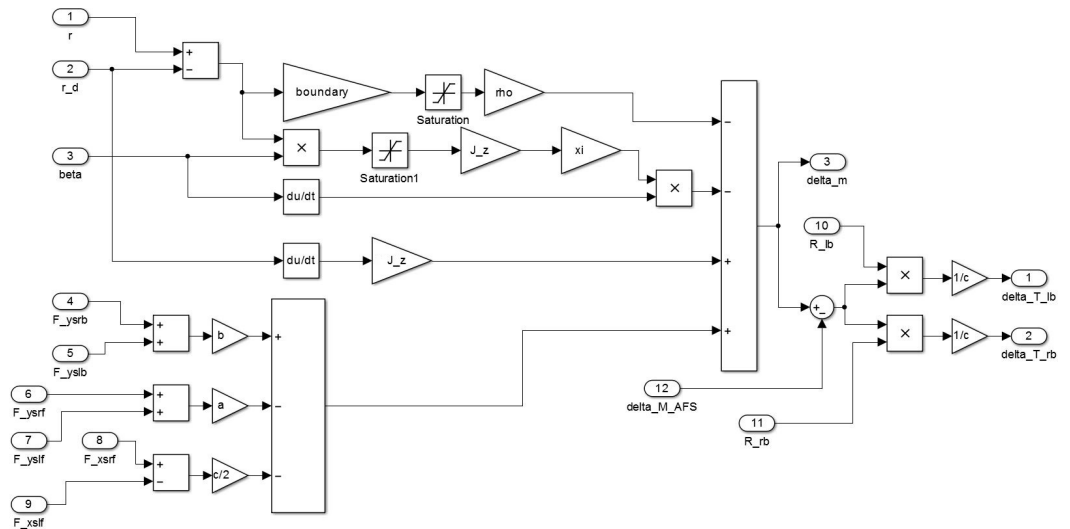
(b) Lateral load shift



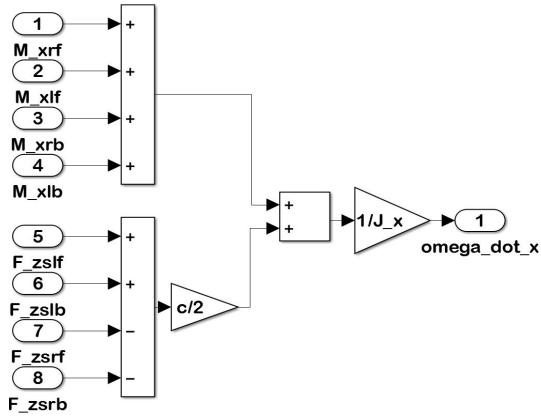
(c) Moment about x-axis



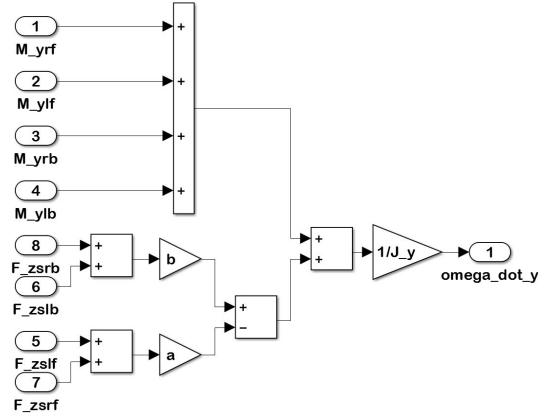
(d) Moment about y-axis



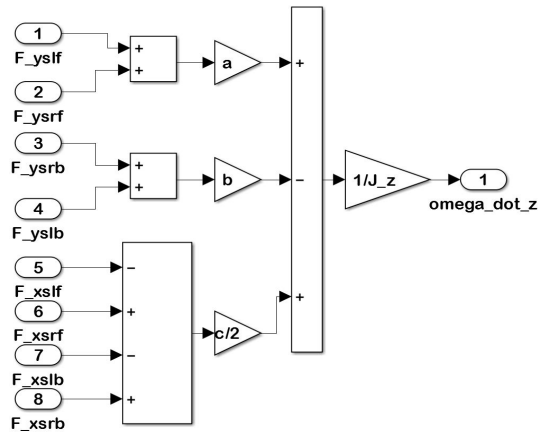
(e) DYC Controller



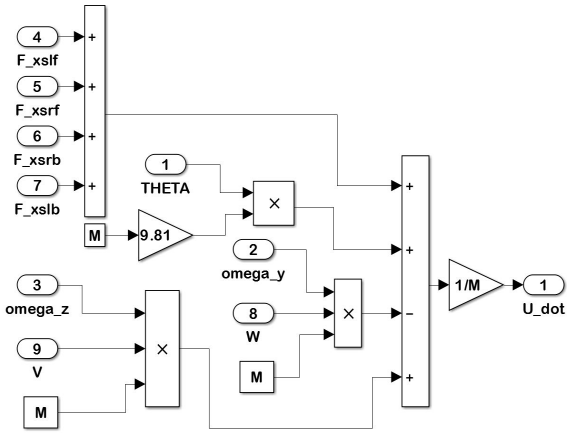
(a) Roll velocity



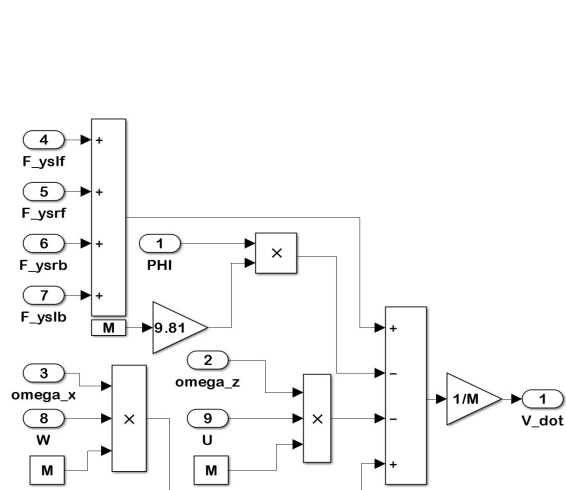
(b) Pitch velocity



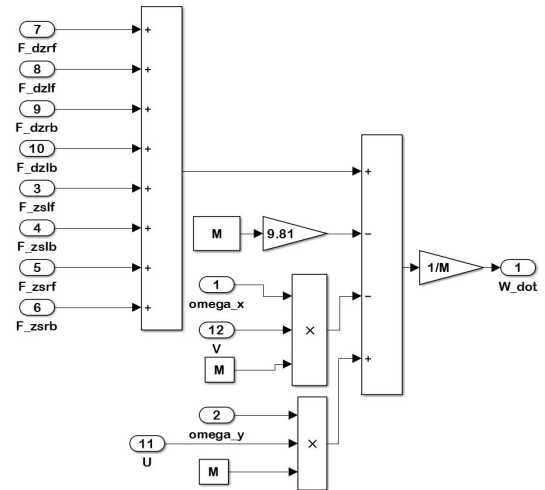
(c) Yaw velocity



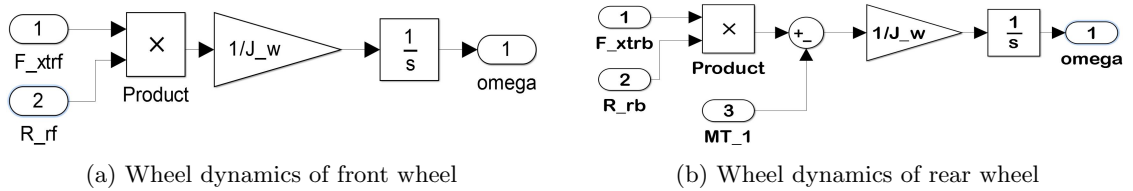
(d) Longitudinal velocity of sprung mass



(e) Lateral velocity of sprung mass



(f) Heave velocity of sprung mass



(a) Wheel dynamics of front wheel

(b) Wheel dynamics of rear wheel

Figure A.6: Wheel dynamics in Simulink

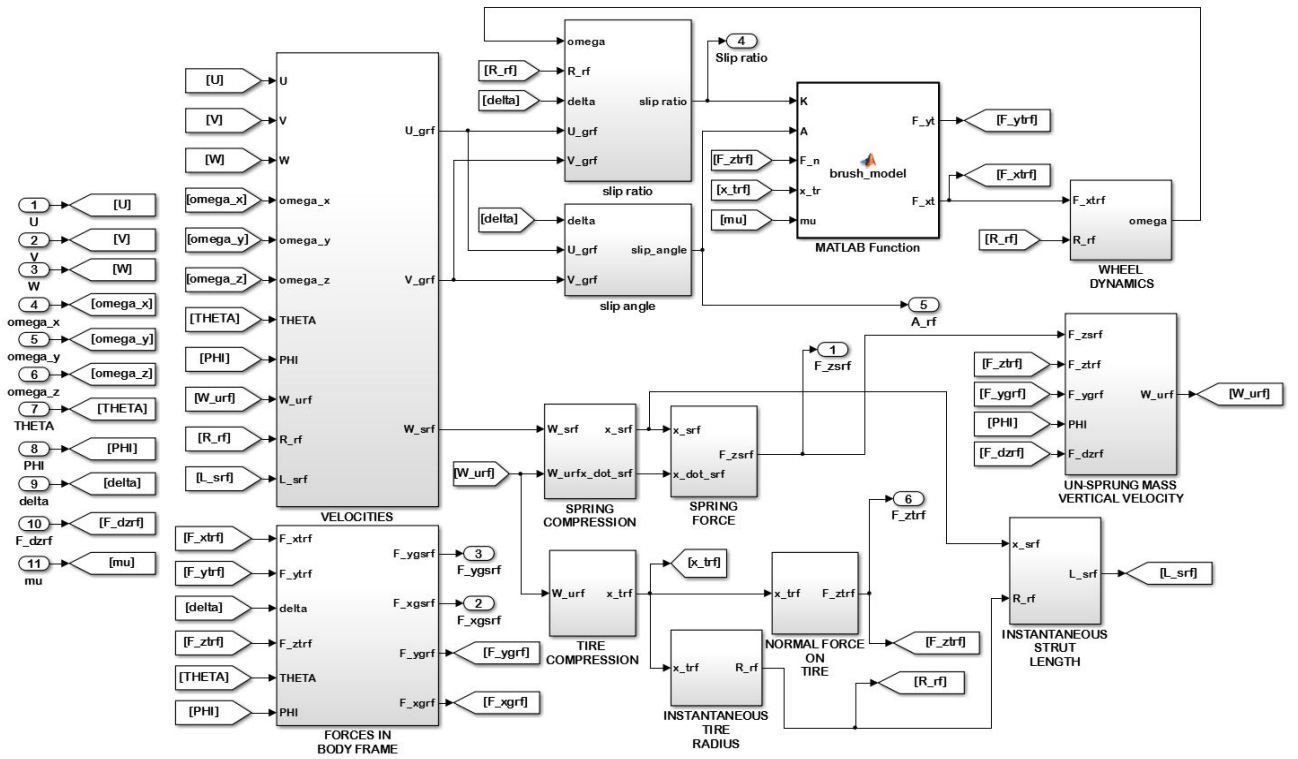


Figure A.7: Dynamics for right-front corner

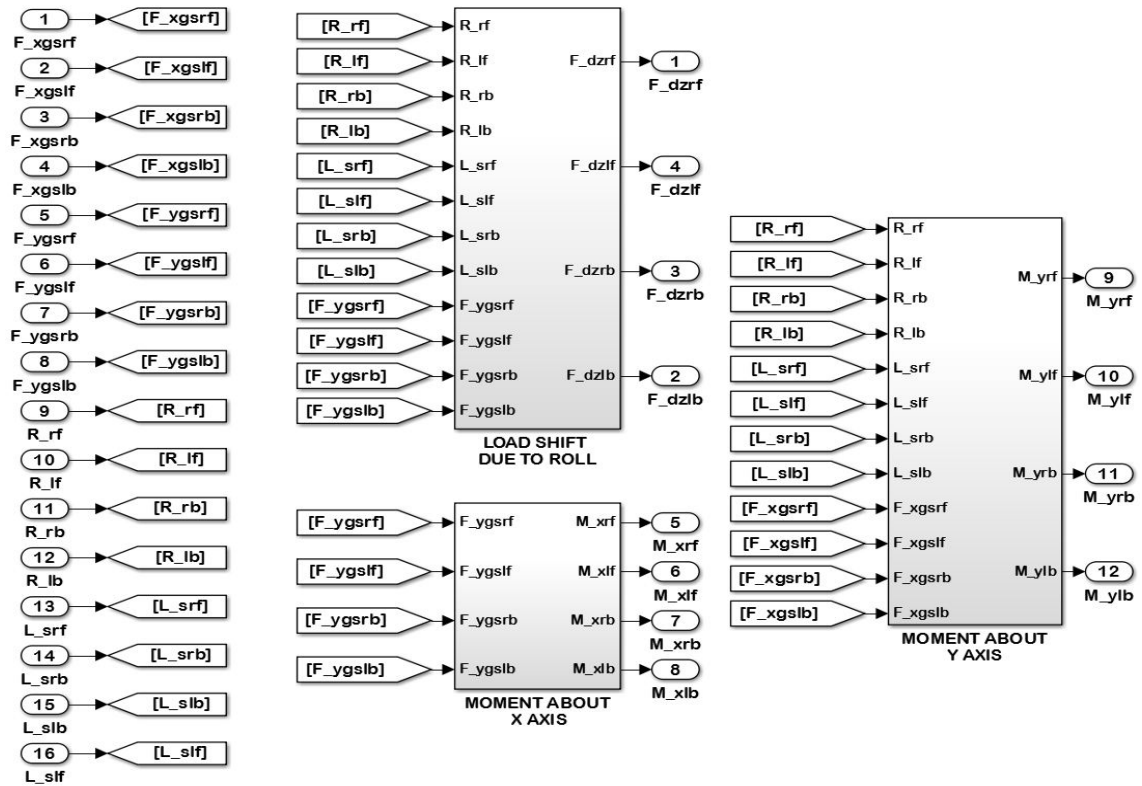


Figure A.8: Details of subsystem 'Assembly'



# References

- [1] Ken Koibuchi, Masaki Yamamoto, Yoshiki Fukada, and Shoji Inagaki. Vehicle stability control in limit cornering by active brake. Technical report, SAE Technical Paper, 1996. [viii](#), [3](#)
- [2] Sanjay Singh. Design of front wheel active steering for improved vehicle handling and stability. Technical report, SAE Technical Paper, 2000. [viii](#), [5](#)
- [3] Chinar Ghike and Taehyun Shim. 14 degree-of-freedom vehicle model for roll dynamics study. Technical report, SAE Technical Paper, 2006. [viii](#), [6](#), [7](#), [8](#), [13](#), [14](#), [15](#)
- [4] B Lee, A Khajepour, and K Behdinan. 2006-01-1022 vehicle stability through integrated active steering and differential braking. *SAE SP*, 2018:185, 2006. [viii](#), [2](#), [4](#), [10](#), [11](#)
- [5] Hans B Pacejka, Egbert Bakker, and Lars Nyborg. Tyre modelling for use in vehicle dynamics studies. *SAE paper*, 870421:1–15, 1987. [viii](#), [x](#), [7](#), [9](#), [10](#), [26](#), [27](#), [28](#), [36](#), [37](#)
- [6] Hans Pacejka. *Tire and vehicle dynamics*. Elsevier, 2005. [viii](#), [8](#), [18](#), [28](#), [29](#), [30](#), [32](#)
- [7] [www.marules.com](http://www.marules.com). Coefficient of friction of various road surfaces. [x](#), [54](#)
- [8] Kiyoka Matsubayashi, Yukinori Yamad, Motomi Iyoda, Shin Koike, Tomoya Kawasaki, and Masanori Tokuda. Development of rear pre-crash safety system for rear-end collisions. In *20th International Technical Conference on the Enhanced Safety of Vehicles (ESV)*, number 07-0146, 2007. [1](#)
- [9] Bo-Chiuan Chen and Huei Peng. Rollover warning of articulated vehicles based on a time-to-rollover metric. *Ann Arbor*, 1001:48109–2125, 1999. [1](#), [2](#)
- [10] Erik Dahlberg. A method determining the dynamic rollover threshold of commercial vehicles. Technical report, SAE Technical Paper, 2000. [1](#)
- [11] Y Watanabe and RS Sharp. Mechanical and control design of a variable geometry active suspension system. *Vehicle system dynamics*, 32(2-3):217–235, 1999. [1](#)

- [12] Jeonghoon Song. Design and evaluation of active front wheel steering system model and controller. *SAE International Journal of Passenger Cars-Mechanical Systems*, 7(1):367–374, 2014. [2](#)
- [13] Azadeh Farazandeh, AKW Ahmed, and Subhash Rakheja. An independently controllable active steering system for maximizing the handling performance limits of road vehicles. *Proceedings of the Institution of Mechanical Engineers, Part D: Journal of Automobile Engineering*, 229(10):1291–1309, 2015. [4](#)
- [14] Edward J Bedner and Hsien H Chen. A supervisory control to manage brakes and four-wheel-steer systems. *SAE paper*, 3:8–11, 2004. [5](#)
- [15] MSC Marc. Url: <http://www.mscsoftware.com/products/cae-tools>. *Marc. aspx*. [7](#), [9](#), [12](#), [34](#), [36](#)
- [16] Nicholas Cooper, David Crolla, Martin Levesley, and Warren Manning. Integration of active suspension and active driveline to ensure stability while improving vehicle dynamics. Technical report, SAE Technical Paper, 2005. [9](#)
- [17] Behrooz Mashadi and Majid Majidi. Integrated afs/dyc sliding mode controller for a hybrid electric vehicle. *International Journal of Vehicle Design*, 56(1-4):246–269, 2011. [9](#)
- [18] Junjie He, DA Crolla, MC Levesley, and WJ Manning. Coordination of active steering, driveline, and braking for integrated vehicle dynamics control. *Proceedings of the Institution of Mechanical Engineers, Part D: Journal of Automobile Engineering*, 220(10):1401–1420, 2006. [9](#), [45](#)
- [19] Chunyun Fu. *Direct yaw moment control for electric vehicles with independent motors*. PhD thesis, RMIT University, 2014. [10](#), [22](#), [42](#)
- [20] SJ Tupling and MR Pierrynowski. Use of cardan angles to locate rigid bodies in three-dimensional space. *Medical and Biological Engineering and computing*, 25(5):527–532, 1987. [22](#)
- [21] Parviz E Nikravesh. *Computer-Aided: analysis of mechanical systems*. 1988. [23](#)
- [22] Reza N Jazar. *Vehicle dynamics: theory and application*. Springer Science & Business Media, 2013. [40](#), [41](#), [47](#)
- [23] Thomas D Gillespie. Fundamentals of vehicle dynamics. Technical report, SAE Technical Paper, 1992. [40](#)
- [24] Jean-Jacques E Slotine, Weiping Li, et al. *Applied nonlinear control*, volume 199. Prentice-Hall Englewood Cliffs, NJ, 1991. [42](#), [43](#), [44](#)

- 
- [25] Kyongsu Yi, Taeyoung Chung, Jeontae Kim, and Seungjong Yi. An investigation into differential braking strategies for vehicle stability control. *Proceedings of the Institution of Mechanical Engineers, Part D: Journal of Automobile Engineering*, 217(12):1081–1093, 2003. [47](#)